Metallamacrocyclic Xanthate Complexes of Co^{II}/ Cu^{II} Derived From Xanthates of Phenolates and Their Use in (2:2) Binuclear *N, O*-Schiff Base Macrocycle Formation: Synthesis, Characterization and *in vitro* Cytotoxicity Studies

Abstract

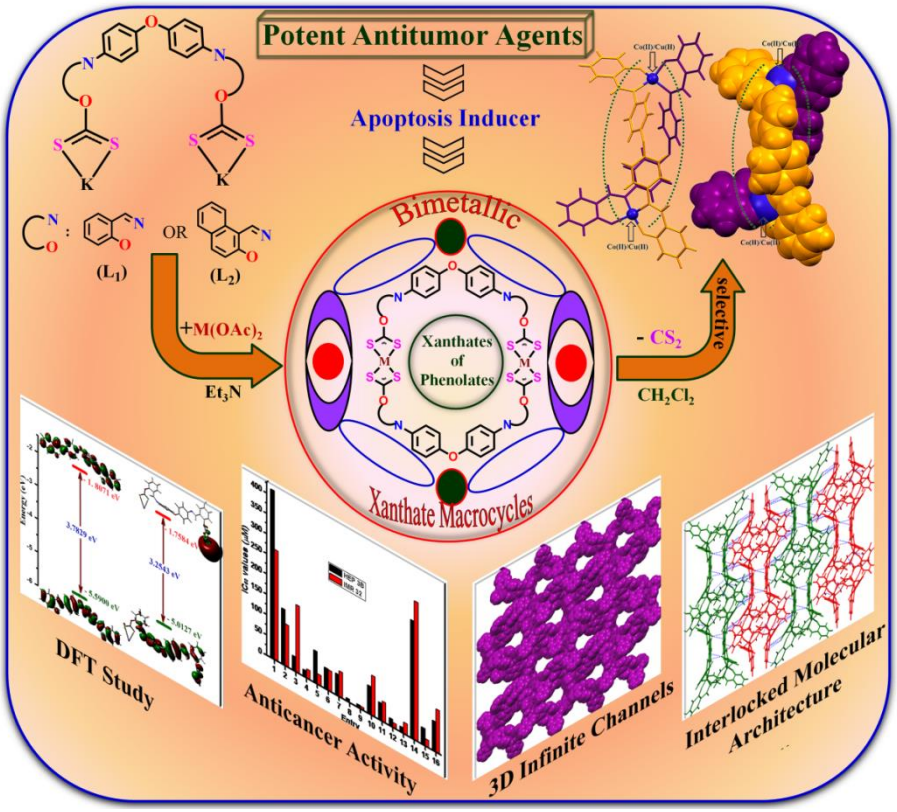

This is the first report on the binuclear Co^{II} or Cu^{II} xanthate macrocyclic complexes of the type [M_2-μ^2-bis-(κ^2*S,S*-xan^1/xan^2)]**1-4** derived from phenolate based polydentate xanthate ligands andtheir facile transformation into [2:2] binuclear *N, O*-bidentate Schiff base macrocycles of the type [M_2-μ^2-bis-(κ^2*N,O*-L^1/L^2)] **5-8**. The unambiguous structures of **5-8** and their crystal packing patters wereinvestigated by single crystal X-ray diffraction study. The geometry of model compounds has been optimized by a DFT method. The *in vitro* cytotoxicity of all the compounds was evaluated against HEP 3B and IMR 32 by the MTT assay and the resulting dataunderlines their better potency than cisplatin.These scaffolds were explored as a novel class of active chemical agents to induce apoptosis.

2.1. Introduction

Among the coordination compounds, discrete molecular metallamacrocyclic rings or cages with diverse cavity size and shape[1] are of particular interest due to their potential applications in catalysis,[2] host-guest chemistry,[3] molecular and ion sensing,[4] separation, transport and storage,[5] in drug delivery, two-phase transport and biosensing.[6] However, control over the size and shape of the metallamacrocyclic rings and product's selectivity is still a challenge for synthetic chemists.[7] Besides, the transition metal complexes have shown the utility as bioinorganic replica to get insight in the mode of action of complexed biological systems or to mimic metalloproteins featuring dinuclear active sites.[8] Further, they offer additional opportunities for development of new therapeutic agents not accessible to organic compounds,[9] by means of varied coordination numbers, geometries, redox states, thermodynamic-kinetic characteristics, and intrinsic properties of both metal ions and ligands. The platinum based anticancer drug cisplatin and its analogues have already proved to be indispensable in cancer chemotherapy. However, the efforts in the evaluation of anticancer drugs have been shifted to non-platinum metal-based agents with improved pharmacological properties and aimed at different targets,[10]to avoid dose-limiting side effects[11] and the emergence of drug resistance associated with platinum chemotherapeutics.[12]In this context, copper complexes have shown encouraging results,[13] mainly due to its redox activity and affinity for binding sites that should be occupied by other metal ions. The altered metabolism of cancer cells and differential response between normal and tumor cells to copper are the basis for the development of copper complexes endowed with antineoplastic characteristics. Further, it has been established that a wide range of natural product bearing macrocyclic motif and their synthetic derivatives have long been clinically used as they endow structural pre-organization with sufficient flexibility for better binding with the target molecules and exhibit high degree of potency as well as selectivity.[14]However, a class of inorganic compounds "metallamacrocyclic structures" are surprisingly underexploited from medical view point especially for cytotoxic activity.

It is well known that, sulfur is an important constituent of biomolecules and plays a crucial role in transporting and addressing the molecule to the targets as well

as in the protection of pharmacophore against untimely exchanges with biomolecules.[11,15] For instance, the diethyldithiocarbamate anion, has been extensively used in Wilson's disease to overcome copper poisoning[16] and for better nephrotoxicity in platinum-based chemotherapy.[17]In addition, it has been shown that sulfur containing compounds exhibit good DNA/protein binding/cleaving and catalytic activity toward glutathione.[18]Even though dithiocarbamates demonstrated neurotoxic effect in animal models as well as in human,[19] only gold and copper dithiocarbamate complexes were studied over past few decades for their anti-cancer activity[20] while other transition metal dithiocarbamate complexes and their structural analogous xanthate complexes were relatively underexplored. 4,4'-diaminodiphenyl ether and its *N*-acetyl derivative towards *Salmonella typhimurium* TA98 and TA100 were reported in 1985 by Tanaka et al.,[21] there is no reports of further investigations of biological properties of 4,4'-diaminodiphenyl ether and its derivatives. Notably, no data are available to assess the mutagenicity or teratogenicity of any derivative of 4,4'-diaminodiphenyl ether to human. Only recently, we have reported bisimine and diamino derivatives of 4,4'-diaminodiphenyl ether bearing polyaromatic *N*-substituents that have shown promising in vitro cytotoxic activity which largely depends on the nature of various *N*-substituents.[22] With the intension to enhance cytotoxicity, we have synthesized potassium salts of 4,4'-bis(*2*-dithiocarbonatobenzylideneamino)diphenyl ether (K_2xan^1) and 4,4'-bis(*2*-dithiocarbonatonaphthylmethylideneamino)diphenyl ether (K_2xan^2). The incorporation of xanthate moiety is expected to enhance the possibility of stacking and intercalation through a number of noncovalent interactions with DNA/proteins and, in turn, cytotoxicity of the ensuing complexes. These phenolate based xanthate **K_2xan^1** and **K_2xan^2** ligands have been used to derive binuclear metallamacrocyclic Co^{II}/ Cu^{II} xanthate complexes **1-4**. We have further demonstrated the selective transformation of **1-4**into corresponding (2:2) binuclear metallamacrocyclic *N*,*O*-Schiff base complexes **5-8**.In a conventional approach for the synthesis of (2:2) binuclear metallamacrocyclic *N*,*O*-Schiff base complexes, lack of selectivity is one of the main barriers; hence the present synthetic methodology would be of great interest. To the best of our knowledge, this is the first report on binuclear metallamacrocyclic xanthate complexes derived from phenolates and their selective transformations into (2:2) binuclear *N*,*O*-Schiff base macrocycles. All the compounds were investigated

for their potential in vitro cytotoxic and apoptosis inducing properties against HEP 3B and IMR 32 human cancer cells.

2.2. ExperimentalSection

2.2.1. Instrumentations

GC analysis was carried out on CLARUS500, PE AutoSystem type GC equipped with FID detector. Powder X-ray diffraction studies were performed on a 'X Calibur, Eos, Gemini' X-ray diffractometer using Cu source, CrysAlisPro data reduction: Agilent Technologies Version 1.171.36.28 program(s) used to process the data and the 'POWDERX' program for indexing the powder XRD data. Flow cytometry studies were performed on Fluorescent Activated Cell Sorter (FACS) analyzer with high speed sorter model BD FACS Aria III.

2.2.2. Ligand precursors L^1 and L^2

To a solution of 2-hydroxybenzaldehyde (3 mmol, 366 mg) or 2-hydroxynaphthaldehyde (3 mmol, 517 mg) in 10 mL of toluene containing 2-3 drops of glacial acetic acid, added 4, 4'-diaminodiphenyl ether (1 mmol, 200 mg) with rigorous stirring. The reaction mixture was refluxed for 2 hrs using Dean-Stark apparatus. This reaction is outlined in Scheme 1. The reaction mixture was cooled at room temperature and solvent was evaporated under vacuum, washed with chilled absolute ethanol followed by diethyl ether to yield the products **L^1**and **L^2**. These compounds were dried under vacuum and samples were taken for analysis.

2.2.3. General procedure for synthesis of K_2xan^1 and K_2xan^2

To a solution of KOH (2.5 mmol, 141 mg) in 25 ml distilled water, added 4,4'-bis(*2*-hydroxyarylmethylideneamino)diphenyl ether precursors **L^1**(1 mmol, 408 mg) or **L^2** (1 mmol, 508 mg) with stirring. After 15 minutes, an excess amount of CS_2 (2 ml) was added and the reaction was allowed to continue at room temperature for 12 h. The solvent was evaporated under vacuum and solid was washed with diethyl ether to yield the product **K_2xan^1** or **K_2xan^2**. The compound was dried under vacuum, stored under a nitrogen atmosphere and samples were taken for analysis. This reaction is outlined in Scheme 2.

2.2.4. General procedure for synthesis of 1-4

To a solution of xanthate ligand **K_2xan^1**(0.5 mmol, 318 mg) or **K_2xan^2** (0.5 mmol, 369 mg) in 20 ml of distilled Et_3N, was added $Co(OAc)_2.4H_2O$ / $Cu(OAc)_2.H_2O$ (0.6 mmol, 149mg) / (0.6 mmol, 120 mg) with rigorous stirring (Scheme 2). The reaction was allowed to continue for 12h. The solid residue was filtered and washed with Et_3N followed by distilled water and hexane to yield the products **1-4**. These products were dried under vacuum, stored under a nitrogen atmosphere and samples were taken for analysis.

2.2.5. General procedure for synthesis of 5-8

Binuclear metallamacrocyclic xanthate complexes (0.5 mmol) **1** (618 mg), **2** (718 mg), **3** (622 mg) or **4** (722mg) were dissolved in dichloromethane and allowed to evaporate the solution at room temperature (Scheme 2). The brownish **5** and **6** (in case of **1** and **2**) and blackish brown **7** and **8** (in case of **3** and **4**) crystalline solids were isolated and washed with distilled water followed by diethyl ether for three times. Solids were dried under vacuum to yield corresponding binuclear metallamacrocyclic bis-*N,O*-Schiff base complexes **5-8**; products were stored under a nitrogen atmosphere and samples were taken for analysis.

Table 1. Micro-, mass- and IR analysis data for compounds **L^1-L^2, K_2xan^1-K_2xan^1** and **1-8**.

Entry	Molecular Formula (MW)	Yield (%)	Mp (°C)	Elemental Analysis (%) Found (calculated)				ES-MS (m/z)	IR data (KBr disk) υ_{max} /cm^{-1}
				C	H	N	S		
L^1	$C_{26}H_{20}N_2O_3$	99	213	76.40 (76.45)	4.95 (4.94)	6.89 (6.86)	…	413.1730 (M+2Li), (42%); 414.1868 (M+2 Li+H), (10%)	3426m br, 3052m, 2990m, 2742m, 1898w, 1618s, 1571s, 1494s, 1411s, 1363s, 1277s, 1187s, 1151s, 1107m, 1031w, 979m, 938w, 910w, 877m, 832s, 747s, 535m, 444w.
L^2	$C_{34}H_{24}N_2O_3$	93	164	80.38 (80.30)	4.72 (4.76)	5.45 (5.51)	…	510.52 (M+H); (30%)	3437s br, 3043s, 2362w, 1619s, 1542s, 1495s, 1325s, 1245s, 1164s, 969s, 830s, 744s, 536m, 492m, 433w.
(K_2xan^1)	$C_{28}H_{18}K_2N_2O_3S_4$	98	205-210 dec.	52.87 (52.80)	2.95 (2.85)	4.49 (4.40)	…	…	3053w, 2990w, 2740w, 2352w, 1897m, 1683m, 1620s, 1572s, 1490s, 1413s, 1362m, 1282s, 1263s, 1188s, 1148s, 1109m, 1031w, 996s, 982m, 911m, 878m, 834s, 780w, 749m, 714w, 670m, 654s, 534s, 521m, 464w, 444m.
(K_2xan^2)	$C_{36}H_{22}K_2N_2O_3S_4$	98	180-185 dec.	58.08 (58.10)	3.12 (3.01)	3.85 (3.80)	…	…	3044w, 2368w, 2344w, 1879w, 1624s, 1545m, 1493s, 1407m, 1328s, 1301m, 1247s, 1212m, 1165s, 1140s, 1084m, 1038w, 998s, 970m, 873w, 830s, 744s, 671m, 656s, 595w, 536m, 491s, 434w.
1	$C_{56}H_{36}Co_2N_4O_6S_8$	99	180-185	54.12 (54.45)	3.05 (2.94)	4.50 (4.54)	20.75 (20.77)	…	3053m, 2991w, 2921m, 2852w, 1897w, 1620s, 1574m, 1505m, 1492s, 1457m, 1411m, 1364m, 1300m, 1283s, 1264m, 1189s, 1152m, 1112m, 1104m, 1031w, 1012w, 983m, 936w, 911m, 879m, 833s, 780w, 749s, 740s, 716w, 652w, 544s, 521m, 464w, 444m.
2	$C_{72}H_{44}Co_2N_4O_6S_8$	96	200-205 dec.	60.25 (60.24)	3.21 (3.09)	3.85 (3.90)	17.70 (17.87)	1436.1 (M+H)	3058w, 2925w, 1684w, 1616s, 1615s, 1601s, 1571s, 1535s, 1492s, 1456s, 1424s, 1388s, 1360s, 1340m, 1303w, 1240s, 1212m, 1183m, 1163m, 1145m, 1110m, 1041w, 1012m, 980m, 895w, 852w, 829s, 745s, 648w, 618w, 559m, 493m, 452w.
3	$C_{56}H_{36}Cu_2N_4O_6S_8$	98	160-165 dec.	54.10 (54.04)	2.99 (2.92)	4.55 (4.50)	20.91 (20.61)	…	3052m, 2359w, 1896w, 1708w, 1614s, 1533s, 1493s, 1464s, 1445s, 1412m, 1381m, 1359m, 1327m, 1283m, 1240s, 1183s, 1149s, 1127m, 1104m, 1029w, 1010m, 982w, 924w, 911w, 877m, 833s, 755s, 740m, 714w, 622m, 522s, 464w, 443w.
4	$C_{72}H_{44}Cu_2N_4O_6S_8$	93	100-105 dec.	59.23 (59.86)	3.35 (3.07)	3.72 (3.88)	17.91 (17.76)	…	3036s, 1928m, 1617s, 1602s, 1574s, 1534s, 1493s, 1456m, 1432m, 1388m, 1366m, 1342w, 1308w, 1240s, 1211m, 1184s, 1163s, 1142m, 1103m, 1041w, 1011w, 982w, 967w, 895w, 872w, 852m, 826s, 778w, 745s, 648w, 551w, 525w, 494m, 454w,

									410w.
5	$C_{52}H_{36}Co_2N_4O_6$	81	170-175 dec.	67.20 (67.10)	3.95 (3.90)	5.96 (6.02)	…	…	3051w, 2925w, 1608s, 1584s, 1560s, 1528s, 1494s, 1462s, 1447s, 1436s, 1376m, 1328m, 1236s, 1181s, 1145s, 1028w, 1012m, 988w, 922w, 876m, 848m, 835m, 756s, 727m, 695w, 596w, 520s, 499m, 424m.
6	$C_{68}H_{44}Co_2N_4O_6$	93	200-205 dec.	72.18 (72.22)	4.05 (3.92)	4.91 (4.95)	…	1131.0 (M+H)	2924s, 2853m, 1732w, 1616s, 1601s, 1574m, 1535m, 1491s, 1455w, 1428w, 1389w, 1361m, 1340w, 1240m, 1212w, 1182s, 1162m, 1141w, 1094w, 1012w, 984w, 853w, 827s, 746m, 668w, 648w, 495w.
7	$C_{52}H_{36}Cu_2N_4O_6.CH_2Cl_2$	90	200-205 dec.	62.13 (62.11)	3.75 (3.74)	5.45 (5.47)	…	931 (M+H)	3033m, 2963m, 2918m, 2848m, 2356w, 1878m, 1708m, 1617s, 1602s, 1574s, 1535s, 1491s, 1455s, 1427s, 1388s, 1365s, 1307m, 1239s, 1211m, 1185s, 1163s, 1142m, 1097m, 1040w, 1011w, 982m, 895w, 853m, 829s, 746s, 647m, 598w, 548m, 525w, 494s, 454m, 411w.
8	$C_{68}H_{44}Cu_2N_4O_6$	95	150-155 dec.	71.60 (71.63)	3.95 (3.89)	4.89 (4.91)	…		3057m, 1936w, 1616s, 1603s, 1573s, 1535s, 1492s, 1456s, 1434m, 1426m, 1386s, 1368s, 1309w, 1238s, 1210m, 1184s, 1163m, 1143w, 1101w, 1041w, 1011w, 982w, 895w, 855m, 827s, 777w, 740m, 718w, 648m, 598w, 551m, 525w, 501m, 455w, 416w.

Table 2. NMR spectral data for compounds **L^1-L^2** and **$K_2(xan)^1$-$K_2(xan)^1$**.

Entry	**NMR Data (ppm)**	
	^{1}H NMR	**^{13}C NMR**
L^1 (CDCl3)	6.970(td, 2*H-Ph*), 7.05(dd, 2*H-Ph*), 7.115(dt, 4*H-Ph*), 7.34(dt, 4*H-Ph*), 7.41(m, 4*H-Ph*), 8.659(s, 2*H*-N=C*H*), 13.277(s, 2*H-OH*).	117.29, 119.16, 119.70, 122.60, 132.25, 133.29, 156.17 (*all corresponds toPh*), 161.19, 161.83(–N=*C*H).
L^2 (CDCl3)	7.159(m, 6*H-Ph*), 7.38(m, 6*H-Ph*), 7.55(td, 2*H-Ph*), 7.754(d, 2*H-Ph*), 7.84(d, 2*H-Ph*), 8.15(d, 2*H-Ph*), 9.39(s, 2*H*-N=C*H*), 15.529(s, 2*H-OH*).	108.97, 118.94, 119.93, 121.72, 121.97, 123.57, 127.43, 128.07, 129.42, 133.10, 136.31, 141.59, 155.05, 155.82 (*all corresponds toPh*), 168.69; (–N=*C*H).
(K_2xan^1) (DMSO-d6)	6.880(m, 4*H-Ph*), 7.110(d, 4*H-Ph*), 7.354(m, 2*H-Ph*), 7.44(d, 4*H-Ph*), 7.645(dd, 2*H-Ph*), 8.97(s, 2*H*-N=C*H*).	115.24, 115.34, 117.57, 119.38, 119.93, 121.42, 123.19, 123.50, 124.36, 127.61, 133.38, 135.63, 144.54, 146.12, 148.93, 158.45 (*all corresponds toPh*), 162.02 (–N=*C*H), 190.86(–CS_2).
(K_2xan^2) (DMSO-d6)	7.05(dd, 2*H-Ph*), 7.18(dd, 4*H-Ph*), 7.36(t, 2*H-Ph*), 7.545(m, 2*H-Ph*), 7.71(dd, 4*H-Ph*), 7.8(d, 2*H-Ph*), 7.93(d, 2*H-Ph*), 8.525(d, 2*H-Ph*), 9.688(s, 2*H*-N=C*H*).	109.14, 118.85, 118.91, 120.10, 120.92, 122.21, 122.72, 122.93, 123.90, 123.95, 127.19, 128.49, 129.44, 133.51, 136.88, 140.63, 155.69, 156.29 (*all corresponds toPh*), 169.62 (–N=*C*H), 190.24 (–CS_2).

2.2.6. Fluorescence study in the presence of metal ions

The stock solutions of metallamacrocyclic complexes **1** and **5** were prepared in DMSO (5×10^{-4} M) and their ability to sense various metal ions was investigated by means of fluorescence spectroscopy at their respective λ_{ex} nm. The fluorescence response of metallamacrocycle in the presence of guest metal ions such as: **G1: Ag^{+}** ($AgSO_4$), **G2: Pb^{2+}**($Pb(OAc)_2$), **G3: Sn^{2+}**($SnCl_2$), **G4: Hg^{2+}**($HgCl_2$), **G5: Cu^{2+}**($Cu(OAc)_2$) was obtained in a typical experiment, described as: 0.1 ml of metal on solution prepared in DMSO (0.015 M) was added to the 2.9 ml of metallamacrocycle solution, mixed properly before emission spectroscopic data was recorded and plotted to evaluate the effect of various metal ions on the emission property of **1** and **5.**

2.2.7. X-ray structure determinations

Single crystals suitable for X-ray crystallographic study were obtained by slow evaporation at 4 °C of dichloromethane solution of **5-7** and a chloroform solution of **8.** The crystals of **7** were also grown by the slow diffusion of hexane in a DMSO solution in order to explore the effect of solvent on crystallization and thus its impact on supramolecular packing in the solid state. Intensity data for **5.*2H₂O*** [$C_{52}H_{36}Co_2N_4O_8$], **6.*2H₂O*** [$C_{68}H_{44}Co_2N_4O_7$], **7.*DMSO*** [$C_{54}H_{40}Cu_2N_4O_7S$], **7.*CH₂Cl₂*** [$C_{54}H_{40}Cl_4Cu_2N_4O_6$] and **8.*CHCl₃.8H₂O*** [$C_{137}H_{105}Cl_3Cu_4N_8O_{22}$] was collected on Oxford X Calibur and Gemini diffractometer respectively equipped with Eos CCD detector at 298 K. Monochromatic Cu-Kα (λ = 1.54184) (in case of **5**) and Mo-*Kα* X-ray (λ=0.71073 Å) (in case of **6-8**) radiations were used for the measurements. Data were collected and reduced by using the ‘‘CrysAlispro’’ program (Version 1.171.37.33 Agilent Technologies, 2014).[24]An empirical absorption correction using spherical harmonics was implemented in ‘‘SCALE3 ABSPACK’’ scaling algorithm. (For 6) The crystal structure was solved by the direct method, and the refinement was carried out by full-matrix least squares against F^2 using SHELXL-97 program package[25] and Olex2 (version 1.2.5) program package. [26]All non-hydrogen atoms were refined anisotropically.

2.2.8. *In vitro* cytotoxic study

2.2.8.1. MTT assay for cell viability/ proliferation

The cell growth inhibition was determined by MTT assay with some modifications.[27]Schiff base precursors (**L^1**, **L^2**), xanthate ligands (**K_2xan^1**, **K_2xan^2**)**,** binuclear xanthate complexes (**1-4**) and binuclear Schiff base complexes (**5-8**) were dissolved in DMSO and then diluted with water. The content of DMSO in each sample was 1%. Cells were seeded in 96-well plates at a density of 1×10^3 cells per well and incubated for 24 h.

These cells were treated with different concentrations of compounds reported in this paper for 6 h (against HEP 3B) and 14 h (against IMR 32). Cisplatin was also screened against both the cell lines under the similar experimental conditions. After removal of the media, culture was incubated with 20 µL of media containing 5 mg/ml stock solution of MTT in PBS and 60 µL of DMEM for 6 h at 37 °C in 5% CO_2 incubator. Formazan crystal formed by metabolically viable cells was dissolved in DMSO and the optical density was measured at 570 nm by ELISA reader (METERTECH-∑960). The number of viable cells was proportional to the extent of formazan production.

2.2.8.2. Annexin V/PI Double Staining for Cell Death Analysis

The cell death assessment was performed using annexin V alexa Fluro 4888 and propidium iodide apoptosis kit, procured from Himedia. For apoptosis measurement, HEP 3B and IMR 32 cells (5×10^6 cells/mL) were treated with selective compounds ($^1/_3$ of the IC_{50} concentration) for 16 hours. After washing in PBS, 1×10^6 cells were resuspended in 100µl of annexin binding buffer. FITC-Annexin V and propidium iodide were added and then incubated for 15 minutes at room temperature in the dark. After the incubation period, 400 µL of annexin-binding buffer was added then kept in an ice bath for 5 minutes. Cells were centrifuged and fixed in 1% formalin. Cells were resuspended in 1% FBS and 0.5% in BSA after centrifugation and then these were analyzed by flow cytometry (BD FACSAria III).

2.3. Results and discussion

2.3.1. Synthesis and characterization

Ligand precursors 4,4'-bis(*2*-hydroxybenzylideneamino) ether (**L^1**) and4,4'-bis(*2*-hydroxynaphthylmethylideneamino)diphenyl ether (**L^2**),bearing phenolic –OH, adjacent to Schiff base moiety, have been **s**ynthesized by using a literature procedure[23] that involve condensation of primary amines with aldehydes in toluene containing a catalytic amount of glacial acetic acid (Scheme 1). The potassium salts of polydentate xanthate ligands (**K_2xan^1** or **K_2xan^2**) were synthesized by the reaction of these phenolates **L^1** or **L^2** with CS_2 in the aqueous KOH solution, shown in Scheme 2. Although, numerous reports support the easy accessibility of xanthate ligands derived from alcohols and wide use in synthetic organic chemistry,[29] the use of xanthates derived from phenolates[28] in the design and development of macrocyclic coordination compounds have scarcely been investigated.[30] In fact only one paper[28] deals with the use of phenolate based xanthate in the synthesis of coordination compound till date. The lack of stability of transition metal xanthate complexes,[31] primarily

limit their use in coordination chemistry. However, we could use phenolate based xanthate **K_2xan^1** and **K_2xan^2** ligands successfully to derive binuclear metallamacrocyclic Co^{II}/ Cu^{II} xanthate complexes **1-4** (Scheme 3) from a metathetical reaction of **K_2xan^1** or **K_2xan^2** with corresponding metal acetates in Et_3N.

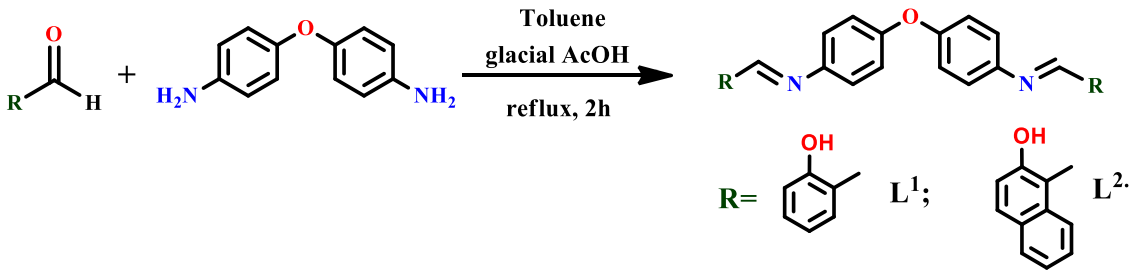

Scheme 1. General scheme for the synthesis of diimines **L^1** and **L^2**.

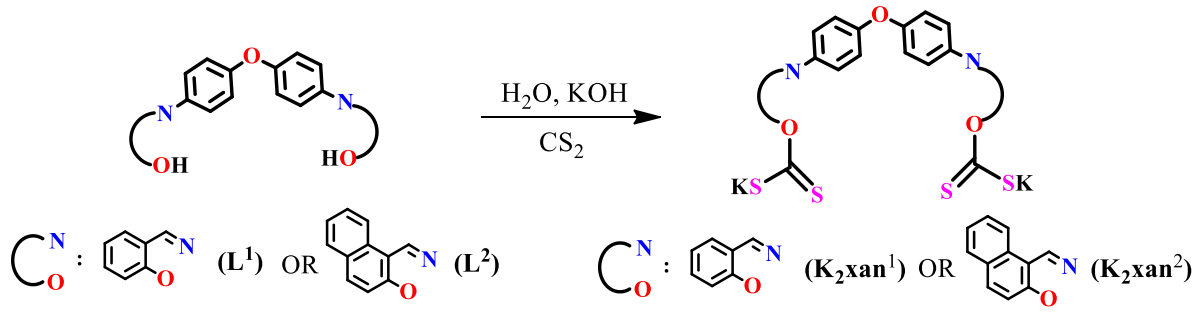

Scheme 2. General scheme for the synthesis of **K_2xan^1** and **K_2xan^2**.

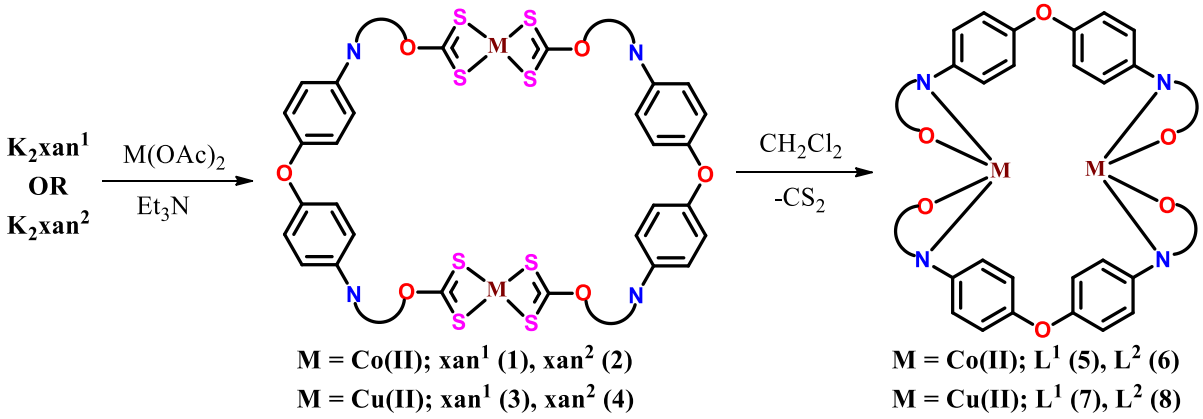

Scheme 3. General synthetic methodology for binuclear Co^{II}/Cu^{II} xanthate metallamacrocycles and their respective binuclear *N,O*-bidentate Schiff-base analogues.

These complexes **1-4** are stable in the solid state over a period of days but are found to be quite unstable, especially in chlorinated solvents. The instability associated with the binuclear metallamacrocyclic Co^{II}/ Cu^{II} xanthate complexes **1-4** helped us to use them further in selective transformation reactions leading to the formation of corresponding (2:2) binuclear metallamacrocyclic *N,O*-Schiff base complexes **5-8**.To the best of our knowledge, this is the first report on binuclear xanthate metallamacrocyclic complexes derived from

phenolates and their selective transformations into (2:2) binuclear *N,O*-Schiff base metallamacrocycles.

Literature suggests that a direct approach to obtain (2:2) binuclear metallamacrocyclic Schiff base complexes suffer the disadvantage of mixture of products with the ratio 1:1, 2:2, 3:3, 4:4 and the $(1:1)_\infty$ polymeric species which are insoluble in most organic solvents.[32] Further reports suggest that the conformational modes of ligand, nuclearity and ultimately the structures of resulting complexes are greatly depend upon the selection of metal ion. For instance, J. Zhang *et. al.* have isolated a dinuclear mesocate structure for Cu^{II} and a pseudo *C*3-symmetrical, torus-like molecular structure for Co^{II} ions with the same ligand system.[33] Hence, in the development of efficient synthetic methodology for the formation of binuclear metallamacrocyclic complexes, lack of selectivity is one of the main barriers. Thus, the present synthetic methodology to obtain (2:2) binuclear metallamacrocyclic Co^{II}/Cu^{II}*N.O*-Schiff base complexes selectively from their respective binuclear metallamacrocylic Co^{II}/Cu^{II} xanthate complexes would be of great interest to the researchers. The presence of Schiff base (-N=C) moiety in close vicinity to the chelated xanthate ($-OCS_2$) moiety in **1-4** causes instability in the solution and enforcing these molecules to undergo a facile transformation into their corresponding binuclear metallamacrocyclic *N, O*-Schiff base complexes selectively in 2:2 stoichiometry *via* evolution of CS_2 fragment, qualitatively detected by GC analysis. The evolution of CS_2 from 1,1-dithiolato complexes in chlorinated solvents have been previously observed.[34] Further, the poor electron flow from the xanthate moieties to the cobalt centres is reflected from DFT study. For instance the charges on the cobalt nucleus (0.052 e) in binuclear xanthate complex **1** are less than the similar charges in its Schiff base analogue **5** (~0.750 e). Thus, lower electron flow at cobalt centres in **1** could be prevented cobalt(II) centres from their ready oxidation, unlike earlier reports.[35]

All the newly synthesized compounds were characterized by elemental, mass, thermogravimetric analysis and relevant spectroscopic techniques. Elemental analysis and spectroscopic data mutually suggest the formation of the desired structures. The microanalysis and spectroscopic data were sufficient to unequivocally assign the structure of potassium salts of xanthate lignads $\mathbf{K_2xan^1}$ and $\mathbf{K_2xan^2}$. The IR spectra of these ligands display characteristic IR bands due to ν(C=N), ν(C-O) and $\nu(CS_2)$ in the region of 1619-1624, 1084-1147 and 982-1038 cm^{-1} respectively. In the ^{1}H NMR spectrum, disappearance of phenolic -OH signals and significant downfield shift of imine (-N=C*H*) signals to the 8.97 and 9.688 ppm are indicative of the formation of $\mathbf{K_2xan^1}$ and $\mathbf{K_2xan^2}$, respectively. In the ^{13}C

NMR spectra, most characteristic signals appeared at 190.86 and 190.24 ppm due to the xanthate (–OCS_2) moiety, apart from the signals appeared in 161.83-168.69 ppm and 108-162 ppm regions due to the imine (-N=CH) and aromatic groups respectively. The IR spectra of binuclear xanthate complexes **1-4** exhibit most characteristic bands in the region 1041-967 cm^{-1}, diagnostic of *S,S* coordination of the xanthate ligands.[36] The appearance of shoulder or split bands in the region of 1041-967 cm^{-1}, is indicative of anisobidentate coordination mode of the xanthate moiety in **1-4**.The absence of –OCS_2 bands and subsequent split of ν(C=N) stretching bands with significant shifting (compared to ν(C=N) bands in L^1 or L^2) in the IR spectra of **5-8** is suggestive of removal of CS_2 moiety and formation ofcorresponding binuclear metallamacrocyclic *N,O*-Schiff base complexes. The structural variations in **K_2xan^1**, its binuclear xanthate complex **1** and corresponding binuclear *N,O*-Schiff base complex **5** can easily be seen in theiroverlapping IR spectra.

The binuclear metallamacrocyclic xanthate complex **2** and binuclear metallamacrocyclic *N,O*-Schiff base complexes **6-7** clearly displayed (M+H) molecular ion peaks along with the other fragmentation peaks. The poor stability of the freshly synthesized xanthate ligands and their metal complexes in solvents, especially chlorinated solvents and low solubility of these compounds in other common organic solvents except DMF/DMSO limited the crystallization attempts. Hence, the powder X-ray diffraction study was performed on representative compounds (**K_2xan^1**, **1, 3, 5** and **7**) to understand structural features such as crystal lattice, lattice parameters. The powder XRD data for these samples have been indexed and refined by least square refinement with the help of commonly used[37]program 'POWDERX'.[38]Notably, the results of the powder XRD analysis for xanthate ligand **K_2xan^1** and its Co^{II}/Cu^{II} complexes **1**/**3** as well as their corresponding Schiff base complexes **5**/**7** do not match due their different their packing patterns in the solid state. The indexing of powder XRD data for **5** and **7** gave the lattice system similar to that obtain from single crystal data with the differences in cell parameters probably arise due to the involvement of solvent of crystallization. The deviation between the experimental and simulated powder XRD patterns of **5** and **7**, suggest that the bulk properties of these materials are different from the single crystals. The differences in the cell parameters probably rise due to the involvement of solvent molecules stabilizing the crystal structure.

The UV–visible absorption (10^{-4} M DMSO solution) and emission (10^{-3} M DMSO solution) properties of ligand precursors (**L^1**, **L^2**), the potassium salt of xanthate ligands

(**K2xan1**, **K2xan2**), binuclear metallamacrocyclic complexes (**1–8**)were investigated at room temperature (Figure 1-2, Table 3).

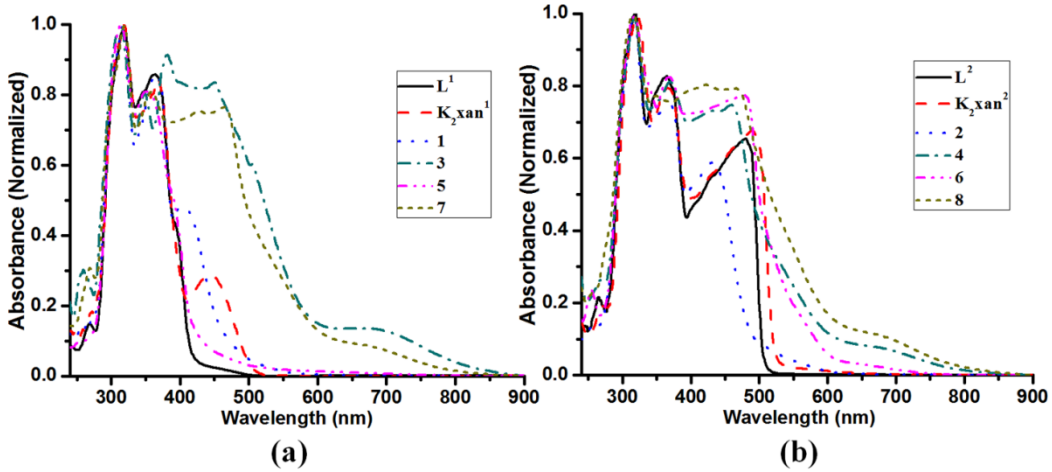

Figure 1. UV-visible absorption spectra of Schiff base precursors, xanthate salts, binuclear xanthate complexes and binuclear Schiff base complexes at room temperature in 10^{-4} MDMSO solution: (a) **L1**, **K2xan1**, **1**, **3**, **5** and **7**;(a) **L2**, **K2xan2**, **2**, **4**, **6** and **8**.

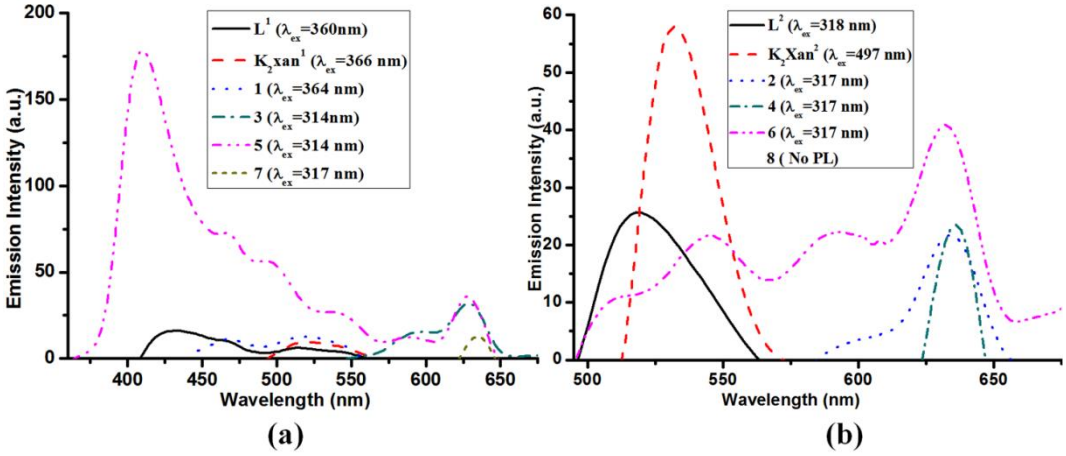

Figure 2. Fluorescence spectra of Schiff base precursors, xanthate salts, binuclear xanthate complexes and binuclear Schiff base complexes at room temperature in 10^{-3} MDMSO solution: (a) **L1**, **K2xan1**, **1**, **3**, **5** and **7**;(a) **L2**, **K2xan2**, **2**, **4**, **6** and **8**.

Table 3. Principal IR, UV-visible and fluorescence bands for **L^1, L^2**, **K_2xan^1**, **K_2xan^2**and Complexes **1-8**.

Entry	UV-Visible data (10^{-4} M DMSO) λ_{max} nm (ε, L mol^{-1} cm^{-1})	Fluorescence data (10^{-3} M DMSO) λ_{em} nm (Intensity)	λ_{ex} (nm)
L^1	320 (15633) π→π*, 364 (13555) n→π*, 395 CT	432 (16.0497), 513 (6.1781)	360
L^2	319 (26530) π→π*, 365 (21589) n→π*, 480 (17534) CT	519 (25.7266)	318
K_2xan^1	319 (26530) π→π*, 367 (21589) n→π*, 444 (7920) CT	520 (9.5477)	366
K_2xan^2	321 (28560) π→π*, 366 (24090) n→π*, 490 (19778) CT	532 (57.9323)	497
1	318 (32593) π→π*, 366 (27634) n→π*, 405 (15852) CT, 531 d-d	469 (11.1489), 519(12.6580)	364
2	316 (53760) π→π*, 367 (39718) n→π*, 433 (34477) CT, 556 d-d	634 (21.6423)	317
3	314 (4903) π→π*, 348 (4032) n→π*, 380 (4534) n→π*, 452 (4156) CT, 683 d-d	628(32.09)	314
4	317 (6527) π→π*, 366 (5346) n→π*, 461(4959) CT, 674 d-d	634 (14.013)	317
5	314 (35817) π→π*, 349 (29221) n→π*, 390 CT, 538 d-d	410 (178.54)	314
6	317 (36314) π→π*, 365 (30300) n→π*, 458 (28921) CT, 565 d-d	545 (21.5474) 634 (40.7225)	317
7	318 (5726) π→π*, 354 (4696) n→π*, 464(4419) CT, 677 d-d	634(12.84)	317
8	317 (5411) π→π*, 352 (4520) n→π*, 423(4379) , 469 (4342) CT, 685 d-d	No fluorescence	317, 352

The differential electronic spectra of **1-8** clearly suggest alterations in the structural features of the molecular framework. The shorter absorption band ~315 nm is assigned to π→π* (phenyl) transitions and the longer absorption band ~360 nm is assigned to n→π* (imine) transitions whereas the absorption bands appeared in 390-490 nm regions are attributable to the intraligand charge transfer transitions in respective compounds.

Expectedly, the imine n→π* transition bands of the ligand precursors **L^1**, **L^2**remain unaffected in corresponding xanthate ligands **K_2xan^1**, **K_2xan^2** and binuclear xanthate complexes **1-4**. However, a distinguishable blue shift of this transition band by 10-15 nm in the binuclear *N,O*-Schiff base complexes **5-8** is observed which clearly underlines the participation of imine moiety in complex formation. The fluorescencespectra of **L^1**and **K_2xan^1**display weak emission bands at 432, 513 and 520 nm upon excitation at λ_{ex} 360 and 318 nm, respectively however **L^2**and **K_2xan^2** display strong emission bands at 519 and 532 nm upon excitation at λ_{ex} 318 and 497 nm respectively with a significant Stokes shift. Among all complexes, **5** is highly fluorescent, displaying a high intensity emission band at 410 nm upon excitation at λ_{ex} 314 with a concomitant Stokes shift of ≈ 138 nm. Expectedly, all the

Cu^{II} complexes display no significant fluorescence properties, as Cu^{II} is a well known fluorescence quencher.[39]The appearance of a number of bands upon excitation of a single wavelength as well as high fluorescence behaviour of the complexes may be attributed to the reduction of photoinduced electron transferprocess on complex formation.[40]

2.3.2. Metal ion sensing

Metallamacrocyclic structures capable of sensing metal ions are of great interest from the view point of biological and environmental perspectives, as they can easily undergo chelation in organic as well as aqueous media.[41] However, the syntheses of sensors capable of efficient sensing and detection of multiple metal ions is challenging.[41] Complexes based on silver find applications in medicine and agriculture; however, its prolonged use leads to irreversible darkening of the skin and mucous membrane.[42] It is well known that metal ions like Pb^{2+}, Sn^{2+}, and Hg^{2+} exhibit number of adverse effects on health and environment. Further, reports underline the presence of an excess copper at tumor site[43] and copper is an important metal pollutant,[44] hence highly sensitive fluorescent sensors for metal ion especially Cu^{2+} ions could be of prime concern. Although most of the metal ions act as fluorescence quenchers,[41] the emission performance of their complexes strongly depends on the nature of ligand and the structure of resulting compounds.

Thus, binuclear xanthate complex **1** and its *N,O*-Schiff base analogue **5** has been selected to explore their potential applicability as a metal ion sensor by means of fluorescence spectrophotometry. (Figure 3-4) Complex **1** fluoresces at two major wavelengths 475 and 525 nm, due to two metal centres having different stereo chemical environment. The addition of Ag^{+} ions to the solution of **1** induces about two fold enhancements in the fluorescence intensity with no change in the emission wavelengths, indicative of favourable interactions of this with the inner environment of **1** without transmetallation reactions. This trend is consistent with Pb^{2+} ions, however, there is comparatively less increase in the fluorescence intensity. Addition of Sn^{2+} ions causes significant blue shifting in the first peak position with almost three foldincreases in the emission intensity. This may be due to transmetallation reaction occurring at one of the cobalt centres of host with guest ions. This is indeed unfavourable as the energy of interaction increases resulting in blue shifting of first emission peak. Meanwhile the second cobalt centre of the molecule remain as spectator as its peak position remains unaffected, but its electronic environment is definitely affected by the transmetalation of the first centre resulting in decrease in intensity. In case of Hg^{2+} ion, interesting phenomena of interaction with **1** is observed. It appears that emission peaks of

both the metallic centres are red shifted and split into doublet. The red shifting may be attributed to strong and favourable interactions resultingin a decrease in the energy of the system. The splitting of the peaks into doublet indicates the multiple emission phenomena occurring due to the difference in the energy levels. Interestingly, addition of Cu^{2+} ions to **1** doubles the intensity of lower wavelength emission peak without a significant change in its position, indicating parallel emissions from 3d to 3d orbitals of the metal ions. Unlike **1**, no significant change in the emission wavelength of binuclear metallamacrocyclic *N*,*O*-Schiff base complex **5** upon addition of different cations (G1-G4) ruled out the possibility of transmetallation reactions at both of cobalt centres of **5**. However, these interactions significantly changed the fluorescence intensity. In contrast to **1**, Cu^{2+} ions are able to '*turn off*' of fluorescence property of receptor **5** completely. Probably, the presence of xanthate moieties enabled complex **1** to interact with Cu^{2+} ions through S...Cu stacking interaction,[45] resulting into extended conjugation and enhanced emission intensity. In summary Ag^{+} and Pb^{2+} ions have successfully enhanced the fluorescence property of receptor **1** suggesting their 'turn on' ability without transmetallation whereas and Cu^{2+} ions have quenched the fluorescence property of receptor *5* suggesting its '*turn off*' ability. Further, both of the macrocycles **1** and **5** can be used as a sensor for various guests G1-G5.[46]

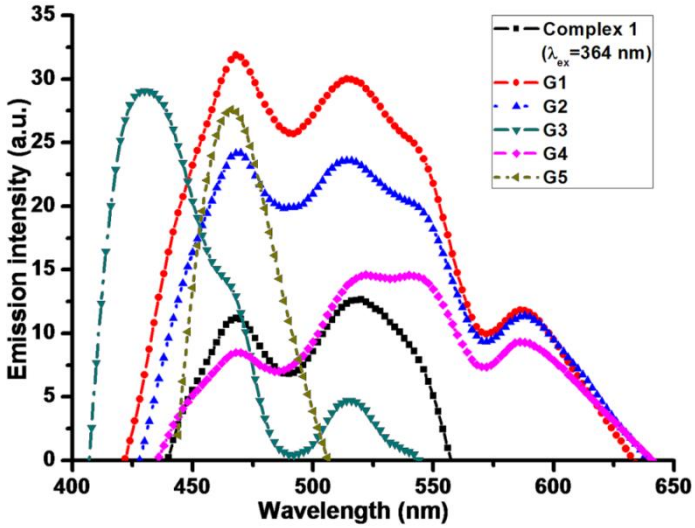

Figure 3. Emission responses of **1** to G1-G5 (G1= Ag^{+}; G2= Pb^{2+}; G3= Sn^{2+}; G4= Hg^{2+}; G5= Cu^{2+}).

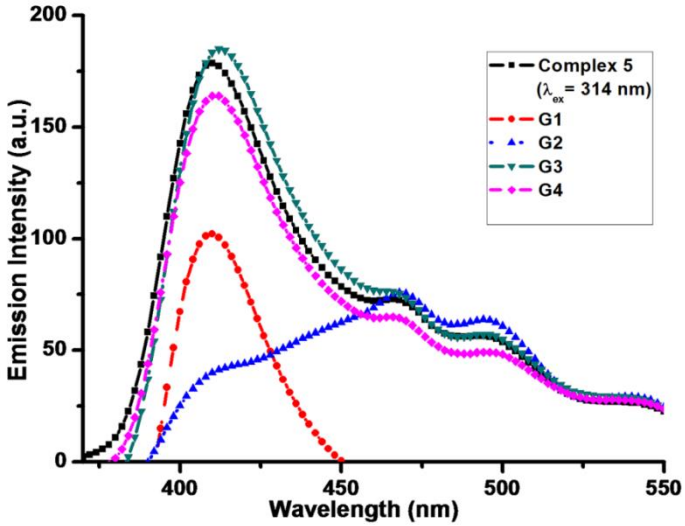

Figure 4. Emission responses of **5** to G1-G5 (G1= Ag^{+}; G2= Pb^{2+}; G3= Sn^{2+}; G4= Hg^{2+}; G5= Cu^{2+}).

2.3.3. Thermogravimetric Analysis

The thermogravimetric analysis of bimetallic xanthate/ *N*,*O*-Schiff base macrocyclic complexes **1-8,** were performed under N_2 atmosphere at a heating rate of 10 °C /min from room temperature to 550 °C. (Table 4)A single or multi stage mass loss for these compounds was observed with DTG and corresponding DTA curves which are ascribed to endothermic and/or exothermic elimination of molecular fragments due to the thermal degradation. The bimetallic xanthate macrocyclic complexes **1-4**, exhibit an insignificant mass loss of ~ 1% in the initial stage, which could be assigned to the loss of solvent impurities. Further mass loss of 12.44, 8.07, 4.2 and 3.52 % observed in the second stage of degradation is attributed to the loss of CS_2/ SCO ligand fragments. The maximum rate of decomposition seen in DTG curves for **1-4** is 360.2, 442.3, 327.8 and 337.6 °C respectively. Contrarily, among bimetallic *N*, *O*-Schiff base complex **5-8**, complex **5** display an endothermic peak at 147.2 °C on the DTA curve without mass loss suggesting phase changes occurring due to its melting. Further, it exhibits a single stage degradation started at 200 °C and continues at 550 °C with a maximum rate of decomposition observed at 269.8 °C on DTG curve. Other complexes **6-8** showed two stages of degradation involving the loss of naphthyl/ CH_2Cl_2 fragments in the first stage followed by a continuous mass loss with a maximum rate of degradation at 467.5, 373.9 and 358.3 °C observed on corresponding DTG curves. It may be noted that the thermogravimetric study of complex **7** has been performed with the crystals obtained from CH_2Cl_2/hexane solvent mixture. The association of two CH_2Cl_2 molecules with the crystals is indeed confirmed by its thermogram, disclosing a mass loss of 14.8% at 212 °C

corresponding to two CH_2Cl_2 molecules (calc. 16.5%). This is consistent with the results of single crystal X-ray analysis of **7**.

Table 4. Thermogravimetric analysis of binuclear xanthate/ *N,O*-Schiff base macrocyclic complexes **1-8.**

Entry	DTA (°C) (μV)	DTG (°C) (μg/min)	Significant Mass loss % (temp range °C)	Inference
1	188.5 (8.21) 360.2 (20.3)	188.1 (45.2)	1.22 % (upto 100) 12.44 % (100-250) 22.71 % (250-550) 36.37 % (50-550)	1st stage: Insignificant mass loss of solvent impurities. 2nd stage: Loss of $2CS_2$ molecules (calc. 12.3 %). 3rd stage: Decomposition continues after 550 °C. - Maximum rate of decomposition observed at 188.1 °C on DTG curve.
2	…	442.3 (62.2)	1.49 % (upto 100) 8.07 % (100-350) 23.43 % (350-550) 32.99 % (100-550)	1st stage: Insignificant mass loss of solvent impurities. 2nd stage: Loss of 2SCO fragment (calc. 8.35 %). 3rd stage: Decomposition continues after 550 °C. - Maximum rate of decomposition observed at 442.3 °C on DTG curve.
3	205.2 (2.57) 298.7 (2.42)	327.8 (145.4)	0.5 % (upto 100) 4.2 % (100-250) 25.4 % (250-550) 30.1 % (50-550)	1st stage: Insignificant mass loss of solvent impurities. 2nd stage: Loss of SCO fragment (calc. 4.8 %). 3rd stage: Decomposition continues after 550 °C. - Maximum rate of decomposition observed at 327.8 °C on DTG curve.
4	264.2 (3.32) 303.5 (4.46) 329.8 (2.84) 362.8 (-1.66)	337.6 (154.0) 353.4 (132.4)	3.52 % (50-100) 35.68 % (100-550) 39.20 %(50-550)	1st stage: Loss of SCO (calc. 4.1 %). 2nd stage: Decomposition continues after 550 °C. - Maximum rate of decomposition observed at 337.6 °C on DTG curve.
5	**147.2 (25.8)**	269.8 (104.7)	47.8 % (200-550)	1st stage: Decomposition continues after 550 °C. - *An endothermic peak at 147.2 °C appeared on DTA curve without mass loss suggesting phase changes occurring due to its melting.* - Maximum rate of decomposition observed at 269.8 °C on DTG curve.
6	…	77.3 (31.8) 459.2 (153.9) 467.5 (158.5)	10.6 % (upto 300) 39.8 % (300-550) 50.4 % (50-550)	1st stage: Loss of naphthyl (calc. 11.23 %). 2nd stage: Decomposition continues after 550 °C. - Maximum rate of decomposition observed at 467.5 °C on DTG curve.
7	212.1 (7.75) 349.1 (6.50)	212.1 (131.6) 373.9 (150.2)	14.8 % (150-250) 35.2 % (250-550) 50.0 % (50-550)	1st stage: Loss of two CH_2Cl_2 (calc. 14.8 %). 2nd stage: Decomposition continues after 550 °C. - Maximum rate of decomposition observed at 373.9 °C on DTG curve.
8	364.6 (39.59)	358.3 (93.1)	12.2 % (50-250) 48.5 % (250-550) 60.7% (100-550)	1st stage: Loss of naphthyl (calc. 16.5%). 2nd stage: Decomposition continues after 550 °C. - Maximum rate of decomposition observed at 358.3 °C on DTG curve.

2.3.4. Crystallographic Study

Molecular structures of **5-8** have been determined crystallographically. The complexes crystallize in orthorhombic Pbca (**5.***2H₂O*), monoclinic $P2_1/c$(**6.***2H₂O*), orthorhombic Pbca(**7.***DMSO*), monoclinic C2/c(**7.***CH₂Cl₂*) and monoclinic $P2_1/c$(**8**.*CHCl₃.8H₂O*) centrosymmetric space groups. The X-ray crystal structure shows one complete molecule in their asymmetric units, except **7**.*CH₂Cl₂* and**8**.*CHCl₃.8H₂O* which contains half and two complete molecules in their asymmetric units, respectively. It may be noted that the poor quality crystal of **8** has limited us to refine the structure and to fix the disordered solvent molecules precisely.The *ORTEP* view at 40 % probability for complexes

is shown in Figure 5a-e. Details about data collection, refinement, and structure solution are recorded in Table 4, and selected geometrical parameters are collected in Table 5.

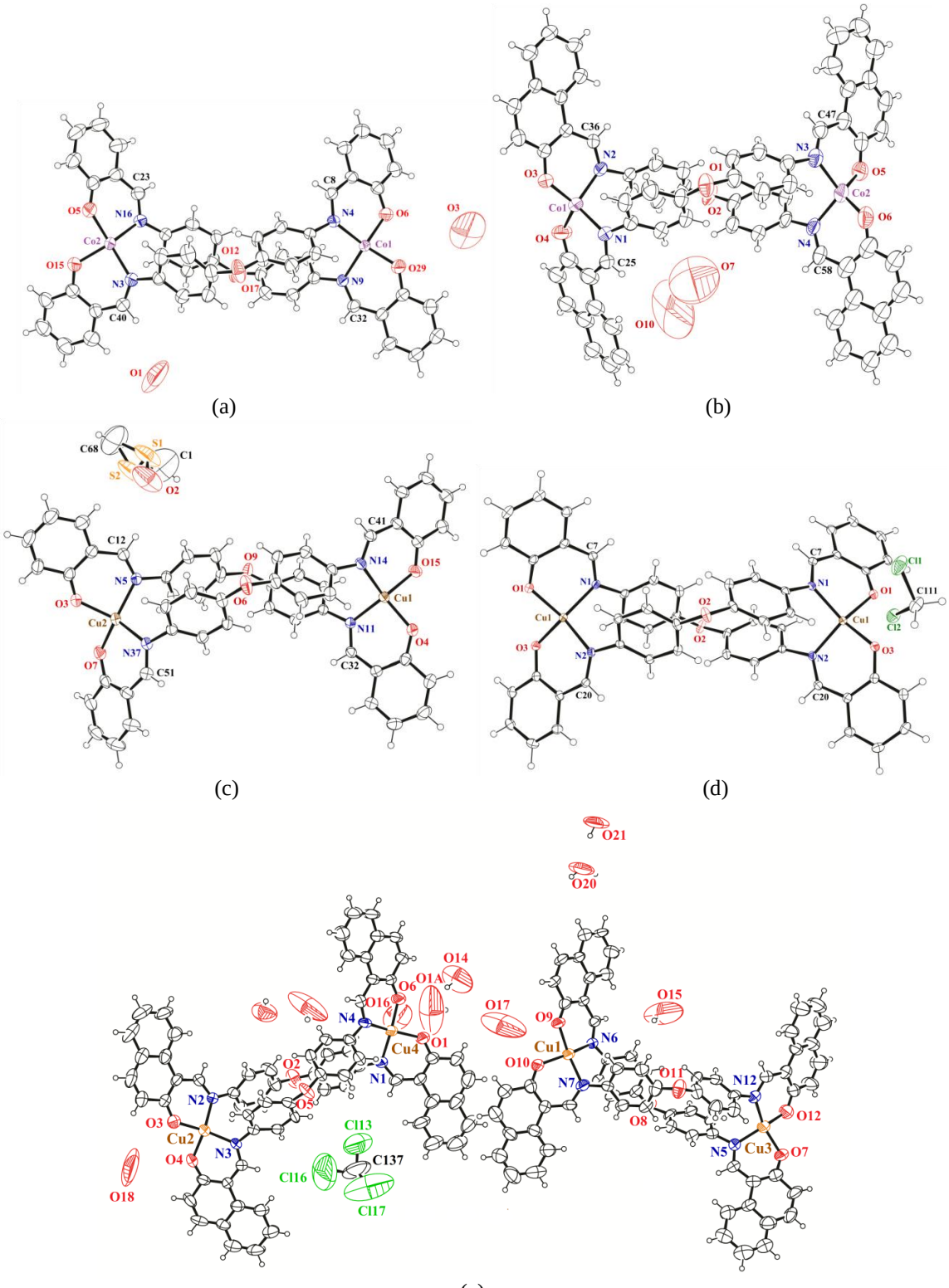

Figure 5. *ORTEP* diagram with atoms labelled showing 40% probability ellipsoids for(a) **5**.$2H_2O$, (b) **6**.$2H_2O$, (c) **7**.*DMSO*, (d) **7**.CH_2Cl_2 and (e) **8**.$CHCl_3.8H_2O$.

Table 4. Crystal data and structure refinement for compounds **5-8**.

Compound	**5.*2H₂O***	**6.*2H₂O***	**7.*DMSO***	**7.*CH₂Cl₂***	**8.*CHCl₃.8H₂O***
Formula	$C_{52}H_{36}Co_2N_4O_8$	$C_{68}H_{44}Co_2N_4O_7$	$C_{54}H_{40}Cu_2N_4O_7S$	$C_{54}H_{40}Cl_4Cu_2N_4O_6$	$C_{137}H_{105}Cl_3Cu_4N_8O_{22}$
Formula weight(amu)	962.71	1146.94	1016.07	1109.80	2575.80
T(K)	293(2)	298.15	295.0	150(2)	298.0
Crystal System	orthorhombic	monoclinic	orthorhombic	monoclinic	monoclinic
Space group	Pbca	$P2_1/c$	Pbca	C2/c	$P2_1/c$
a(Å)	26.3438(6)	11.840(3)	26.2828(4)	16.5132(3)	19.0398(9)
b(Å)	12.3067(3)	12.679(3)	12.25878(17)	14.6766(2)	21.6349(7)
c(Å)	28.9628(7)	37.680(8)	28.8218(4)	19.2170(3)	31.0856(15)
α(°)	90.00	90.00	90.00	90.00	90.00
β(°)	90.00	95.358(4)	90.00	96.1890(10)	100.470(5)
γ(°)	90.00	90.00	90.00	90.00	90.00
Cell volume ($Å^3$)	9389.9(4)	5632(2)	9286.2(2)	4630.24(13)	12591.7(10)
Z	8	4	8	4	4
Completeness to theta (%)	(θ = 72.16) 100	(θ = 26.08) 99.7	(θ = 27.36) 96.27	(θ = 25.00) 99.8	(θ = 26.08) 99.7
$\rho_{calc}g/cm^3$	1.362	1.353	1.4535	1.592	1.359
μ/mm^{-1}	6.017	0.649	1.020	1.209	0.803
F(000)	3952.0	2360.0	4176.0	2264.0	5304.0
Radiation	CuKα (λ = 1.54184)	MoKα (λ = 0.71073)	Mo Kα (λ = 0.71073)	MoKα (λ = 0.71073)	MoKα (λ = 0.71073)
2θ range for data collection/°	9.84 to 144.32	3.4 to 52.16	6.38 to 54.72	6.88 to 50	6.58 to 50
Index ranges	$-32 \le h \le 32$, $-15 \le k \le 15$, $-35 \le l \le 35$	$-14 \le h \le 14$, $-15 \le k \le 15$, $-46 \le l \le 46$	$-33 \le h \le 33$, $-15 \le k \le 15$, $-37 \le l \le 37$	$-19 \le h \le 19$, $-16 \le k \le 17$, $-22 \le l \le 22$	$-28 \le h \le 22$, $-29 \le k \le 25$, $-46 \le l \le 36$
Reflections collected	23584	58626	54461	17040	160890
Independent reflections	9250 [R_{int} = 0.0385, R_{sigma} = 0.0507]	11179 [R_{int} = 0.0774, R_{sigma} = 0.0678]	10504 [R_{int} = 0.0344, R_{sigma} = 0.0255]	4085 [R_{int} = 0.0177, R_{sigma} = 0.0151]	22172 [R_{int} = 0.1895, R_{sigma} = 0.5255]
Data/restraints/parameters	9250/0/601	11179/78/631	10504/0/622	4085/0/316	22172/443/1591
Goodness-of-fit on F^2	1.105	1.021	1.053	1.070	0.827
Final R indices [I>2σ(I)]	R_1 = 0.0687, wR_2 = 0.2077	R_1 = 0.0837, wR_2 = 0.2259	R_1 = 0.0392, wR_2 = 0.1042	R_1 = 0.0247, wR_2 = 0.0693	R_1 = 0.0874, wR_2 = 0.2347
R indices (all data)	R_1 = 0.1093, wR_2 = 0.2288	R_1 = 0.1681, wR_2 = 0.2584	R_1 = 0.0551, wR_2 = 0.1148	R_1 = 0.0285, wR_2 = 0.0702	R_1 = 0.2005, wR_2 = 0.2618
Largest diff. peak/hole / e $Å^{-3}$	0.78/-0.26	0.93/-0.64	0.41/-0.61	0.42/-0.57	1.48/-0.45

Table 5. Selected structural parameters of **5-7**from single crystal X-ray study.

Selected Bonds	Bond lengths (Å)	Selected Bonds	Bond angles (°)
	5.*2H₂O*		
O_6—Co_1	1.900(4)	N_4—Co_1—O_6	94.58(17)
O_{29}—Co_1	1.889(4)	N_9—Co_1—O_{29}	95.34(18)
O_5—Co_2	1.883(4)	N_9—Co_1—O_6	141.8(2)
O_{15}—Co_2	1.901(4)	N_4—Co_1—O_{29}	140.9(2)
N_4—Co_1	1.954(4)	N_3—Co_2—O_{15}	91.84(19)
N_9—Co_1	1.987(4)	N_{16}—Co_2—O_5	93.25(18)
N_3—Co_2	1.971(5)	N_3—Co_2—O_5	148.8(2)
N_{16}—Co_2	1.984(5)	N_{16}—Co_2— O_{15}	146.2(2)
N_3—C_{40}	1.287(7)	N_3—C_{40}— C_{52}	126.4(5)
N_{16}—C_7	1.438(7)	N_{16}—C_7— C_{14}	120.2(5)
N_4—C_{19}	1.418(7)	N_4—C_8— C_{13}	127.0(5)
N_9—C_{36}	1.430(6)	N_9—C_{32}— C_{64}	127.9(5)
		C_{39}—O_{17}— C_{34}	115.4(5)
		C_{31}—O_{12}— C_{43}	118.1(4)
	6.*2H₂O*		
O_3—Co_1	1.892(4)	N_1—Co_1—O_4	94.55(19)
O_4—Co_1	1.906(4)	N_2—Co_1—O_3	93.51(16)
O_5—Co_2	1.885(5)	N_1—Co_1—O_3	125.23(18)
O_6—Co_2	1.900(5)	N_2—Co_1—O_4	121.89(19)
N_1—Co_1	1.981(4)	N_3—Co_2—O_5	94.1(2)
N_2—Co_1	1.975(4)	N_4—Co_2—O_6	93.6(2)
N_3—Co_2	1.981(4)	N_3—Co_2—O_6	123.1(2)
N_4—Co_2	1.982(5)	N_4—Co_2—O_5	119.4(2)
N_1—C_{25}	1.297(7)	N_3—C_{47}— C_{48}	127.3(5)
N_2—C_{36}	1.298(7)	N_4—C_{58}— C_{59}	127.5(6)
N_3—C_{47}	1.311(7)	N_2—C_{36}— C_{37}	127.7(5)
N_4—C_{58}	1.308(7)	N_1—C_{25}— C_{26}	129.5(6)
		C_4—O_1— C_7	116.8(4)
		C_{16}—O_2— C_{19}	118.1(4)
	7.DMSO		
O_{15}— Cu_1	1.892(17)	O_4—Cu_1— N_{14}	144.84(8)
O_4—Cu_1	1.901(4)	O_{15}—Cu_1— N_{11}	144.0(9)
N_{14}—Cu_1	1.975(18)	N_{14}—Cu_1— O_{15}	95.00(8)
N_{11}—Cu_1	1.949(18)	N_{11}—Cu_1— O_4	94.33(7)
O_3— Cu_2	1.908(17)	O_3— Cu_2— N_5	91.68(8)
O_7—Cu_2	1.888(17)	O_7— Cu_2— N_{37}	93.48(8)
N_5—Cu_2	1.976(19)	O_3— Cu_2— N_{37}	148.30(8)
N_{37}—Cu_2	1.981(2)	O_7— Cu_2— N_5	150.88(8)
N_5—C_{12}	1.293(3)	N_{14}—C_{41}— C_{18}	127.8(2)
N_{37}—C_{51}	1.298(3)	N_{11}—C_{32}— C_{20}	126.5(2)
N_{14}—C_{41}	1.288(3)	N_{37}—C_{51}— C_{26}	127.7(2)
N_{11}—C_{32}	1.304(3)	N_5—C_{12}— C_{54}	126.1(2)
		C_8—O_6— C_{27}	117.58(18)
		C_{29}—O_9— C_{43}	115.44(19)
	7.CH_2Cl_2		
O_1— Cu_1	1.893(13)	O_3—Cu_1— N_2	94.92(6)
O_3—Cu_1	1.888(12)	O_1—Cu_1— N_1	94.11(6)
N_2—Cu_1	1.976(14)	N_2—Cu_1— O_1	145.89(6)
N_1—Cu_1	1.957(14)	N_1—Cu_1— O_3	145.29(6)
N_2—C_{20}	1.298(2)	C_6— C_7— N_1	125.87(17)
		C_{19}— C_{20}— N_2	126.81(16)
		C_{11}— O_2—C_{24}	115.91(13)

In all the complexes, each Co^{II} or Cu^{II} centre is bonded to the available coordination sites of Schiff bases $\mathbf{L^1}$ and $\mathbf{L^2}$ through two imine nitrogen and two phenolic oxygen atoms. The angles between the two O−M−N planes deviates largely from coplanarity and O−M−O, and N−M−N angles differ significantly from 90° in all

the molecules. The geometry around the metal ions in **5-8** is thus essentially distorted tetrahedral. It appears that M–O and M–N bond lengths around one metal centre in binuclear Co^{II} complexes **5**, **6** is comparable with the similar distances around other metal centre whereas these distances deviate significantly in binuclear Cu^{II} complex **7** (Table 3). It is noteworthy that the Co–O (1.883-1.906 Å) and Co-N (1.954-1.987 Å) bond distances in binuclear Co^{II} complexes **5-6** are significantly longer than the similar distances observed in other Schiff base square planar Co^{II} complex (1.835-1.847 Å for Co–O and 1.861-1.864 Å for Co–N).[47] However, longer Cu–O (1.888-1.976 Å) and shorter Cu-N (1.949-1.976 Å) bond distances are observed as compared to the other Schiff base planar Cu^{II}complex (1.874 Å for Cu–O and 2.009 Å for Cu–N),[48] which are indeed consistent with the similar measurements observed in analogous tetrahedral Cu^{II} complex reported elsewhere.[32a]In all the binuclear complexes, the ethereal bond angle of one linker appeared in the normal range[23] 117.5-118.1º while the similar angle associated with second linker is decreased significantly to 115.4-116.8º. This inward bending of the diphenyl ether linkers suggests flexibility in the coordinated ligands, essential for the formation of macrocyclic structures. Further, the unique coordination geometry adopted by Co^{II} or Cu^{II} ions and the presence of two arc shaped ligands form double helical molecular unit of **5-8** as exemplified in Figure 6.

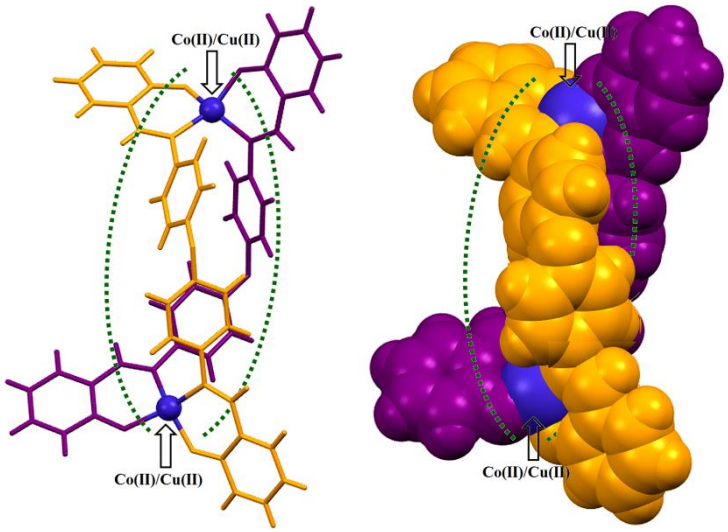

Figure 6. General representation of double helical molecular unit formed in **5-8**.

Evidently, the presence of phenyl/naphthyl rings and different metal centrescertainly induce a significantdifference in the electronic nature as well as stereochemical conformations (dihedral angles) of the molecules. The aromatic moieties present in the molecular framework potentially provide a hydrophobic surface

capable of participating in noncovalent interactions such as *π*...*π*, CH...*π*, CH...O, Cl...O and/ or O...S in compounds **5-7**. For instance, the intermolecular interactions H61...*π*, H49...*π* (**5**.*2H₂O*) and H39...*π* (**7**.*DMSO*) lead to the formation of infinite 1D helical chain with a helical pitch of 28.963Å and 28.822 Å, respectively. A representative view is provided in Figure 7a for **7.**DMSO (Other views are provided in annexure). The presence of *N*-naphthyl substituents in **6.***2H₂O* alters the packing pattern and indeed forms, infinite 1D saw shape molecular stacking along b-axis involving H6...*π* or H15...*π* and *π*...*π* interactions. (Figure 7b) Mutually all the noncovalent interactions in **5**.*2H₂O*, **6.***2H₂O* and **7.** *DMSO* lead to the formation of an infinite 3D molecular network consisting of voids occupied by corresponding solvent molecules, that are translated in an infinite channel as shown in Figure 7c-e. In case of 7.CH_2Cl_2, solvent molecules played a crucial role in directing the crystal packing patterns of this molecule. For instance, ***π...π*** and Cl...O interactions lead to an attractive helical arrangement along c axis, however, all these noncovalent interactions mutually leads to the formation of a 3D infinite supramolecular assembly consisting relatively smaller voids occupied by CH_2Cl_2 molecules, compared to 7. DMSO. Moreover, the two closing π...π interactions involve half of the linker moiety of two molecules which oriented adjacent molecule in *anti* fashion. Notably, differential stereoelectronic factors associated with CH_2Cl_2 molecules have efficiently tuned the noncovalent interactions, involving CH_2Cl_2 molecules in CH...O interactions that together with effective CH...π, π...π interactions have resulted into the formation of unique 3D interlocked undulated architecture as illustrated in Figure 7f.

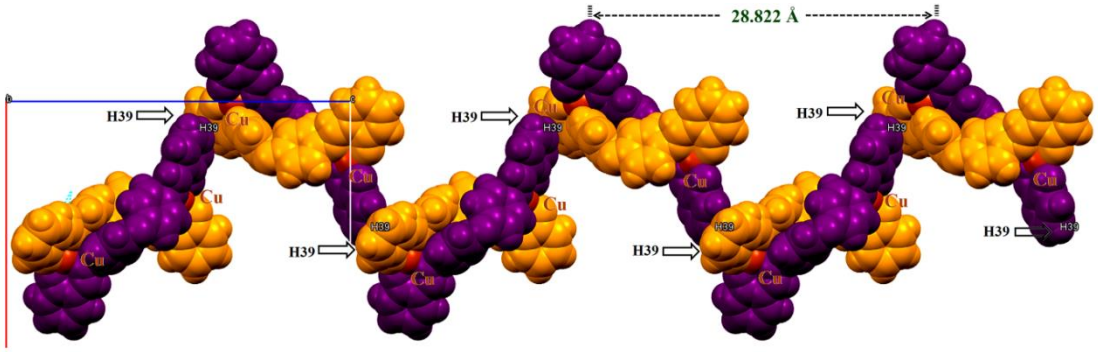

(a)

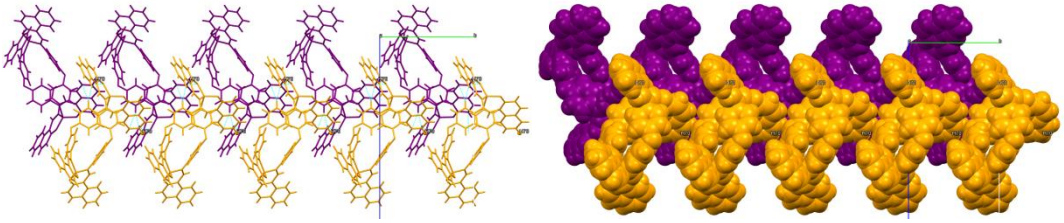

(b)

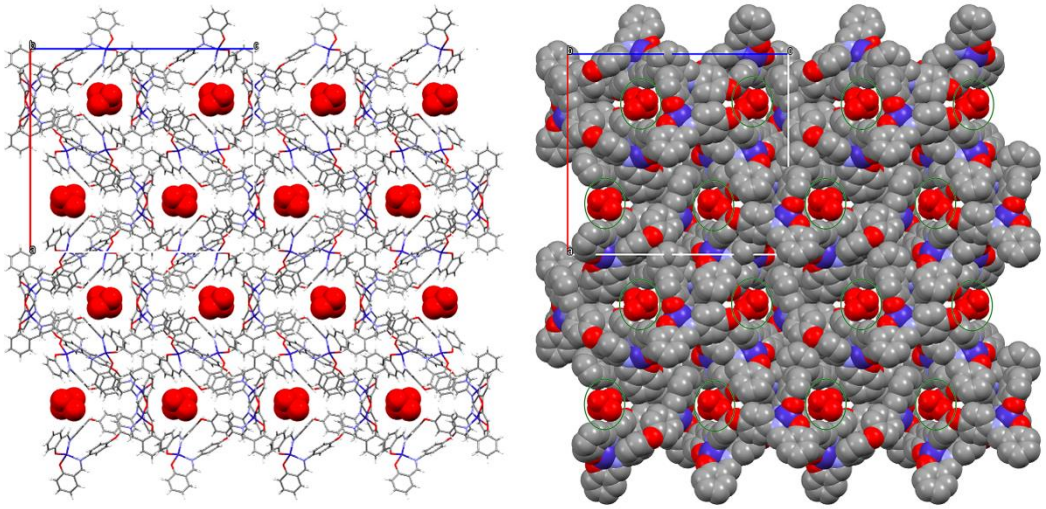

(c)

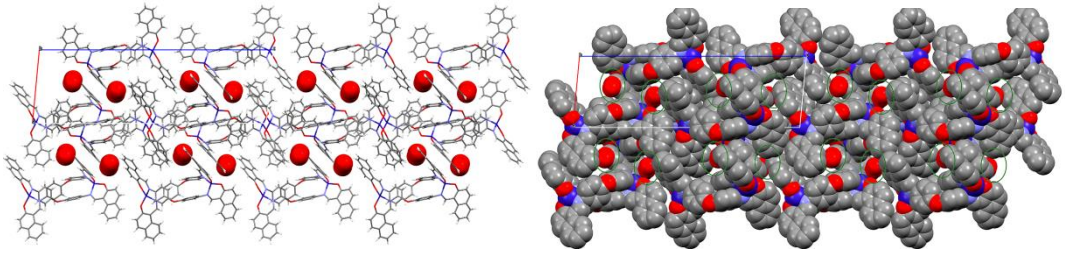

(d)

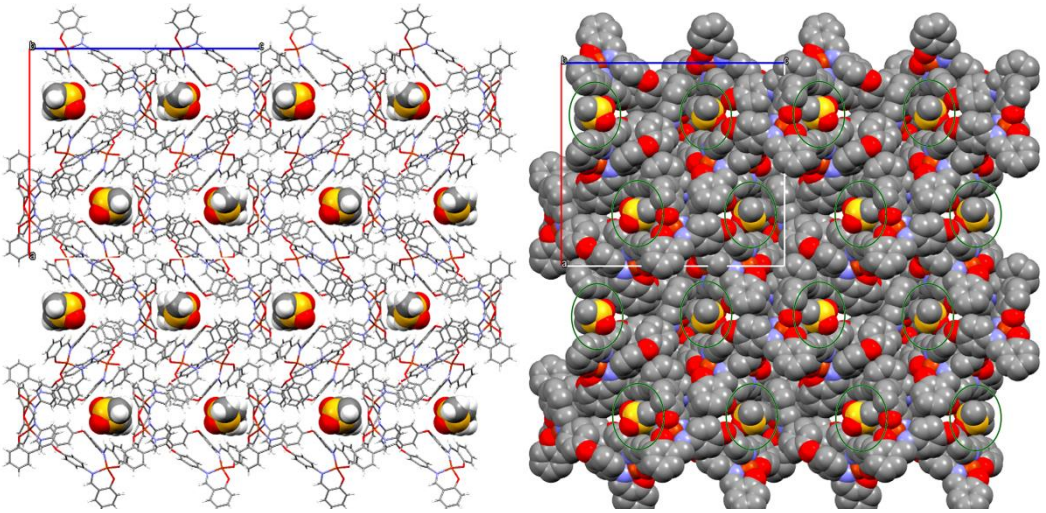

(e)

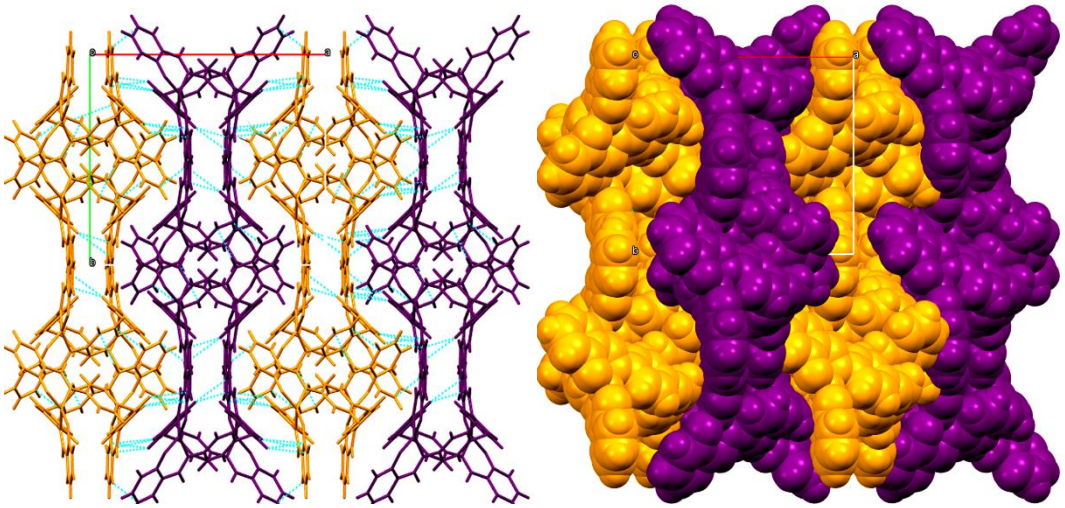

(f)

Figure 7. (a) CH...π interactions forming infinite 1D helical chain, (b) packing pattern illustrating infinite 1D saw shape molecular stacking, (c-e) 3D supramolecular assembly formed through noncovalent interactions capped stick and spacefill model (H are omitted for clarity) a view along *b*-axis (2.2.2) for **5.*2H₂O***, **6.*2H₂O*** and **7.DMSO** respectively, (f) Formation of 3D infinite interlocked undulated architecture through noncovalent interaction in **7**.CH_2Cl_2.

2.3.5. Theoretical Investigations

The DFT calculations were performed for representative compounds *ca* **L[1]**, **K₂xan[1]**, binuclear xanthate macrocycles **1, 3** and their corresponding binuclear Schiff base macrocyclic derivatives **5, 7**. All calculations were performed with the Gaussian 03 program suite.[49]The geometry for all the model compounds discussed herein was fully optimized (Figure 8) by density functional theory at the DFT B3LYP/lanl2dz level. Such a type of basis set has been used with good success in a number of studies involving similar species, having good agreement with experimental results.[50] Molecular orbitals were generated using GaussView 3.0 program.

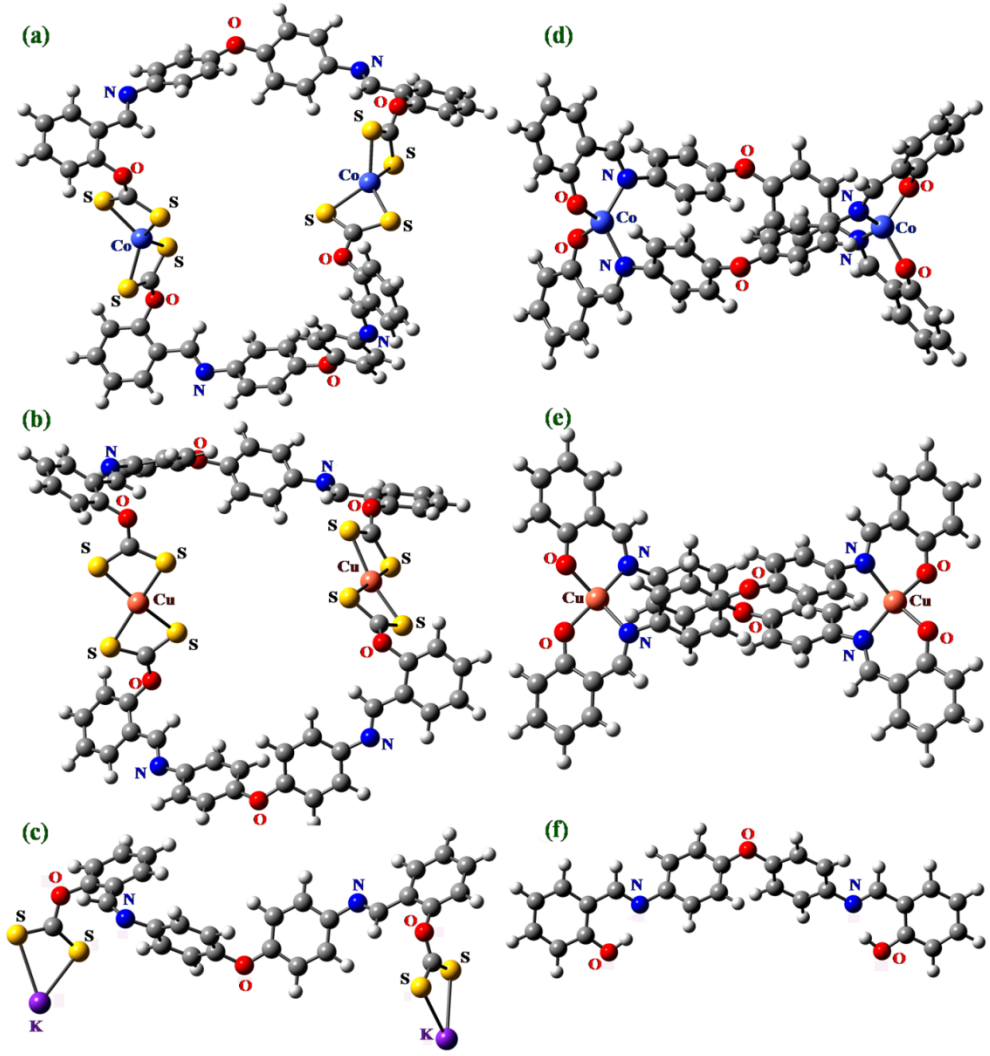

Figure 8. An optimized geometry for the minimum energy conformation atB3LYP/lanl2dz level for **1** (a), **2** (b), **Kxan-1** (c), **5** (d), **7** (e), $\mathbf{L_1}$ (f).

The calculated structural parameters for complex **5** and **7** are comparable to their structural parameters obtained from X-ray crystallography (Table 6). The calculated HOMO-LUMO gaps are comparable with the experimental UV-visible absorption data (Table S4) and further validate the computed data and optimized structures. The flexibility associated with the linker leading to inward bending of the both of the xanthate moieties of $\mathbf{K_2xan^1}$ in the optimized structure suggests complementary ligand, essential for the formation of metallamacrocyclic xanthate complexes **1-4**. It appears that the optimized structures adopt a unique orientation to diminish the steric and electronic factors associated with them. For instance, boat shaped macrocyclic architectures are obtained as a lower energy conformation in case of binuclear xanthate complexes **1** and **3**, whereas double helical macrocyclic

architectures are obtained for binulear *N, O*-Schiff base complexes **5** and **7**. These architectures are exemplified in Figure 9-10.

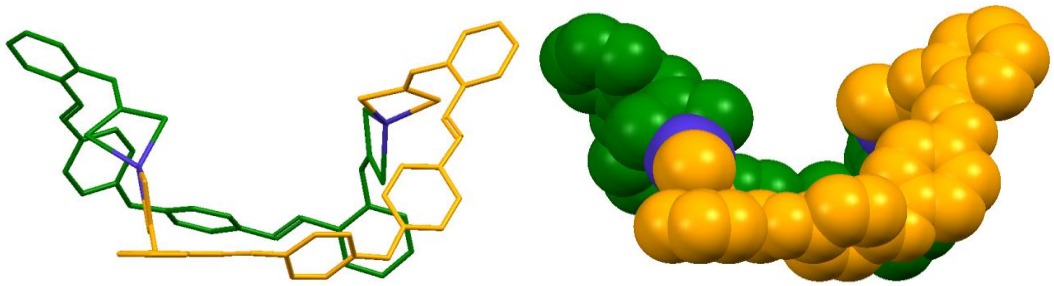

(a) (b)

Figure 9. Complex **1** forming boat shaped macrocyclic architecture represented by capped sticks (a) and spacefill (b) models.

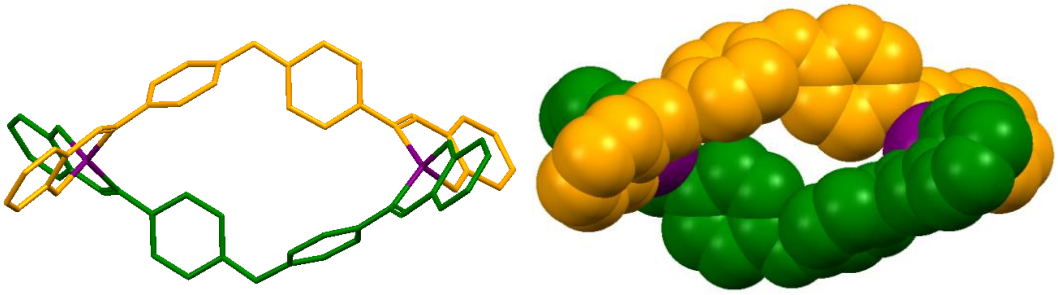

(a) (b)

Figure 10. Complex **5** forming double helical macrocyclic architecture represented by capped sticks (a) and spacefill (b) models.

An optimized geometry of complexes **1**, **5** and **7** suggests distorted tetrahedral coordination sphere at both the metal centres, however complex **3** adopts distorted square planar geometry around both the Cu^{II}centres. The geometrical parameters of the binuclear *N, O*-Schiff base macrocyclic complexes **5** and **7** are well compared with their experimental parameters obtained from single crystal X-ray study (Table 6) and these validate the optimized electronic structural models of compounds under investigation. The small difference between the geometrical parameters obtained theoretically and from X-ray crystallography of compound **5** is probably emerged due to the presence of a large number of non-covalent interactions offered by the spacer moiety intending an extra stability to the macrocyclic architecture.

Table 6. Selected structural parameters obtained from theoretical investigations and X-ray study for**1**, **3, 5** and **7**.

Entry	Selected Bond	Bond Length (Å) Theoretical	Bond Length (Å) X-ray	Selected Bond	Bond Length (Å) Geometrical	Bond Length (Å) X-ray
5	O–Co	1.917, 1.921	1.890, 1.900, 1.906, 1.884	O–Co–N	94.08, 94.54	94.62, 95.29, 93.46, 91.71
	N–Co	2.047, 2.043	1.991, 1.953, 1.972, 1.985	O–Co–O	117.61	94.24, 91.07
	N–C (imine)	1.312, 1.309	1.284, 1.288, 1.301	N–Co–N	123.70	101.00, 101.29
	O–C (ether)	1.387, 1.381	1.381, 1.396, 1.384, 1.379	C–C–N	128.16, 128.43	127.14, 127.68, 126.35, 126.88
	Co_1–Co_2	11.259	11.750	C–N–Co	118.64, 118.65, 119.32	122.70, 121.61, 122.85, 121.95
				C–O–Co	124.93, 126.49	126.75, 127.47, 124.63, 128.86
				C–O–C (ether)	118.88	115.42, 117.92
7	O–Cu	1.930	1.888, 1.893	O–Cu–N	93.33	94.11-94.92
	N–Cu	2.029	1.957, 1.976	N–Cu–N	104.34	98.12
	N–C	1.421	1.299-1.434	O–Cu–O	96.22	92.80
				N–Cu–O	139.48-139.53	145.29-145.89
				C–C–N	128.20	125.87-126.82
				C–N–Cu	122.10-122.11	121.48-122.76
				C–O–Cu	128.84-128.85	123.16-127.69
				C–O–C	118.32	115.91

Table 7. Computational calculation data for complex **1**, **3, 5, 7**

Sr.	Entry	Energy (10^6 Kcal/mol)	HOMO-LUMO Band gap (eV)	Theoretical λ_{max} value (experimental λ_{max} value) nm
1	**1**	-3.9543	3.4645	358 (366)
2	**3**	-4. 0184473	3.3941	365 (380)
3	**5**	-1.8599	3.5688	347 (349)
4	**7**	-1.9238968	3.6303	342 (359)

Frontier molecular orbital analysis: The character of the frontier orbitals and the HOMO–LUMO energy gap greatly contribute to the photo-physical properties of the complexes and thus analysis of frontier molecular orbitals need prime consideration for prediction of the possible reactivity of the molecule.[51]

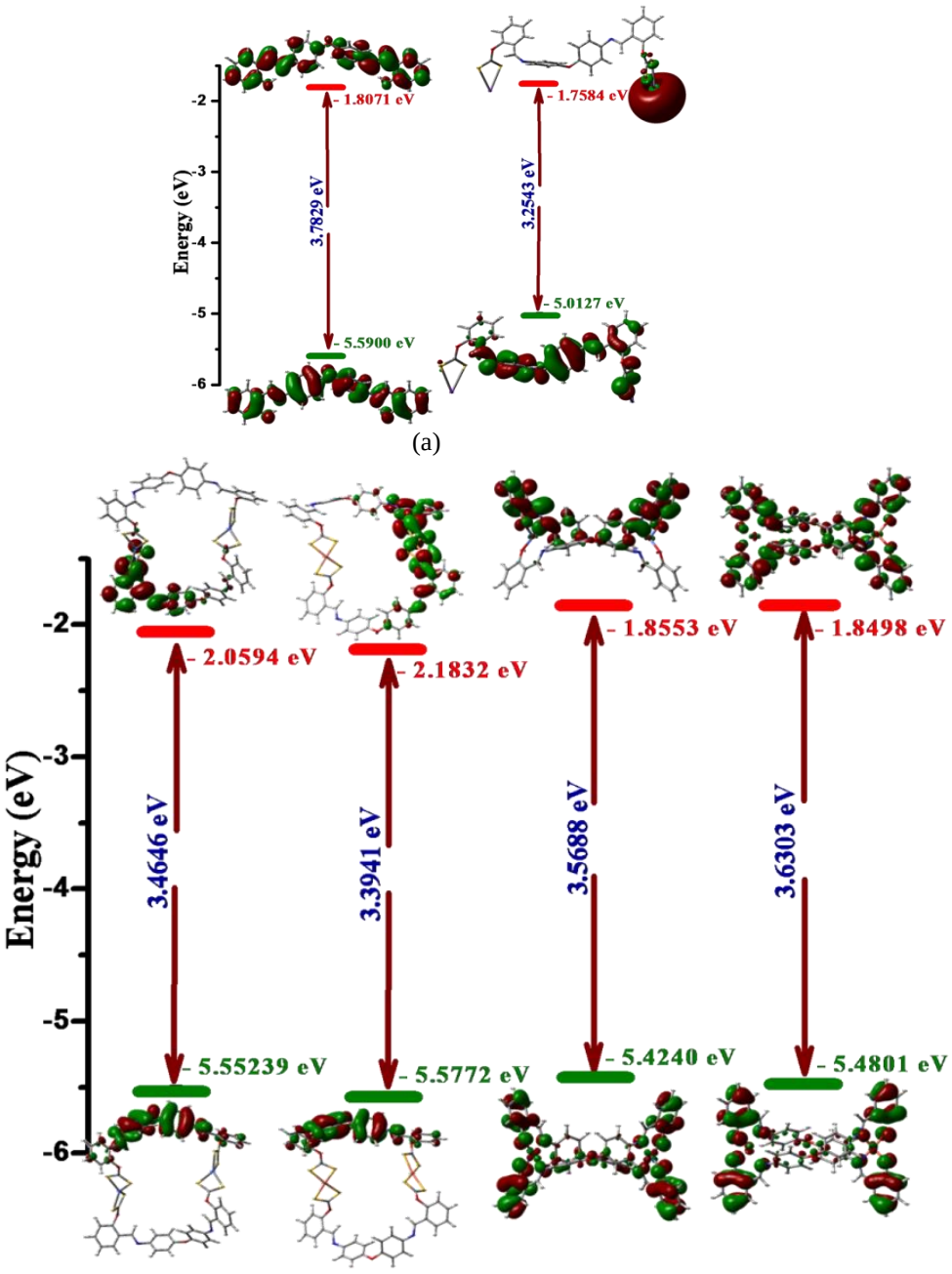

Figure 11. Comparison of the frontier molecular orbitals derived from DFT calculation at the B3LYP/LAN2DZ level; for (a) $\mathbf{L^1}$and $\mathbf{K_2xan^1}$, (b) **Complexes 1**, **3**, **5** and **7**.

Due to the effective conjugation, HOMO and LUMO in $\mathbf{L^1}$ are delocalized over all the phenyl rings, whereas HOMO of $\mathbf{K_2xan^1}$ is mainly delocalized over phenyl rings adjacent to ethereal oxygen and to a little extent to the xanthate moieties. Expectedly, LUMO of $\mathbf{K_2xan^1}$ is mainly localized over a xanthate moiety and potassium attached to xanthate as illustrated in Figure 11a. The electron density in the HOMO for binuclear xanthate complexes **1** and **3** is predominantly delocalized over the phenyl moieties adjacent etherial with oxygen, while metal chelated xanthate moieties are mainly

contributed for LUMO as shown in Figure 11b. The transformation of the binuclear xanthate complexes to their corresponding binuclear N,O-Schiff base analogues can be explained by the localization of LUMO at metal chelated xanthate moiety in complexes **1** and **3** which emphasizes the vulnerability of xanthate moiety under nucleophilic conditions. The HOMO for **5** and **7** is predominantly delocalized over spacer moiety; the π-orbitals of two peripheral phenyl moieties of linker unit are commonly contributing to the high extent for the delocalization of the HOMO. However, the LUMO in **5** is mainly delocalized over the length of one of the ligand portions and it is delocalized over peripheral phenyl moieties in **7** with minor contribution by the phenyl moieties attached to the ethereal oxygen. On the other hand, for both the compounds the contribution from the metal atom in their HOMOs and LUMOs is extremely negligible. Thus, frontier molecular analysis suggests that the chelated xanthate moiety can preferentially react with nucleophilic species and all the complex molecules can show an efficient CH-π and π-π donor-acceptor ability.

Furthermore, the significant decrease in the energy difference between HOMO-LUMO is observed upon the reaction of $\mathbf{L^1}$ (3.7829 eV) with CS_2 leading to the $\mathbf{K_2xan^1}$(3.2543 eV), due to higher electron density and extended conjugation. We have also found that the energies of HOMO and LUMO of **1**and **3** are lower than that of **5** and **7**, energy difference between HOMOs is smaller but LUMOs are greatly differentiated by energy. The energy difference between HOMO-LUMO for xanthate complexes (3.4646 eV for **1** and 3.3941 eV for **3**) is significantly lower compared to their corresponding Schiff base complexes (3.5688 eV for **5** and 3.6303 eV for **7**), could be due to the presence of flexible skeletal structures of the xanthate ligand. Additionally, this study also revealed the greater contribution of copper towards decrease of the HOMO-LUMO energy difference in xanthate complexes in spite of identical molecular framework except metal centres, however a reverse trend is observed in Schiff base complexes. The lower energies of HOMO in copper containing complexes (**3** and **7**) over their cobalt centered congeners (**1** and **5**) also suggest their superior stability. Interestingly, the HOMO–LUMO energy gap values for the entire investigated compound are in the range of 3.38-3.79 eV which reveals the possible semiconducting properties of the compounds[52] and increases the potential applicability of this class of compounds towards semiconducting materials.

The electrostatic potential (ESP) of molecules is widely used as a powerful tool for exploring the properties and locating potential sites within the molecules for the interactions with other moieties and thus it provides insights into molecular association. For instance, the surface property of drug molecules reveals the potential sites of interactions with biomolecules which is useful to estimate the mode of action.[53]

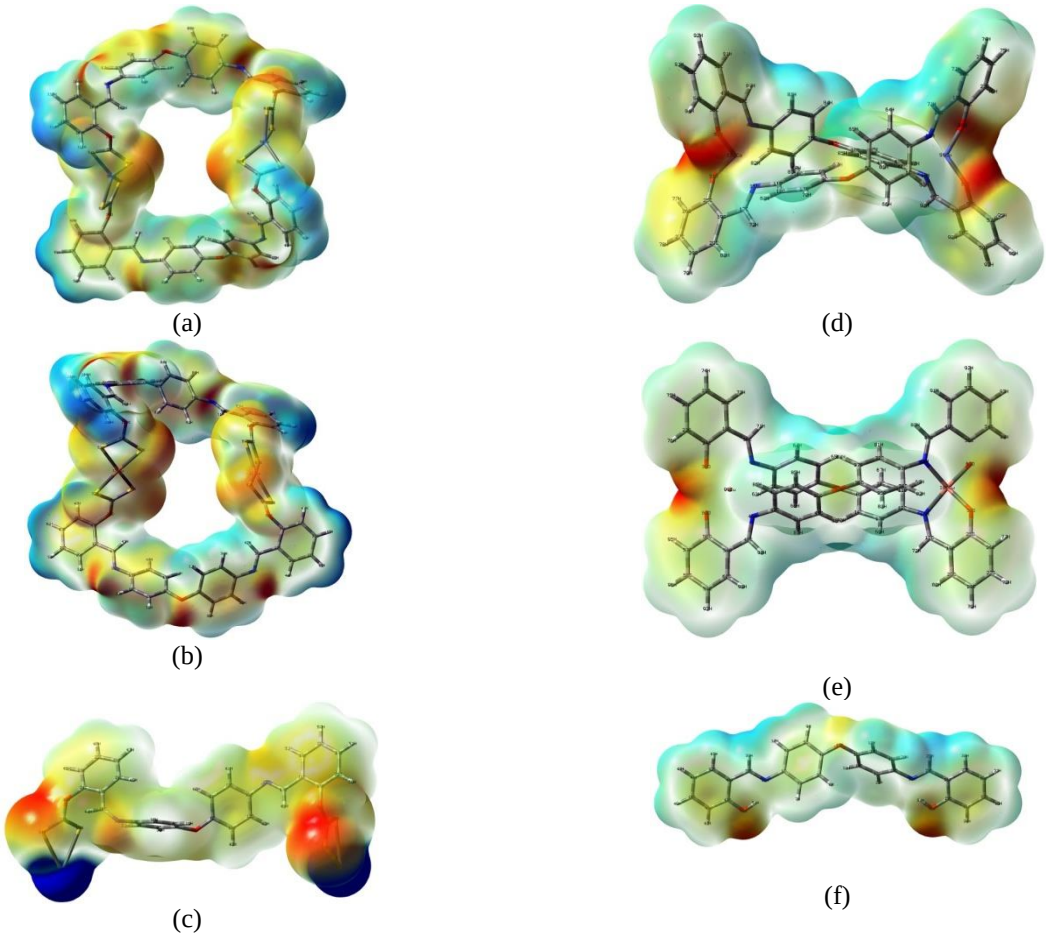

Figure 12. Graphical representation of electron density from total SCF density (isoval= 0.0004; mapped with ESP) for **a-f:** Complex **1**, **3**, **K_2xan^1**, **5**, **7** and **L^1** respectively **(**Red colour indicates negative potential whereas blue colour indicates negative potential).

The localization of slight negative potential around –OH in **L^1** and very high positive potential around potassium centres and quite negative potential around sulfur atoms in **K_2xan^1** can be clearly seen in Figure 12. Furthermore, the localization of low positive potential at aromatic hydrogen atoms moderately negative potential around N/O/S in macrocyclic complex **1** (a), **3** (b), **5** (d) and **7** (e) could be clearly revealed from the mapping of electrostatic potential surface (Figure 12). This has indeed generated a scope for the use of these macrocyclic complexes with variable cavity size and tuneable electronic environment as ditopic receptors to interact with suitable guest species (*vide supra*). Gejji et al. have depicted the exploitation of molecular

electrostatic potential from density functional calculations to understand the host-guest interactions.[54] In this context, the surface potential of binuclear xanthate macrocyclic complexes **1** and its Schiff base analogue **5** clearly explain thesensing ability of various metal ions using fluorescence spectroscopy (*vide supra*).

2.3.6. *In vitro* cytotoxic activity

All the newly synthesized compounds **L^1,L^2**, **K_2xan^1**, **K_2xan^2**, binuclear metallamacrocyclic complexes **1-8** were screened against the malignant cell lines HEP 3B (Hepatoma) and IMR 32 (Neuroblastoma) for their in vitro cytotoxicity by the MTT assay.[27] The cytotoxicity these compounds were compared with clinically used antineoplastic drug cisplatin and lead compound 4,4'-diaminodiphenyl ether **(L)**. The 50% inhibition concentration (IC_{50}) values obtained after incubation for all the compounds against HEP 3B (6 h) and IMR 32 (14 h) are summarized in Table 8.

Table 8. *In vitro* cytotoxicity MTT assay IC_{50} (μM) for entry **1-16** against HEP 3B and IMR 32 cancer cell lines.

Entry	Compound	Antitumor activity (IC_{50} values)	
		HEP 3B μM (1mL) ±SE	IMR 32 μM (1mL) ±SE
1[a]	L	415.4±2.15	272.423±2.40
2	L^1	137.76±13.93	103.985±3.30
3	L^2	36.65±5.03	166.854±11.03
4	K_2xan^1	17.8135±2.94	23.194±1.36
5	K_2xan^2	79.537±6.13	26.192±1.29
6	1	52.943±1.30	51.802±2.86
7	2	54.37±0.29	64.372±3.74
8	3	8.1349±0.82	1.848±0.31
9	4	8.7586±1.74	7.337±0.58
10	5	69.725±3.57	99.658±6.55
11	6	43.449±4.67	50.142±2.50
12	7	19.163±2.05	13.211±1.07
13	8	14.340±1.33	28.763±1.35
14	Co^{II}	290.87±4.05	343.169±17.14
15	Cu^{II}	42.92±4.26	19.033±2.85
16	Cisplatin	74.621±1.27	107.848±0.30

([a]: IC_{50} value taken from ref-22) (The data are expressed as μM concentration and value represents the average of three sets of independent experiments.)

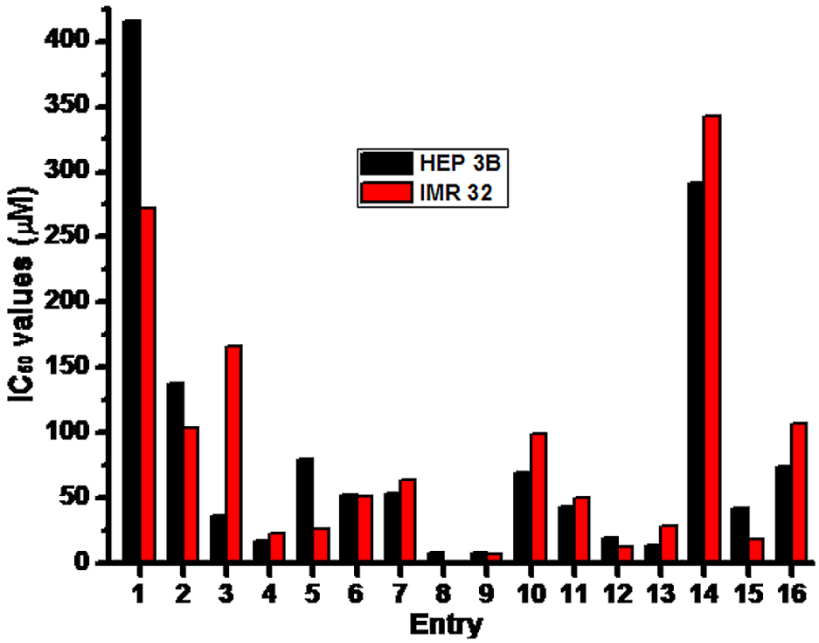

Figure 13. *In vitro* cytotoxicity (IC_{50}) for entries **1-16** against malignant HEP 3B and IMR 32 cells.

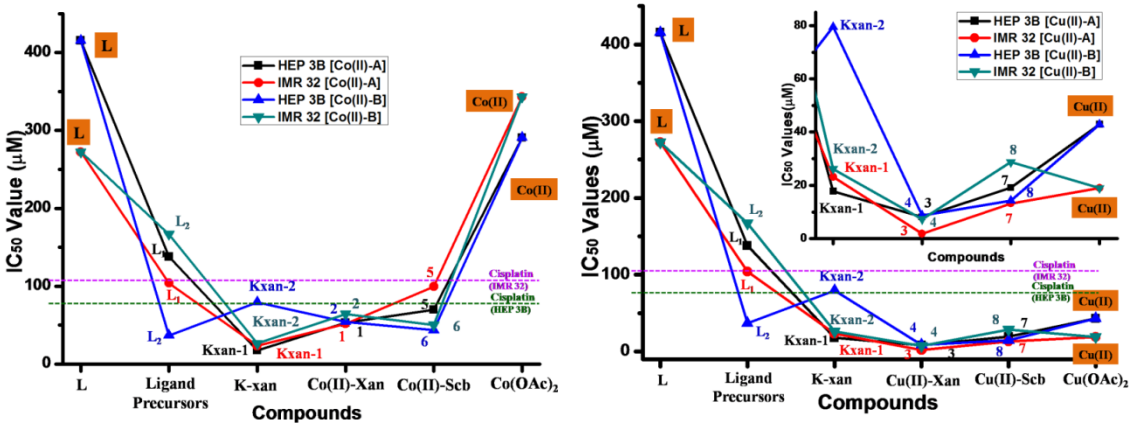

Figure 14. Effect of functionality changes on in vitro cytotoxicity againstHEP 3B and IMR 32 cells.

The condensation of salisaldehyde with lead compound, L resulted into L^1 with ≈ 3 fold increased cytotoxicity (IC50: 137.76±13.93 μM against HEP 3B and 103.985±3.30 μMagainst IMR 32). However, condensation of 2-hydroxy naphthaldehyde with **L** resulted into $\mathbf{L^2}$with >10 and two fold increased cytotoxicity against HEP 3B (36.65±5.03 μM) and IMR 32 (166.854±11.03 μM) cell lines, respectively. The cytotoxicity of L^1 and L^2 further augmented on the formation of their respective xanthate salts and ensuing complexes, particularly copper xanthate complexes. All binuclear xanthate complexes displayed comparable cytotoxic activity, except **3** which exhibits differential activity against both the cell lines. Interestingly, binuclear Cu^{II}xanthate complexes were found extremely active against both the cell lines (IC50: 8.1349±0.82 μM (**3**), 8.7586±1.74 μM (**4**) against HEP 3B and 1.848±0.31 μM (**3**) and 7.337±0.58 μM (**4**) against IMR 32) and this projects them in the vein of

good candidates as potent antitumor agents. Unlike binuclear xanthate analogues, binuclear *N, O*-Schiff base complexes could not preserve the cytotoxic activity. Binuclear Cu^{II} *N, O*-Schiff base complexes **7** and **8** exhibit 2-7 fold better potency than that of cobalt analogues **5-6**. The overall data suggest that **K_2xan^1**, **K_2xan^2**, and complex **1-8** are more cytotoxic against both the cell lines than clinically used antineoplastic drug cisplatin (Table 8). In general, all the complexes bearing copper centre are more potent compared to their cobalt bearing congeners probably due to the predominant favouring of Cu^{II} ion in biological systems than that of cobalt.

Our hypothesis on binuclear Co^{II}/Cu^{II} xanthate complexes that might involve multiple mode of action leading to the cell death, can be explained by several previously observed effects of isostructural dithiocarbamate complexes and complexes derived from *N, O*- donor ligands. 1,1-dithio moieties are known to exert cytotoxicity through antiangio-genesis effects, inhibition of numerous metalloenzymes and NF-KB-related gene-expression and modulation of cellular metabolism, which lead to tissue damage.[55] The decomposition and metabolic products of a transition metal 1,1-dithio complexes in vivo, *ca* free 1,1-dithio moieties, CS_2 are reportedly able to arrest the cell proliferation.[56] Dou and co-workers reported several studies concerning the cytotoxic activity of discrete, transition metal complexes, including complexes based on *S*, *N* and/ or *O*- donor ligands.[57]Electrochemical and stability data[20c] suggests that the most stable dithiocarbamate complexes proved to be most cytotoxic in vitro and also against the cisplatin-resistant.Recent investigations highlights the electronic density analysis of different dithiocarbamate metal complexes to correlate their toxicity as well as the ability to inhibit proteasome and induce apoptosis in human cancer cells.[58] It has appeared that the dithiocarbamate complexes holding higher electronic density over sulfur atom within the complex are more active against the JAMM domain of the 26S proteasome.[58] Due to the presence of almost similar structural and electronic features in dithiocarbamate and xanthate complexes, analogous mode of action for the antitumor activity could be expected for both of them.Beyond this, the possibility of transchelation reactions with physiological molecules and metabolic products of xanthate complexes could alter the intracellular metal constitutions which lead to the cytotoxic activity. Further, cobalt and copper complexes are also known to target DNA under physiological conditions via an oxidative pathway[59]and induce cytotoxicity.[60]

It appears that the structural sub-units such as metal ions, various *N*-substituents, xanthate/ Schiff base functionalities are essentially controlling the cytotoxic activity of the compounds. (Figure 14) Among the investigated compounds, **L^1**, **L^2**, **K_2xan^1** and **K_2xan^2** can be classified as moderate cytotoxic agents, binuclear *N*, *O*-Schiff base analogues as good, whereas binuclear xanthate complexes can be excellent antitumor agents; especially **3-4** displaying optimum cytotoxic ability (Figure 14) against both the cell lines. In analogy with the recent investigations,[61] we have calculated the stereo-electronic parameters such as highest occupied molecular orbital (HOMO), lowest unoccupied molecular orbital (LUMO) energies, dipole moment and charges on the N/O/S/M atoms using density functional theory (DFT). Calculated stereoelectronic parameters and experimental IC_{50} values against HEP 3B and IMR 32 cells for model compounds are summarized in Table S11.These parameters are known to provide insight in the mechanisms related to membranes transportations, revealing possible interactions with biological macromolecules or intracellular receptors and thus provide a possible rationalization for the structure activity relationships (SARs) of these compounds. The stability and reactivity of the molecules towards possible biological receptors such as electron rich or electron deficient regions are reportedly depends on the frontier orbitals,[62] asHOMO energy is closely related to susceptibility to electrophilic attack while LUMO energy is closely related to susceptibility to nucleophilic attack.

Among the model complexes **1**, **3** and **5**, **7**bearings similar ligand framework, complexes **3** and **7** with lower HOMO energy and lower dipole moment (greater lipophilicity) (Table S11) exhibit higher cytotoxicity, suggestive of higher bioavailability at the site of action and reaction in the biological conditions. Notably, complex **3** bearing negative charge on copper and positive charges on sulfur atoms exhibits higher reactivity towards biological receptors, which could underline the extraordinary ability of **3** to arrest the cell growth against both the cell lines. These theoretical parameters correlate well with the experimental results since complex **3** is the most active against both the cell lines.

2.3.7. Induction of apoptosis in human cancer HEP 3B and IMR 32 cells

In higher organisms, apoptosis is a key process for boy haemostasis during development, embryonic development, the immune system, and ageing. It is also known to playan important role in many pathological conditions like cancer and neurodegeneration.[63] Apoptotic cell death is postulated to be the crucial mechanism in natural tumor suppression and cancer treatment, which abolish abnormal malignant cells and reduce the tumor size.[64] Thus, it is important to develop novel chemical agents to specifically induce apoptosis for therapeutic purposes. Addition to MTT assay, the 'Flow Cytometry' is considered as the analytical tool for investigation of potency, not only for cell viability, but also to evaluate membrane and chromosomal damage, cell-cycle analysis and morphological changes. Hence, for quantification of the extent of apoptotic and necrotic cell death, flow cytometry studies were performed upon treatment of some representative compounds on **HEP 3B** and **IMR 32** cells.(Table 9) The flow-cytometric density plot (Figure 15) illustrates the induction of apoptosis in **HEP 3B** and **IMR 32** cells after the treatment with **K_2xan^1** and binuclear metallamacrocyclic complexes **1**, **3**, **6** and **7.**

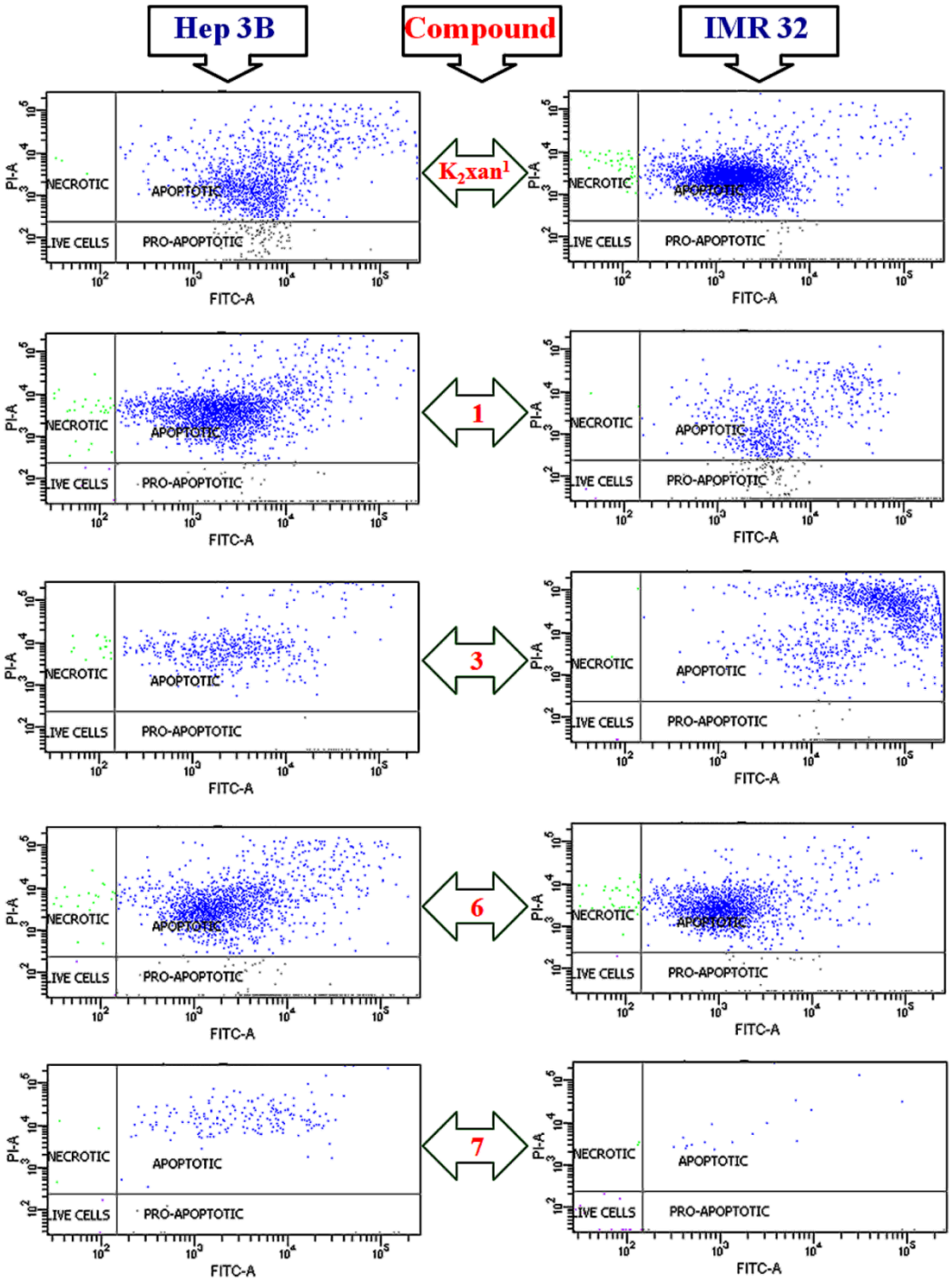

Figure 15. Flow cytometry density plots of HEP 3B and IMR 32 upon treatment with **K_2xan[1]**, binuclear macrocyclic complexes **1**, **3**, **6** and **7**.

With reference to Table 9, less than 1% live cell population was observed for both the cell lines after treatment which reinforced the extreme cytotoxicity of the compounds investigated by MTT assay. Interestingly, apoptotic cell populations *viz*. 32.1%, 70.2%, 13.5%, 62.3% 10.9% were observed ofHEP 3B cells, whereas 76.3%, 19.5%, 51.9%, 54.3% 1.2% of IMR 32 cells were observed,after the treatment, of

K_2xan^1, **1**, **3**, **6** and **7**, respectively. It may be noted that 64.1% of pro-apoptotic HEP 3B cells were observed upon treatment of **K_2xan^1** whereas 77.3% and 43.2% of pro-apoptotic IMR 32 cell population was observed upon treatment of **1** and **3,** respectively.

Table 9. Apoptotic/ necrotic population of HEP 3B and IMR 32 cells upon treatment with K_2xan^1, binuclear metallamacrocyclic complexes **1**, **3**, **6** and **7**.

Sample	HEP 3B (%)				IMR 32(%)			
	Necrotic	Apoptotic	Live cells	Pro-apoptotic	Necrotic	Apoptotic	Live cells	Pro-apoptotic
K_2xan^1	3.8	32.1	0.0	64.1	21.2	76.3	0.0	2.5
1	25.8	70.2	0.2	3.8	3.0	19.5	0.2	77.3
3	85.9	13.5	0.0	0.5	4.8	51.9	0.1	43.2
6	30.8	62.5	0.1	6.7	43.3	54.3	0.0	2.3
7	88.3	10.9	0.2	0.5	97.6	1.2	1.0	0.3
Control	0.1	0.0	99.8	0.1	0.1	0.0	99.7	0.2
Cisplatin	10.3	30.4	0.0	59.3	...	...	...	...

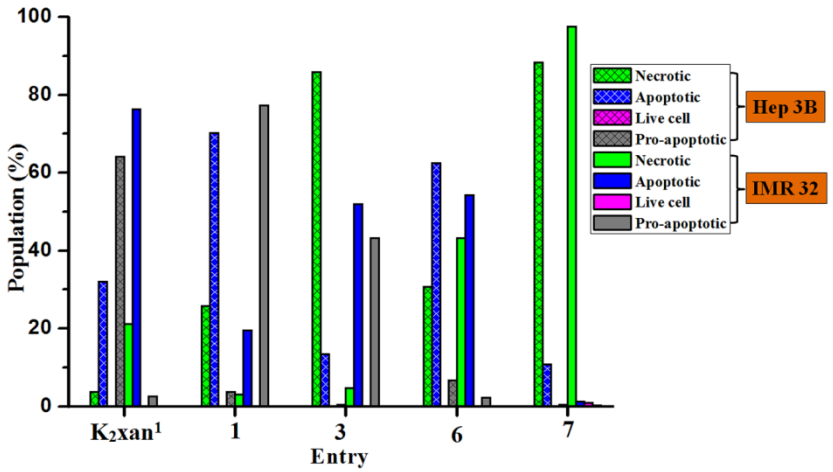

Figure 16. Flow cytometry data revealing apoptotic/ necrotic/live cell population of HEP 3B and IMR 32 cells upon treatment of **K_2xan^1**, binuclear macrocyclic complexes **1**, **3**, **6** and **7**.

Further,HEP 3B and IMR 32 cells treated with **7** and HEP 3Bcells treated with **3**,predominantly dyed with propidium iodide and evident for the induction of necrosis to the great extent, whereas IMR 32 cells treated with **6** showedsimultaneous binding of annexin V and propidium iodide, an indicative of transition state of apoptosis to necrosis (late apoptosis and secondary necrosis).[65] Apoptosis inducing ability of compounds **K_2xan^1**, **1** and **6** is clearly reflected by the sum of apoptotic and pro-apoptotic cell populations (96.2%, 74% and 69.2% for HEP 3B; 78.8%, 96.8% and 56.6% for IMR 32) of treated cells. The distinct behaviour of binuclear metallamacrocyclic xanthate complex **3** towards both the cell lines is also reflected by the sum of apoptotic and pro-apoptotic cell populations of 95.1% (IMR 32) and 14% (Hep 32). The differential apoptotic, pro-apoptotic and necrotic cell populations in

treated HEP 3B and IMR 32 cells put forward the hypothesis of the involvement of distinct receptors in the cytotoxic activity. (Figure 16)

2.4. Conclusion

The current study allows us to put forward newer facets of metallamacrocyclic xanthate complexes of the type [M_2-μ^2-bis-(κ^2*S*,*S*-xan^1/xan^2)]**1-4** derived from phenolate based polydentate xanthate ligands in the development of [2:2] binuclear *N*, *O*- bidentate Schiff base macrocycles of the type [M_2-μ^2-bis-(κ^2*N*,*O*-L^1/L^2)]. The single crystal x-ray diffraction study reveals the unambiguous structures of **5-8** and itunderlines the compatibility of the linker framework for the formation of double helical macrocyclic assembly. It also depicted the great dependence of unique coordination geometry of metal centre on crystal packing patterns. The geometry of model compounds have been optimized by DFT method. The in-vitrocytotoxic activity of all the compounds was evaluated against HEP 3B and IMR 32 by the MTT assay. Interestingly, binuclear metallamacrocyclic Cu^{II}xanathate complex **3** was found most active against both the cell lines and cytotoxicity data confirms their better potency than cisplatin, a well known antineoplastic drug. Flow cytometric investigations project this structural class of active chemical agents to induce apoptosis, required for major therapeutic implication in cancer therapy.

2.5. References

1. Jones, C. J. *Chem. Soc. Rev.* **1998**, *27*, 289. (b) Swiegers, G. F.; Malefetse, T. J. *Chem. Rev.* **2000**, *100*, 3483. (c) Leininger, S.; Olenyuk, B.; Stang, P. *Chem. Rev.* **2000**, *100*, 853. (d) Holliday, B. J.; Mirkin, C. A. *Angew. Chem., Int. Ed.* **2001**, *40*, 2022. (e) Eddaoudi, M.; Moler, D. B.; Li, H.; Chen, B.; Reineke, T. M.; O.-Keeffe, M.; Yaghi, O. M. *Acc. Chem. Res.* **2001**, *34*, 319. (f) Farha, O. K.; Hupp, J. T. *Acc. Chem. Res.* **2010**, *43*, 1166.
2. (a) Ito, H.; Kusukawa, T.; Fujita, M. *Chem. Lett.* **2000**, *29*, 598. (b) Cacciapaglia, R.; Stefano, S. D.; Mandolini, L. *Acc. Chem.Res.* **2004**, *37*, 113. (c) Fiedler, D.; Leung, D. H.; Bergman, R. G.; Raymond, K. N. *Acc. Chem. Res.* **2005**, *38*, 349. (d) Pluth, M. D.; Bergman, R. G.; Raymond, K. N. *Acc. Chem. Res.***2009**, *42*, 1650. (e) Corma, A.; García, H.; L-Xamena, F. X. *Chem. Rev.*

2010, *110*, 4606. (f) Fox, O. D.; Cookson, J.; Wilkinson, E. J. S.; Drew, M. G. B.; MacLean, E. J.; Teat, S. J.; Beer, P. D. *J. Am. Chem. Soc*. **2006**, *128*, 6990. (g) Fielder, D.; Bergman, R. G.; Raymond, K. N. *Angew. Chem., Int. Ed.* **2004**, *43*, 6748. (h) Yoshizawa, M.; Takeyama, Y.; Okano, T.; Fujita, M. *J. Am. Chem. Soc.* **2003**, *125*, 3243. (i) Merlau, M. L.; Meija, M. P.; Nguyen, S. T.; Hupp, J. T. *Angew. Chem., Int. Ed.* **2001**, *40*, 4239. (j) Bell, Z. R.; Harding, L. P.; Ward, M. D. *Chem. Commun.* **2003**, 2432. (k) Fiedler, D.; Pagliero, D.; Brumaghim, J. L.; Bergman, R. G.; Raymon, K. N. *Inorg. Chem.* **2004**, *43*, 846. (l) Leung, D. H.; Fiedler, D.; Bergman, R. G.; Raymond, K. N. *Angew. Chem., Int. Ed.* **2004**, *43*, 963. (m) Argent, S. P.; Riis-Johannessen, T.; Jeffery, J. C.; Harding, L. P.; Ward. M. D. *Chem. Commun*. **2005**, 4647.

3. (a) Fujita, M. *Chem. Soc. Rev.* **1998**, *27*, 417. (b) Hawthorne, M. F.; Zheng, Z. *Acc. Chem. Res.* **1997**, *30*, 267. (c) Beer, P. D.; Gale, P. A. *Angew. Chem., Int. Ed.* **2001**, *40*, 486. (d) Chen, B.; Xiang, S.; Qian, G. *Acc. Chem. Res.* **2010**, *43*, 1115. (e) Uppadine, L. H.; Weeks, J. M.; Beer, P. D. *J. Chem. Soc., Dalton Trans.* **2001**, 3367. (g) Wong, W. W. H.; Cookson, J.; Evans, E. A. L.; McInnes, E. J. L.; Wolowska, J.; Maher, J. P.; Bishop, P.; Beer, P. D. *Chem. Commun*. **2005**, 2214. (h) Beer, P. D.; Berry, N. G.; Drew, M. G. B.; Fox, O. D.; Padilla-Tosta, M. E.; Patell, S. *Chem. Commun.* **2001**, 199. (i) Webber, P. R. A.; Drew, M. G. B.; Hibbert, R.; Beer, P. D. *Dalton Trans*., **2004**, 1127.
4. (a) Beer, P. D. *Acc. Chem. Res.* **1998**, *31*, 71. (b) E.-Aroussi, B.; Guénée, L.; Pal, P.; Hamacek, J. *Inorg. Chem.* **2011**, *50*, 8588.
5. (a) Sanchez, C.; Julián, B.; Belleville, P.; Popall, M. *J. Mater. Chem.* **2005**, *15*, 3559. (b) Mueller, U.; Schubert, M.; Teich, F.; Puetter, H.; S.-Arndt, K. Pastré, J. *J. Mater. Chem.* **2006**, *16*, 626. (c) Finsy, V.; Verelst, H.; Alaerts, L.; D.-Vos, D.; Jacobs, P. A.; Baron, G. V.; Denayer, J. F. M. *J. Am. Chem. Soc.* **2008**, *130*, 7110. (d) Duan, L.; Wu, Z.-H.; Ma, J.-P.; Wu, X.-W.; Dong, Y.-B. *Inorg. Chem.* **2010**, *49*, 11164.
6. Cougnon, F. B. L. Sanders, J. K. M. *Acc. Chem. Res.* **2012**, *45*, 2211.
7. Kirchner, M.T.; Bläser, D.; Boese, R. *Chem. Eur. J.* **2010**, *16*, 2131.
8. (a) Olguín, J.; Kalisz, M.; Clérac, R.; Brooker, S. *Inorg. Chem*., **2012**, *51*, 5058. (b) Gavrilova, A. L.; Bosnich, B. *Chem. Rev*. **2004,** *104*, 349. (c) Klingelea, J.; Dechert, S.; Meyer, F. *Coord. Chem. Rev*. **2009**, *253*, 2698.

9. (a) Hambley, T. W. Dalton Trans. **2007**, 4929. (b) Orvig, C.; Abrams, M. J. *Chem. Rev*. **1999**, 99, 2201. (c) Thompson, K. H.; Orvig, C. *Dalton Trans*. **2006**, 761.
10. Bruijnincx, P. C. A.; Sadler, P. J. *Curr. Opin. Chem. Biol*. **2008**, *12*, 197.
11. (a) Jung, Y. W.; Lippard, S. J. *Chem. Rev*. 2007, *107*, 1387. (b) Singh, S. K.; Joshi, S.; Singh, A. R.; Saxena, J. K.; Pandey, D. S. *Inorg. Chem*. **2007**, *46*, 10869. (c) Gupta,R. K.; Pandey,R.; Sharma, G.; Prasad, R.; Koch, B.; Srikrishna, S.; Li,P.-Z.;Xu,Q.; Pandey, D. S. *Inorg. Chem*. **2013**, *52*, 3687. (d) Gupta,R. K.; Sharma,G.; Pandey,R.; Kumar,A.; Koch,B.; Li, P.-Z.; Xu, Q.; Pandey, D. S. *Inorg. Chem*. **2013**, *52*, 13984.
12. (a) Kaluđerović, G. N.; Kommera, H.; H.-Hawkins, E.; Paschke, R.; G.-Ruiz, S. *Metallomics***2010**, *2*, 419. (b) Boulikas, T.; Pantos, A.; Bellis, E.; Christofis, P. *Cancer Ther*. **2007**, *5*, 537. (c) van Zutphen, S.; Reedijk, J. *Coord. Chem. Rev*. **2005**, *249*, 2845. (d) Gust, R.; Beck, W.; Jaouen, G.; Schoenenberger, H. *Coord. Chem. Rev*. **2009**, *253*, 2760. (e) Gust, R.; Beck, W.; Jaouen, G.; Schoenenberger, H. *Coord. Chem. Rev*. **2009**, *253*, 2742.
13. (a) Wang, T.; Guo, Z. J. *Curr. Med. Chem*. **2006**, *13*, 525. (b) Tisato, F.; Marzano, C.; Porchia, M.; Pellei, M.; Santini, C. *Med. Res. Rev*. **2010**, *30*, 708. (c) Tardito, S.; Marchio, L. *Curr. Med. Chem*. **2009**, *16*, 1325. (d) Duncan, C.; White, A. R. *Metallomics***2012**, *4*, 127. (e) Marzano, C.; Pellei, M.; Tisato, F.; Santini, C. *Med. Chem*. **2009**, *9*, 185.
14. (a) Driggers, E.M.; Hale, S. P.; Lee, J.; Terrett, N. K. *Nat. Rev. Drug Discov*.**2008**, *7*, 608. (b) Mallinson, J.; Collins, I. *Future Med. Chem.* **2012**, *4*, 1409. (c) Mann A. Conformational restriction and/or steric hindrance in medicinal chemistry. In: *The Practice Of Medicinal Chemistry*, Wermuth CG (Ed.). Academic Press, London, UK 2008.
15. Alama, A.; Tasso, B.; Novelli, F.; Sparatore, F. *Drug Discovery Today***2009**, *14*, 500.
16. Rehman, Z.; Shah, A.; Muhammad, N.; Ali, S.; Qureshi, R.; Meetsma, A.; Butler, I. S. *Eur. J. Med. Chem.***2009**, *44*, 3986.
17. Bodenner, D. L.; Dedon, P. C.; Keng, P. C. *Cancer Res.* **1986**, *46*, 2745.
18. (a) Suda, Y.; Arano, A.; Fukui, Y.; Koshida, S.; Wakao, M.; Nishimura, T.; Kusumoto, S.; Sobel, M. *Bioconjugate Chem.* **2006**, *17*, 1125. (b) Mahon, A. B.;

Arora, P. S. *Chem. Commun.* **2012**, *48*, 1416. (d) Stoffregen, S. A.; Griffin, A. K. K.; Kostic, N. M. *Inorg. Chem.* **2005**, *44*, 8899. (c) Dougan, S. J.; Habtemariam, A.; McHale, S. E.; Parsons, S.; Sadler, P. J. *Proc. Natl. Aacad. Sci. U.S.A.* **2008**, *105*, 11628. (d) Esposito, B. P.; Najjar, R. *Coord. Chem. Rev.* **2002**, *232*, 137.

19. (a) Tonkin, E. G., Valentine, H. L., Zimmerman, L. J., and Valentine, W. M. *Toxicol. Appl. Pharmacol.* **2003**, *189*, 139. (b) Valentine, H. L.; Viquez, O. M.; Amarnath, K.; Amarnath, V.; Zyskowski, J.; Kassa, E. N.; Valentine, W. M. Chem. Res. Toxicol. 2009, 22, 218. (c) Johnson, D. J., Graham, D. G., Amarnath, V., Amarnath, K., Valentine, W. M. *Toxicol. Appl. Pharmacol.* **1998**, *148*, 288.
20. (a) Ronconi, L.; Giovagnini, L.; Marzano, C.; Bettío, F.; Graziani, R.; Pilloni, G.; Fregona, D. *Inorg. Chem.* **2005**, *44*, 1867. (b) Giovagnini, L.; Sitran, S.; Montopoli, M.; Caparrotta, L.; Corsini,M.; Rosani,C.; Zanello,P.; Dou, Q. P.; Fregona, D. *Inorg. Chem.* **2008**, *47*, 6336. (c) Keter,F. K.; Guzei, I. A.; Nell, M.; van Zyl, W. E.; Darkwa, J. *Inorg. Chem.* **2014**, *53*, 2058. (d) Ronconi, L.; Marzano, C.; Zanello, P.; Corsini, M.; Miolo, G.; Maccá, C.; Trevisan, A.; Fregona, D. *J. Med. Chem.* **2006,** *49*, 1648.
21. Tanaka, K.; Ino, T.; Sawahata, T.; Marui, S.; Igaki, H.; Yashima,H. *Mutat. Res.* **1985**, *143*, 11.
22. Singh, V. K.; Kadu, R.; Roy, H. *Eur. J. Med. Chem.***2014**, *74*, 552.
23. Kadu, R.; Singh, V. K.; Verma, S. K.; Raghavaiah, P.; Shaikh M. M. *J Mol. Struct*. **2013**, *1033*, 298.
24. ‘‘CrysAlispro’’ program (Version 1.171.37.33 Agilent Technologies, 2014).
25. Sheldrick, G.M. SHELXL-97: program for crystal structure refinement, University of Göttingen, Göttingen, Germany, 1997.
26. Olex2 (version 1.2.5) program package: Dolomanov, O.V.; Bourhis, L.J.; Gildea, R.J.; Howard, J.A.K.; Puschmann, H., OLEX2: A complete structure solution, refinement and analysis program. *J. Appl. Cryst.*, **2009**, *42*, 339.
27. Manosroi, J.; Dhumtanom, P.; Manosroi, A. *Cancer Lett.***2006**, *235*, 114.
28. Kalgotra, N.; Gupta, B.; Kumar, K.; Pandey, S. K. *Phosphorus, Sulfur, and Silicon*, **2012**, *187*, 364.

29. Veetil, A. T.; Šolomek, T.; Ngoy, B. P.; Pavlíková, N.; Heger, D.; Klán, P. *J. Org. Chem*. **2011**, *76*, 8232.
30. Beer, P. D.; Cowley, A. R.; Jeffery, J. C.; Paul, R. L.; Wong, W. W.H. *Polyhedron***2003**, *22*, 795.
31. Johnson, A. L.; Hill, M. S.; K.-Köhn, G.; Molloy, K. C.; Sudlow, A. L. *Inorg. Chem. Commun*. **2014**, *49*, 8.
32. (a) Yoshida,N.; Oshio, H.; Ito, T., *J. Chem. Soc., Perkin Trans. 2*, **1999**, 975. (b) Arbuse, A.; Mandal, S.; Maji, S.; Martínez, M. A.; Fontrodona, X.; Utz, D.; Heinemann, F. W.; Kisslinger, S.; Schindler, S.; Sala, X.; Llobet, A. *Inorg. Chem*. **2011**, *50*, 6878.
33. Pang, Y.; Cui, S.; Li, B.; Zhang, J.; Wang, Y.; Zhang, H. *Inorg. Chem.*, **2008**, *47*, 10317.
34. Plyusnin, V. F.; Kolomeets, A. V.; Grivin, V. P.; Larionov, S. V.; Lemmetyinen, H. *J. Phys. Chem. A***2011**, *115*, 1763.
35. (a) Verma, S. K.; Singh, V. K. *Polyhedron***2015**, *85*, 971. (b) Hogarth, G.; R.-Brent, E.-J. C.-R. C. R.; Kabir, S. E.; Richards I.;, W.-Ely, J. D. E. T.; Zhang, Q. *Inorg. Chim. Acta***2009**, *362*, 2020.
36. (a) Coucouvanis, D. *Prog. Inorg. Chem.* **1979**, *26*, 301. (b)Rajput, G.; Singh, V.; Singh, S. K.; Prasad, L. B.; Drew, M. G. B.; Singh,N. *Eur. J. Inorg. Chem.* 2012, 3885.
37. (a) Chauhan H. P. S.; Bakshi, A. *J Therm. Anal. Calorim.*,**2011**, 105, 937. (b) Singhal, A.; Dutta, D. P.; Tyagi, A. K.; Mobin, S. M.; Mathur, P.; Lieberwirth,I. *J. Organomet. Chem.*, **2007**, 692, 5285.
38. 'POWDERX'' – A program for indexing and refinement of X-ray data written by Dr. V. K. Wadhavan, Bhabha Atomic research Centre, private communication.
39. Gupta, R. K.; Pandey, R.; Singh, R.; Srivastava, N.; Maiti, B.; Saha, S.; Li, P.; Xu, Q.; Pandey, D. S. *Inorg. Chem.*, **2012**, *51*, 8916.
40. Sreedaran, S.; Bharathi, K. S.; Rahiman, A. K.; Jagadish, L.; Kaviyarasan, V.; Narayanan, V. *Polyhedron***2008**, *27*, 2931.
41. (a) Royzen, M.; Durandin, A.; Young, V. G., Jr.; Geacintov, N. E.; Canary, J. W. *J. Am. Chem. Soc*. **2006**, *128*, 3854. (b) Zhang, X.; Shiraishi, Y.; Hirai, T. *Org. Lett*. **2007**, *9*, 5039. (c) Domaille, D. W.; Que, E. L.; Chang, C. *J. Nat.*

Chem. Biol. **2008**, *4*, 168. (d) Ray, D.; Bharadwaj, P. K. *Inorg. Chem*. **2008**, *47*, 2252.

42. (a) Jung, W. K.; Koo, H. C.; Kim, K. W.; Shin, S.; Kim, S. H.; Park, Y. H. *Appl. Environ. Microbiol*. **2008**, *74*, 2171. (b) Melaiye, A.; Simons, R. S.; Milsted, A.; Pingitore, F.; Wesdemiotis, C.; Tessier, C. A.; Youngs, W. J. *J. Med. Chem*. **2004**, *47*, 973. (c) Melaiye, A.; Sun, Z.; Hindi, K.; Milsted, A.; Ely, D.; Reneker, D. H.; Tessier, C. A.; Youngs, W. J. *J. Am. Chem. Soc*. **2005**, *127*, 2285. (d) Butkus, M. A.; Labare, M. P.; Starke, J. A.; Moon, K.; Talbot, M. *Appl. Environ. Microbiol*. **2004**, *70*, 2848. (g) Petering, H. G. *Pharmacol. Ther. A***1976**, *1*, 127. (e) Russell, A. D.; Hugo, W. B. *Prog. Med. Chem*. **1994**, *31*, 351. (f) Silver, S.; Phung, L. T.; Silver, G. *J.Ind. Microbiol. Biotechnol*. **2006**, *33*, 627.
43. (a) Xie, H.; Kang, Y. J. *Curr. Med. Chem*. **2009**, *16*, 1304. (b) Yoo, J. Y.; Pradarelli, J.; Haseley, A.; Wojton, J.; Kaka, A.; Bratasz, A.; Alvarez-Breckenridge, C. A.; Yu, J.-G.; Powell, K.; Mazar, A. P.; Teknos, T. N.; Chiocca, E. A.; Glorioso, J. C.; Old, M.; Kaur, B. *Clin. Cancer Res*. **2012**, *18*, 4931. (c) Wang, F.; Jiao, P.; Qi, M.; Frezza, M.; Dou, Q. P.; Yan, B. *Curr. Med. Chem*. **2010**, *17*, 2685. (d) Ishida, S.; McCormick, F.; S.-McCune, K.; Hanahan, D. *Cancer Cell***2010**, *17*, 574.
44. (a) Que, E. L.; Domaille, D. W.; Chang, C. *J. Chem. Rev*. **2008**, *108*, 1517. (b) Barceloux, D. G.; Barceloux, D. *J. Clin. Toxicol*. **1999**, *37*, 217. (c) Yardim, M. F.; Budinova, T.; Ekinci, E.; Petrov, N.; Razvigorova, M.; Minkova, V. *Chemosphere***2003**, *52*, 835. (d) Løvstad, R. A. *BioMetals***2004**, *17*, 111. (e) Sarkar, B. In Metal ions in biological systems; Siegel, H., Siegel, A., Eds.; Marcel Dekker: New York, 1981; Vol. 12, pp 233.
45. S. K. Verma, R. Kadu, V. K Singh, *Synth. React. Inorg. Metal-Org. Nano-Metal Chem*. **2014**, *44*, 441.
46. Pandey, R.; Kumar, P.; Singh, A. K.; Shahid, M.; Li, P.-z.; Singh, S. K.; Xu, Q.; Misra, A.; Pandey, D. S. *Inorg. Chem.* **2011**, *50*, 3189.
47. Kochem, A. Kanso, H. Baptiste, B. Arora, H. Philouze, C. Jarjayes, O. Vezin, H. Luneau, D. Orio, M. Thomas, F. *Inorg. Chem*. **2012**, *51*, 10557.
48. Yoshida, N.; Ito, N.; Ichikawa, K. *J. Chem. Soc., Perkin Trans. 2*, **1997**, 2387.

49. Frisch, M. J.; Trucks, G. W.; Schlegel, H. B.; Scuseria, G. E.; Robb, M. A.; Cheeseman, J. R.; Montgomery Jr., J. A.; Vreven, T.; Kudin, K. N.; Burant, J. C.; Millam, J. M.; Iyengar, S. S.; Tomasi, J.; Barone, V.; Mennucci, B.; Cossi, M.; Scalmani, G.; Rega, N.; Petersson, G. A.; Nakatsuji, H.; Hada, M.; Ehara, M.; Toyota, K.; Fukuda, R.; Hasegawa, J.; Ishida, M.; Nakajima, T.; Honda, Y.; Kitao, O.; Nakai, H.; Klene, M.; Li, X.; Knox, J. E.; Hratchian, H. P.; Cross, J. B.; Adamo, C.; Jaramillo, J.; Gomperts, R.; Stratmann, R. E.; Yazyev, O.; Austin, A. J.; Cammi, R.; Pomelli, C.; Ochterski, J. W.; Ayala, P. Y.; Morokuma, K.; Voth, G. A.; Salvador, P.; Dannenberg, J. J.; Zakrzewski, V. G.; Dapprich, S.; Daniels, A. D.; Strain, M. C.; Farkas, O.; Malick, D. K.; Rabuck, A. D.; Raghavachari, K.; Foresman, J. B.; Ortiz, J. V.; Cui, Q.; Baboul, A. G.; Clifford, S.; Cioslowski, J.; Stefanov, B. B.; Liu, G.; Liashenko, A.; Piskorz, P.; Komaromi, I.; Martin, R. L.; Fox, D. J.; Keith, T.; A.-Laham, M. A.; Peng, C. Y.; Nanayakkara, A.; Challacombe, M.; Gill, P. M. W.; Johnson, B.; Chen, W.; Wong, M. W.; Gonzalez, C.; Pople, J. A.; Gaussian, Inc., Wallingford, CT, **2004**.
50. Salehzadeh, S.; Bayat,M. *Comp. Theor.Chem*. **2011**, *965*, 131.
51. Vladimirova, K. G.; Freidzon, A. Y.; Kotova, O. V.; Vaschenko, A. A.; Lepnev, L. S.; Bagatur'yants, A. A.; Vitukhnovskiy, A. G.; Stepanov, N. F.; Alfimov, M. V. *Inorg. Chem.* **2009**, *48*, 11123.
52. Verma, S. K.; Singh, V. K. *Polyhedron***2015**, *85*, 971.
53. (a) Gadre, S. R.; Bhadane, P. K. *Resonance*, **1999**, *4*, 11. (b) Bulat, F. A.; T.-Labbé, A.; Brinck, T.; Murray, J. S.; Politzer, P. *J Mol Model***2010**, *16*, 1679. (c) Politzer, P.; Laurence, P. R.; Jayasuriya, K. *Environ. Health Perspect.***1985**, *61*, 191.
54. Peerannawar, S. R.; Gejji S. P., *Phys. Chem. Chem. Phys*., **2012**, ***14***, 8711.
55. (a) Bach, S. P.; Chinery, R.; O'Dwyer, S. T.; Potten, C. S.; Coffey, R. J.; Watson, A. J. *Gastroenterology* **2000**, *118*, 81. (b) Daniel, K. G.; Chen, D.; Orlu, S.; Cui, Q. C.; Miller, F. R.; Dou, Q. P. *Breast Cancer Res.* **2005**, *7*, R897. (c) Segovia, N.; Crovetto, G.; Lardelli, P.; Espigares, M. J. Appl. Toxicol. 2002, 22, 353. (d) Viquez, O. M.; Valentine, H. L.; Amarnath, K.; Milatovic, D.; Valentine, W. M. Toxicol. Appl. Pharmacol. 2008, 229, 77. (e) Chabicovsky, M.; P.-Grassauer, E.; Seipelt, J.; Muster, T.; Szolar, O. H. J.; Hebar, A.;

Doblhoff-Dier, O. Basic Clin. Pharmacol. Toxicol. 2010, 107, 758. (f) Nagy, E. M.; Sitran, S.; Montopoli, M.; Favaro, M.; Marchiò, L.; Caparrotta, L.; Fregona, D. *J Inorg. Biochem*. **2012**, *117*, 131. (g) Qian, Y.; Ma, G.-Y.; Yang, Y.; Cheng, K.; Zheng, Q.-Z.; Mao, W.-J.; Shi, L.; Zhao, J.; Zhu,H.-L. *Bioorg. Med. Chem*. **2010**, *18*, 4310.

56. (a) Amarnath, V.; Amarnath, K.; Valentine, W. M. *Curr. Top. Toxicol.***2007**, *4*, 39. (b) Garcia, J. I.; Humeres, E. *J. Org. Chem.* **2002**, *67*, 2755. (c) Humeres, E.; Debacher, N. A.; Franco, J. D.; Lee, B. S.; Martendal, A. *J. Org. Chem.* **2002**, *67*, 3662. (d) Humeres, E., Debacher, N. A., and Sierra, M. M. *J. Org. Chem.* **1999**, *64*, 1807.
57. (a) Milacic, V.; Chen, D.; Ronconi, L.; Landis-Piwowar, K. R.; Fregona, D.; Dou, Q. P. *Cancer Res.* **2006**, *66*, 10478–10486. (b) Chen, D.; Cui, Q. Z. C.; Yang, H. J.; Dou, Q. P. *Cancer Res.* **2006**, *66*, 10425–10433. (c) Daniel, K. G.; Gupta, P.; Harbach, R. H.; Guida, W. C.; Dou, Q. P. *Biochem. Pharmacol.* **2004**, *67*, 1139. (d) Chen, D.; Frezza, M.; Shakya, R.; Cui, Q. C.; Milacic, V.; Verani, C. N.; Dou, Q. P. *Cancer Res.* **2007**, *67*, 9258. (e) Daniel, K. G.; Chen, D.; Orlu, S.; Cui, Q. C.; Miller, F. R.; Dou, Q. P. *Breast Cancer Res*. **2005**, *7*, R897. (f) Chen, D.; Peng, F.; Cui, Q. C.; Daniel, K. G.; Orlu, S.; Liu, J.; Dou, Q. P. *Front. Biosci*. **2005**, *10*, 2932.
58. (a)Cvek, B.; Milacic, V.; Taraba, J.; Dou, Q. P. *J. Med. Chem*. **2008**, *51*, 6256. (b) Milacic, V.; Chen, D.; Giovagnini, L.; Diez, A.; Fregona, D.; Dou, Q. P. *Toxicol. Appl. Pharmacol.***2008**, *231*, 24.
59. (a) M. N.; Patel, M. R.; Chhasatia, Gandhi, D. S. Bioorg. *Med. Chem. Lett*. **2009**, *19*, 2870. (b) Wang, X.-Y.; Zhang, J.; Li, K.; Jiang, N.; Chen, S.-Y.; Lin, H.-H.; Huang, Y.; Ma, L.-J.; Yua, X.-Q. *Bioorg. Med. Chem*. **2006**, *14*, 6745. (c) Buchtik, R.; Travnicek, Z.; Vanco, J.; Herchel, R.; Dvorak, Z. *Dalton Trans*. **2011**, *40*, 9404. (d) Bhat, S. S.; Kumbhar, A. A.; Heptullah, H.; Khan, A. A.; Gobre, V. V.; Gejji, S. P.; Puranik, V. G. *Inorg. Chem*. **2011**, *50*, 545. (e) G.-Gimenez, L. J.; G.-Alvarez, M.; L.-Gonzalez, M.; Macias, B.; Borras, J.; Alzuet, G. *J. Inorg. Biochem*. **2009**, *103*, 923. (f) Buchtik, R.; Travnicek, Z.; Vanco, J. *J. Inorg. Biochem*. **2012**, *116C*, 163. (g) Arjmand, F.; Muddassir, M. *Chirality***2011**, *23*, 250.

60. Chin, L. F.; Kong, S. M.; Seng, H. L.; Khoo, K. S.; Vikneswaran, R.; Teoh, S. G.; Ahmad, M.; Khoo, S. B. A.; Maah, M. J.; Ng, C. H. *J. Inorg. Biochem*. **2011**, *105*, 339.

61. (a) Piazzi, L.; Cavalli, A.; Belluti, F.; Bisi, A.; Gobbi, S.; Rizzo, S.; Bartolini, M.; Andrisano, V.; Recanatini, M.; Rampa, A. *J. Med. Chem*. **2007**, *50*, 4250. (b) Ferreira, I. P.; de Lima, G. M.; Paniago, E. B.; Rocha, W. R.; Takahashi, J. A.; Pinheiro, C. B.; Ardisson, J. D. *Eur. J. Med. Chem*. **2012**, *58*, 493. (c) Soares, M. A.; Lessa, J. A.; Mendes, I. C.; Da Silva, J. G.; dos Santos, R. G.; Salum, L. B.; Daghestani, H.; Andricopulo, A. D.; Day, B. W.; Vogt, A.; Pesquero, J. L.; Rocha, W. R.; Beraldo, H. *Bioorg. Med. Chem*. **2012**, *20*, 3396.

62. Parrilha, G. L.; da Silva, J. G.; Gouveia, L. F.; Gasparoto, A. K.; Dias, R. P.; Rocha, W. R.; Santos, D. A.; Speziali, N. L.; Beraldo, H. *Eur. J. Med. Chem*. **2011**, *46*, 1473.

63. (a) Jiang, W.; Fu, Y.; Yang, F.; Yang, Y.; Liu, T.; Zheng, W.; Zeng, L.; Chen, T. *ACS Appl. Mater. Interfaces* **2014**, *6*, 13738.(b)Kim, G.; Kim, W.; Kim, K.; Lee, J. *Appl. Phys. Lett*. **2010**, *96*, 021502.

64. (a) Wlodkowic, D.; Faley, S.; Zagnoni, M.; Wikswo, J. P.; Cooper, J. M. *Anal. Chem*. **2009**, *81*, 5517. (b) Wlodkowic, D.; Skommer, J. Z.; Darzynkiewicz, *Cytometry, Part A*, **2008**, *73*, 496. (c) Hanahan, D.; Weinberg, R. A. *Cell* **2000**, *100*, 57. (d) Wlodkowic, D.; Skommer, J.; Faley, S.; Darzynkiewicz, Z.; Cooper, J. M. *Exp. Cell Res.***2009**, *315*, 1706.

65. (a) Oltmanns, D.; Z.-Kolbe, S.; Mueller, A.; B.-Wuest, U.; Schaefer, M.; Eder, M.; Haberkorn, U.; Eisenhut, M. *Bioconjugate Chem.* **2011**, *22*, 2611. (b) Herrmann, S. M.; S.-Osthoff, K.; Lauber, K. J. *Immunol*. **2009**, *183*, 8138.

2.6. Annexures:

2.6.1. Spectral Characterization

Mass spectra

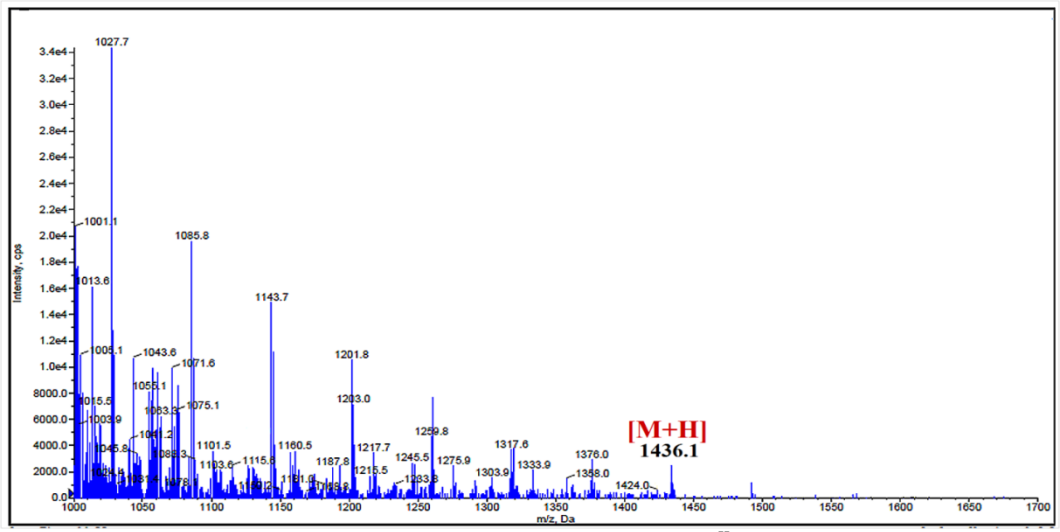

Annexure 1. ES-MS of binuclear metallamacrocyclic Co^{II} xanthate complex **2**.

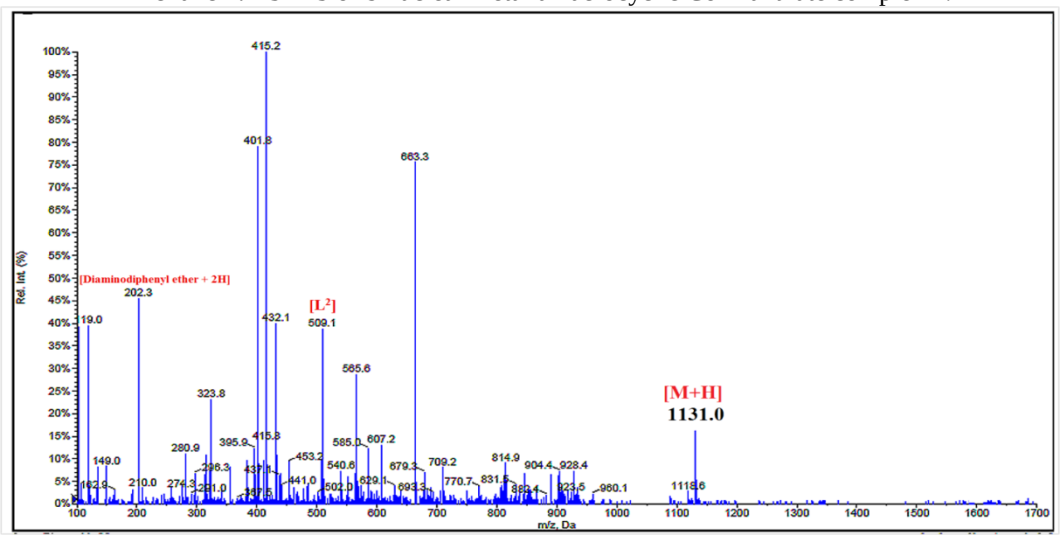

Annexure 2. ES-MS of binuclear metallamacrocyclic Co^{II}*N, O*-Schiff base complex **6.**

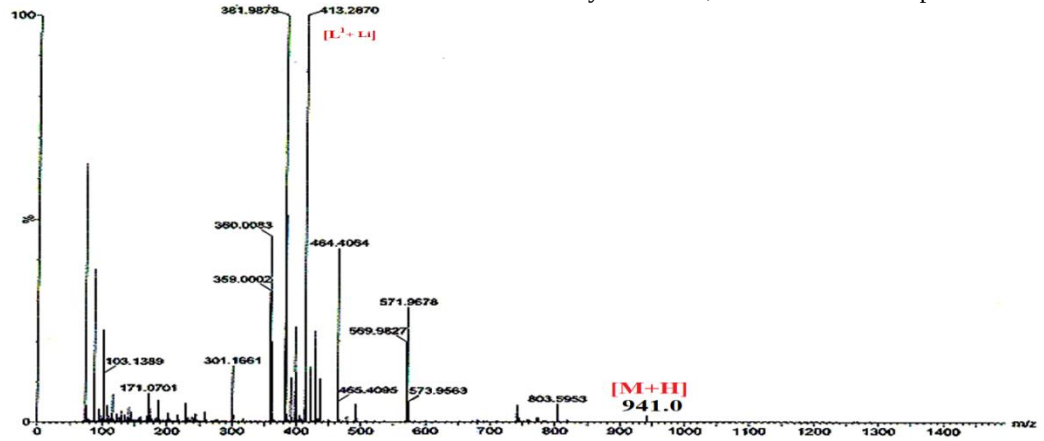

Annexure 3. MALDI-TOF MS of binuclear metallamacrocyclic Cu^{II}*N, O*-Schiff base complex **7**.

The stacked IR spectra of **K_2xan^1**, its binuclear xanthate complex **1** and corresponding binuclear *N*,*O*-Schiff base complex **5** as well as **K_2xan^1**, its binuclear xanthate complex **3** and corresponding binuclear *N*,*O*-Schiff base complex **7** are given in following figure, which clearly reveal the structural variations.

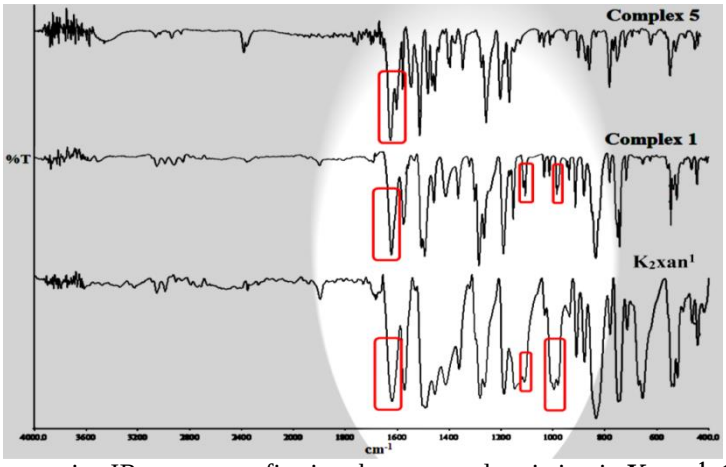

Annexure 4: Representative IR spectra confirming the structural variation in **K_2xan^1**, **1** and **5**.

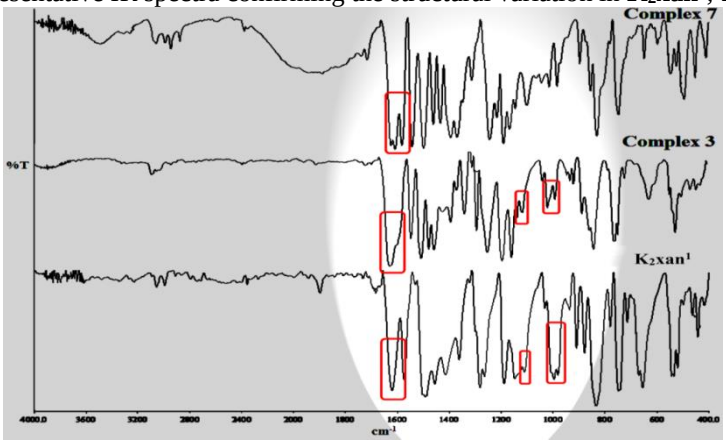

Annexure 5: Representative IR spectra confirming the structural variation in **K_2xan^1**, **3** and **7**.

NMR spectral data

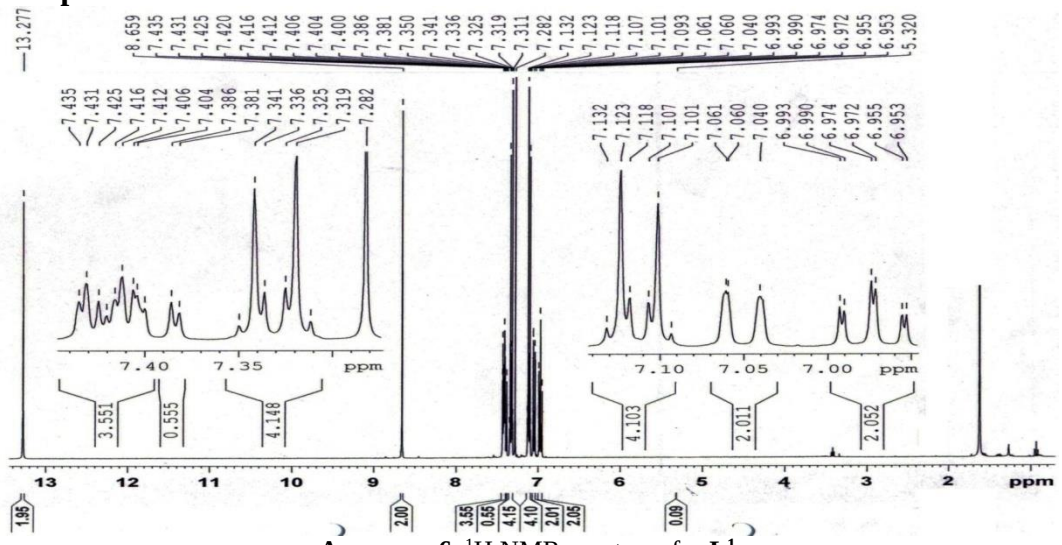

Annexure 6. ^{1}H NMR spectrum for **L^1**

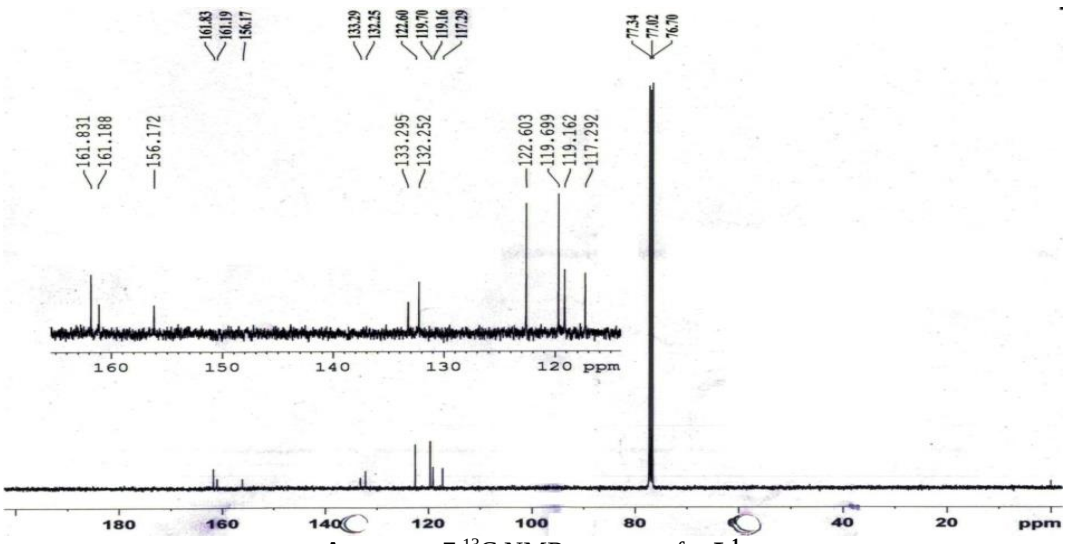

Annexure 7. ^{13}C NMR spectrum for **L[1]**

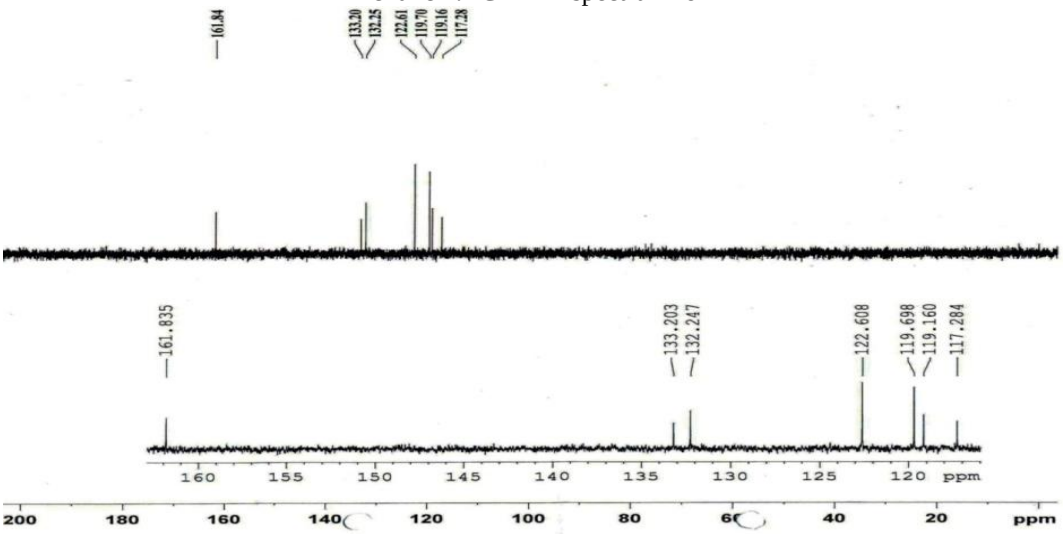

Annexure 8. DEPT-135 NMR spectrum for **L[1]**

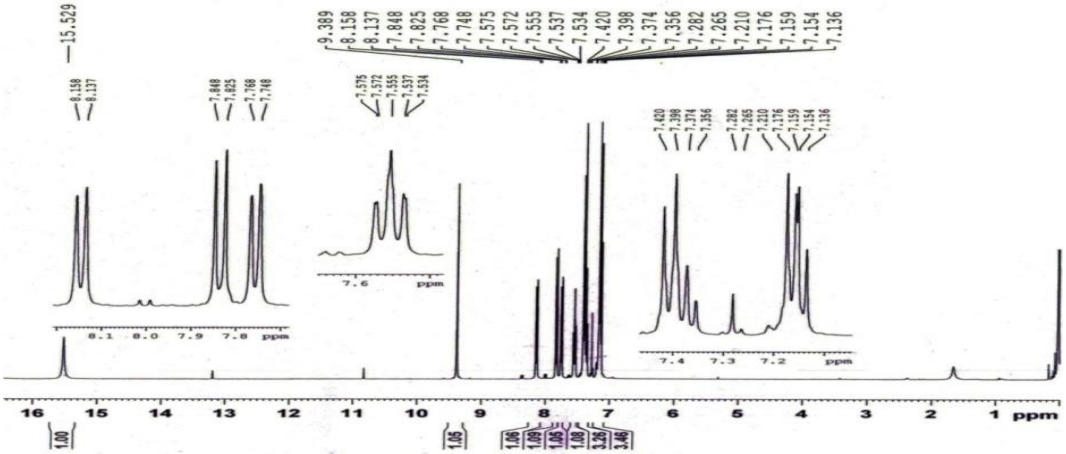

Annexure 9. ^{1}H NMR spectrum for **L[2]**

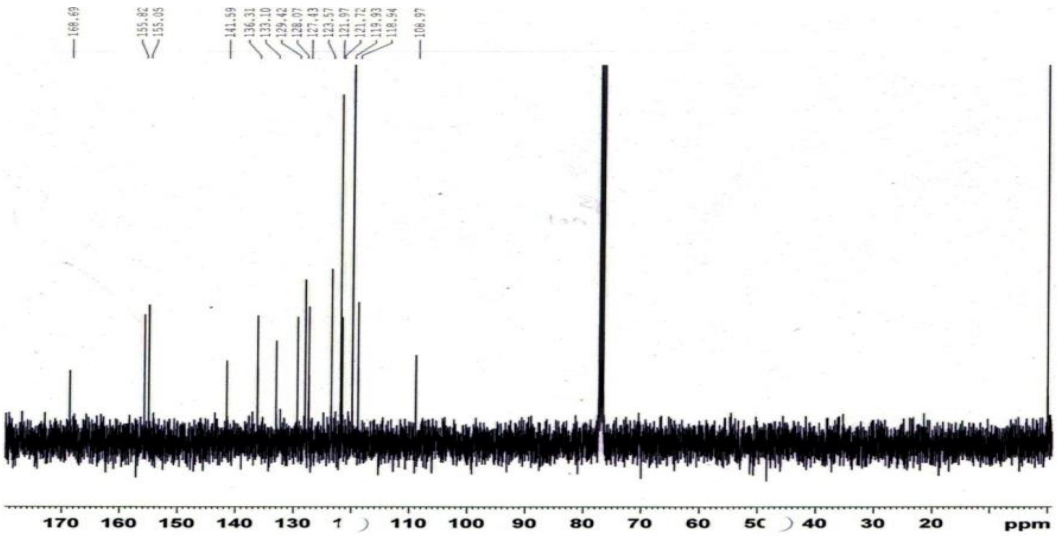

Annexure 10. ^{13}C NMR spectrum for **L[2]**

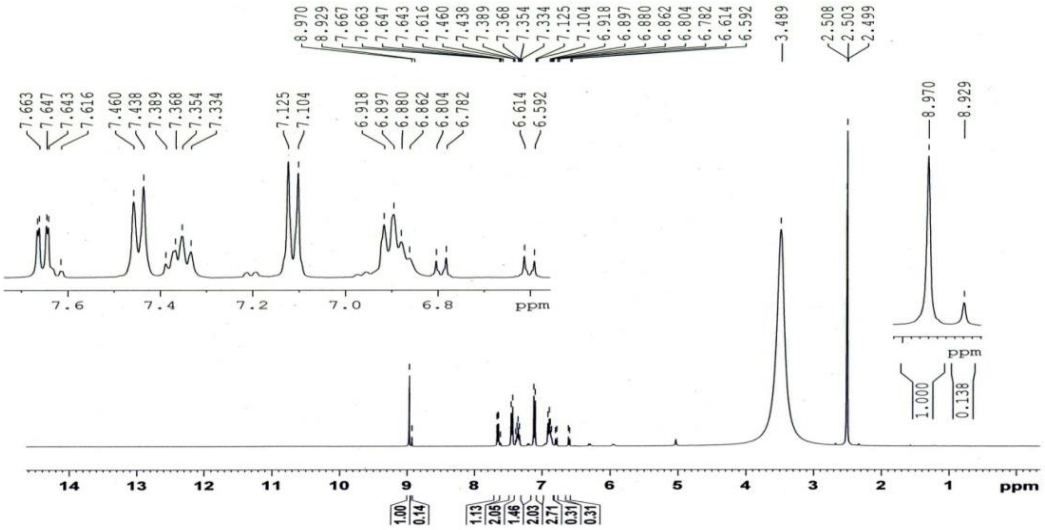

Annexure 11. ^{1}H NMR spectrum for **K_2xan[1]**

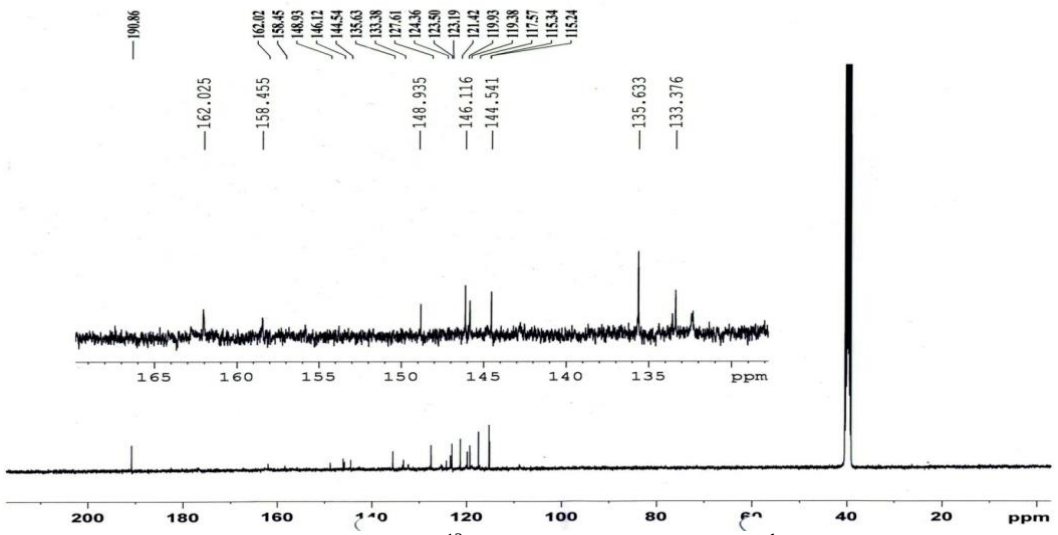

Annexure 12. ^{13}C NMR spectrum for **K_2xan[1]**

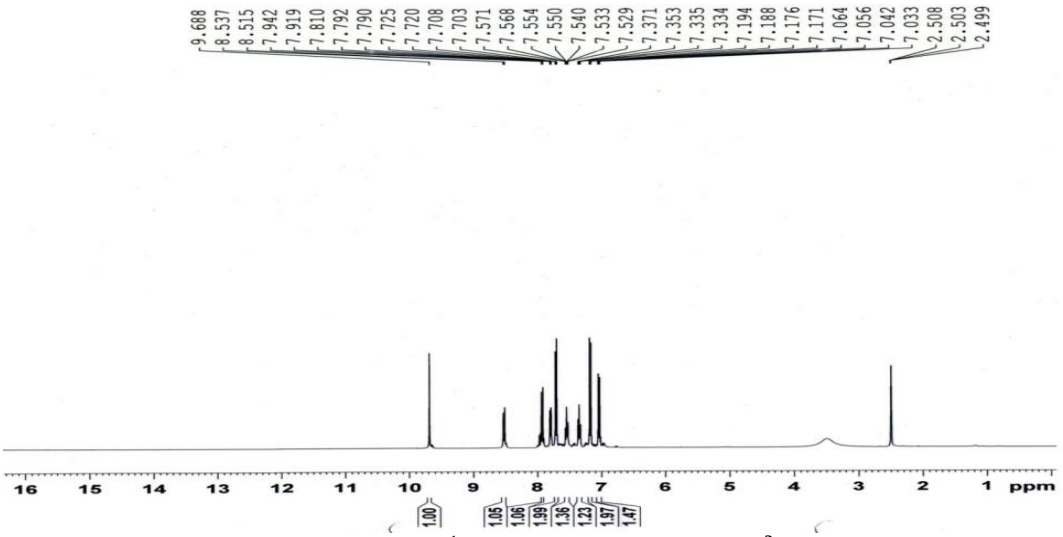

Annexure 13. ^{1}H NMR spectrum for **K$_2$xan^2**

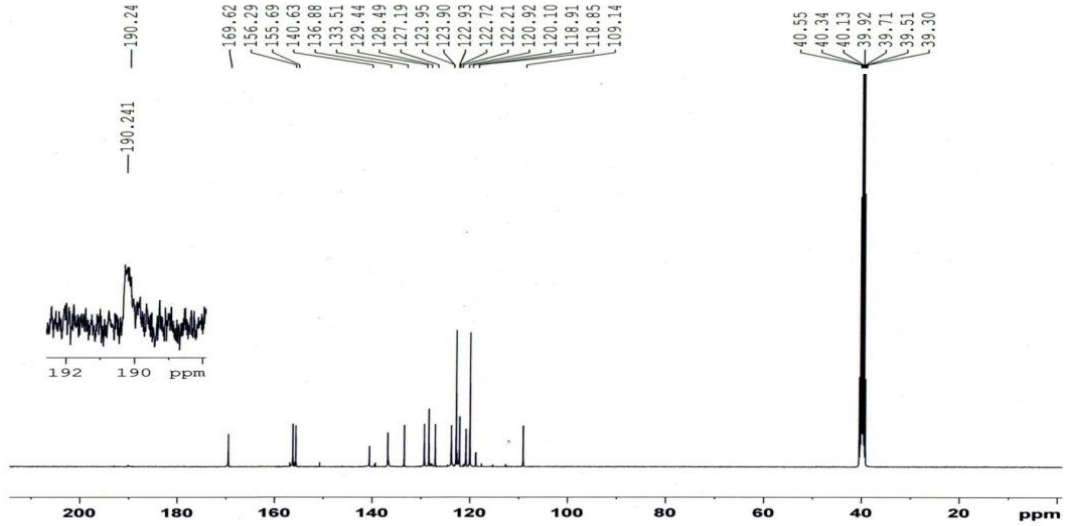

Annexure 14. ^{13}C NMR spectrum for **K$_2$xan^2**

2.6.2. Powder XRD.

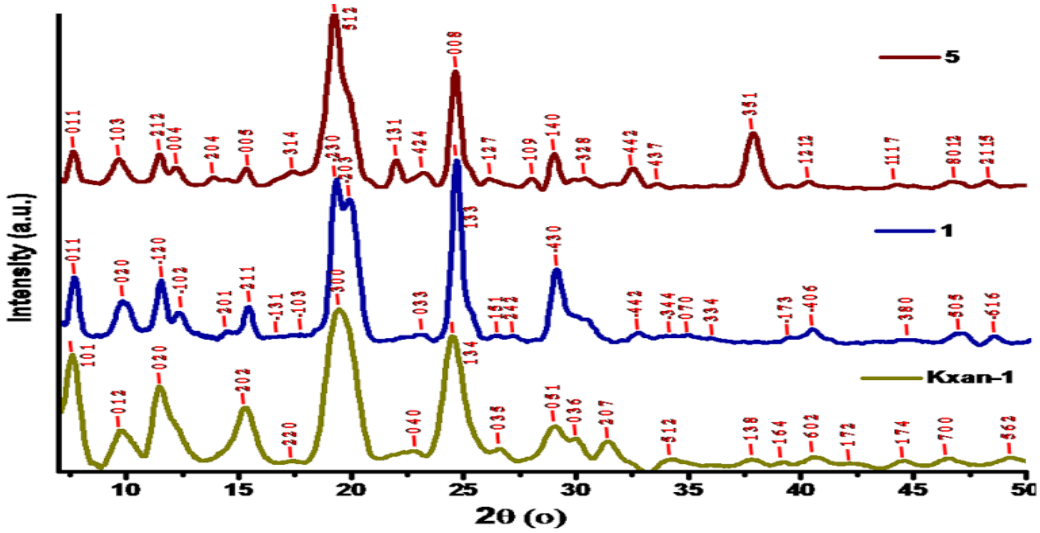

Annexure 15. Powder X-ray diffraction pattern for a set of compounds **K$_2$xan^1,1** and **5**

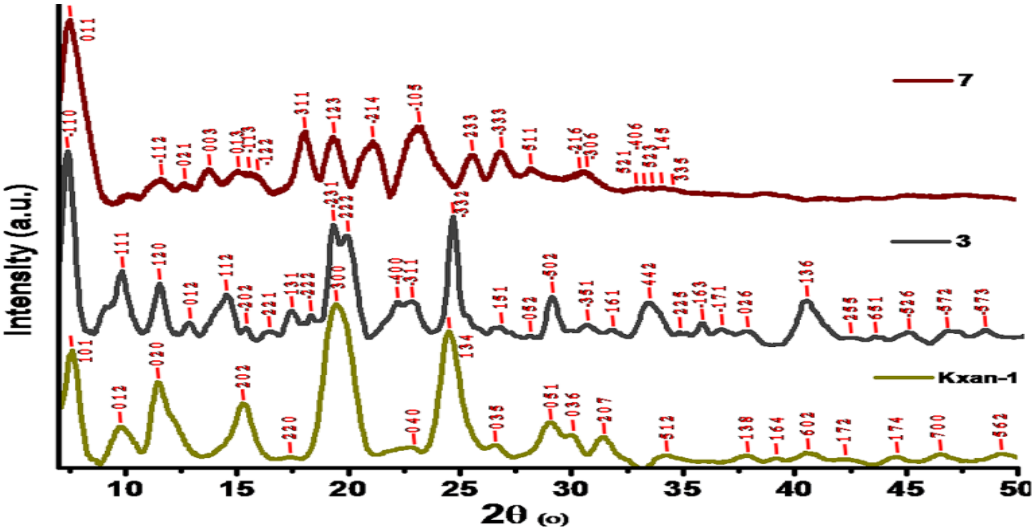

Annexure 16. Powder X-ray diffraction pattern for a set of compounds **K$_2$xan^1,3** and **7.**

The powder XRD data for these samples have been successfully indexed and refined by least square refinement with the help of commonly used[2]program[3] 'POWDERX' and the details of the indexed peak are given below.

Table A1. Power X-ray diffraction data for **K$_2$xan^1**, **1, 3, 5** and **7**.

Powder pattern line	h	k	l	2θ			d spacing		Intensity
				Exp.	Calc.	Diff	Exp.	Calc.	
(a) Kxan-1: *Orthorhombic(P)*: ***a*** = 13.66 Å, ***b*** = 15.5 Å, ***c*** = 21.9 Å; ***α*** = ***β*** = ***γ*** = 90º.									
1	1	0	1	7.619	7.627	-0.009	11.60344	11.59019	25.63
2	0	1	2	9.838	9.89	-0.051	8.98996	8.9434	9.02
3	0	2	0	11.483	11.417	0.066	7.70575	7.75	18.69
4	2	0	2	15.263	15.289	-0.026	5.805	5.79509	14.07
5	2	2	0	17.32	17.305	0.014	5.11985	5.12409	2.36
6	3	0	0	19.453	19.495	-0.042	4.563	4.55333	35.61
7	0	4	0	22.908	22.95	-0.042	3.88204	3.875	4.52
8	1	3	4	24.522	24.57	-0.048	3.63006	3.62308	29.67
9	0	3	5	26.629	26.681	-0.052	3.34736	3.34101	4.98
10	0	5	1	29.081	29.092	-0.01	3.07046	3.0694	9.95
11	0	3	6	30.004	29.973	0.031	2.97812	2.98113	7.23
12	2	0	7	31.448	31.45	-0.002	2.84453	2.84436	6.63
13	5	1	2	34.23	34.32	-0.09	2.6195	2.61281	2.72
14	1	3	8	37.79	37.767	0.023	2.38051	2.38188	2.68
15	1	6	4	39.134	39.115	0.019	2.30179	2.30288	2.1
16	6	0	2	40.502	40.467	0.035	2.22716	2.229	3.26
17	1	7	2	42.134	42.157	-0.023	2.1446	2.14347	1.93
18	1	7	4	44.641	44.637	0.004	2.02979	2.02996	2.42
19	7	0	0	46.537	46.537	0	1.95142	1.95143	2.95
20	5	6	2	49.268	49.251	0.017	1.84946	1.85006	3.06
21	4	2	10	50.919	50.914	0.005	1.7933	1.79345	1.94
(b) 1: *Monoclinic (P)*:***a*** = 14.5 Å, ***b*** = 18.03 Å, ***c*** = 15.35 Å;***α*** = ***γ*** = 90ºand***β*** = 99.1º.									
1	0	1	1	7.683	7.62	0.063	11.49785	11.59306	1.25
2	0	2	0	9.82	9.811	0.009	9.00002	9.00809	0.86
3	-1	2	0	11.522	11.599	-0.077	7.67391	7.62287	1.18
4	-1	0	2	12.321	12.32	0.002	7.17773	7.17873	0.67
5	2	0	1	14.492	14.495	-0.003	6.10719	6.10592	0.36
6	2	1	1	15.398	15.31	0.088	5.74981	5.78283	0.75
7	-1	3	1	16.704	16.693	0.011	5.30297	5.30644	0.28
8	-1	0	3	17.692	17.667	0.025	5.0091	5.01614	0.31
9	-2	3	0	19.275	19.282	-0.007	4.60117	4.59942	2.83
10	-2	0	3	19.847	19.841	0.006	4.46979	4.47121	2.51
11	0	3	3	22.998	22.996	0.002	3.8641	3.86435	0.3
12	1	3	3	24.588	24.559	0.029	3.61765	3.6219	3.15
13	1	5	1	26.343	26.377	-0.033	3.38043	3.37623	0.29
14	2	4	2	27.079	27.041	0.038	3.29029	3.29484	0.29
15	-4	3	0	29.006	29.035	-0.028	3.07587	3.07292	1.37

16	-4	4	2	32.63	32.659	-0.029	2.74208	2.73972	0.33
17	-3	4	4	34.158	34.175	-0.017	2.62283	2.6216	0.29
18	0	7	0	34.816	34.83	-0.014	2.57472	2.57374	0.3
19	3	3	4	35.797	35.773	0.024	2.50643	2.50807	0.25
20	-1	7	3	39.317	39.314	0.003	2.28973	2.28991	0.26
21	-4	0	6	40.303	40.31	-0.007	2.23597	2.23561	0.39
22	3	8	0	44.459	44.453	0.005	2.03614	2.03638	0.22
23	5	0	5	46.979	46.969	0.01	1.9326	1.933	0.33
24	-6	1	6	48.394	48.415	-0.021	1.87934	1.87858	0.28
25	-7	1	5	49.951	49.944	0.007	1.82436	1.82459	0.21
26	-8	0	1	50.389	50.386	0.003	1.80953	1.80962	0.22

(c) 3: *Monoclinic (P)*: ***a*** = 16.2 Å, ***b*** = 17.6 Å, ***c*** = 15.0 Å;***α*** = ***γ*** = 90º and ***β*** = 96.15º.

1	-1	1	0	7.418	7.44	-0.022	11.90844	11.87299	2.87
2	1	1	1	9.816	9.877	-0.061	9.00346	8.94781	1.15
3	1	2	0	11.517	11.458	0.059	7.67723	7.71664	0.97
4	0	1	2	12.841	12.893	-0.052	6.88836	6.86074	0.41
5	1	1	2	14.5	14.514	-0.015	6.10404	6.09798	0.81
6	-2	0	2	15.355	15.304	0.052	5.76569	5.78502	0.34
7	2	2	1	16.476	16.491	-0.015	5.37596	5.371	0.28
8	1	3	1	17.397	17.354	0.043	5.09336	5.10601	0.58
9	-2	2	2	18.264	18.343	-0.079	4.85355	4.83291	0.52
10	-2	3	1	19.271	19.28	-0.009	4.60208	4.60006	1.82
11	2	2	2	19.856	19.829	0.027	4.46783	4.4739	1.66
12	-4	0	0	22.124	22.074	0.05	4.01464	4.0236	0.7
13	-3	3	1	22.776	22.769	0.007	3.90114	3.90234	0.72
14	-3	3	2	24.581	24.602	-0.021	3.61867	3.6156	1.94
15	1	5	1	26.725	26.736	-0.011	3.33303	3.3317	0.34
16	0	5	2	28.033	28.03	0.003	3.18038	3.18073	0.22
17	-5	0	2	29.005	28.992	0.014	3.076	3.0774	0.78
18	-3	5	1	30.578	30.607	-0.029	2.92123	2.91855	0.38
19	1	6	1	31.704	31.692	0.012	2.82005	2.82105	0.3
20	4	4	2	33.32	33.337	-0.017	2.68683	2.6855	0.7
21	2	2	5	34.68	34.701	-0.021	2.58453	2.583	0.27
22	-1	6	3	35.675	35.671	0.003	2.51473	2.51494	0.4
23	-1	7	1	36.539	36.571	-0.032	2.45719	2.45514	0.31
24	0	2	6	37.577	37.601	-0.024	2.39167	2.39019	0.28
25	1	3	6	40.35	40.346	0.004	2.23349	2.23369	0.72
26	2	5	5	42.142	42.136	0.006	2.14254	2.14284	0.19
27	6	5	1	43.357	43.328	0.029	2.08528	2.08662	0.21
28	-5	2	6	44.829	44.802	0.027	2.02017	2.02133	0.27
29	-5	7	2	46.64	46.632	0.007	1.94587	1.94617	0.29
30	-5	7	3	48.298	48.298	0	1.88287	1.88287	0.31
31	2	8	4	50.076	50.049	0.026	1.82011	1.821	0.22

(d) 5: *Orthorhombic(P)*: ***a*** = 26.4 Å, ***b*** = 12.4 Å, ***c*** = 28.9 Å; ***α*** = ***β*** = ***γ*** = 90º.

1	0	1	1	7.669	7.758	-0.089	11.52802	11.39535	6.54
2	1	0	3	9.707	9.773	-0.067	9.11165	9.04967	5.3
3	2	1	2	11.503	11.548	-0.046	7.69266	7.66242	6.15
4	0	0	4	12.229	12.25	-0.021	7.23732	7.225	3.96
5	2	0	4	13.916	13.973	-0.057	6.3636	6.33774	2.35
6	0	0	5	15.351	15.329	0.022	5.77169	5.78	3.77
7	3	1	4	17.405	17.417	-0.012	5.09508	5.0916	3.31
8	5	1	2	19.266	19.275	-0.009	4.60686	4.60468	29.43
9	1	3	1	22.003	21.982	0.021	4.03965	4.04342	5.15
10	4	2	4	23.248	23.216	0.033	3.82592	3.83121	3.07
11	0	0	8	24.634	24.643	-0.008	3.6137	3.6125	19.66
12	1	2	7	26.144	26.15	-0.006	3.40841	3.40765	2.09
13	1	0	9	28.032	27.99	0.041	3.183	3.18762	2.11
14	1	4	0	29.024	29	0.024	3.07635	3.07884	6.17
15	3	2	8	30.381	30.384	-0.002	2.94198	2.94175	2.16
16	4	4	2	32.507	32.505	0.002	2.75424	2.75445	3.83
17	4	3	7	33.585	33.549	0.037	2.66828	2.67111	1.3
18	3	5	1	37.862	37.816	0.046	2.37616	2.37892	9.6
19	1	2	12	40.313	40.319	-0.006	2.23716	2.23684	1.62
20	11	1	7	44.245	44.259	-0.014	2.04703	2.04644	1.14
21	8	0	12	46.716	46.69	0.025	1.94437	1.94537	1.67
22	2	1	15	48.292	48.297	-0.005	1.88451	1.88432	1.7
23	13	2	6	50.971	50.976	-0.005	1.7916	1.79144	3.74
24	0	1	1	7.669	7.758	-0.089	11.52802	11.39535	6.54

(e) 7: *Monoclinic (P)*: ***a*** = 16.8 Å, ***b*** = 15.0 Å, ***c*** = 19.4 Å;***α*** = ***γ*** = 90º and ***β*** = 96.15º**.**

1	0	1	1	7.517	7.466	0.051	11.7514	11.83181	4.02
2	-1	1	2	11.623	11.69	-0.067	7.60747	7.56428	0.94
3	0	2	1	12.686	12.663	0.023	6.97228	6.9848	0.86
4	0	0	3	13.747	13.773	-0.025	6.43629	6.42452	1.12

5	0	1	3	15.077	14.991	0.085	5.8717	5.90494	1.1
6	-1	1	3	15.405	15.404	1E-3	5.74709	5.74761	1.06
7	-1	2	2	15.638	15.547	0.092	5.66202	5.69519	1.05
8	3	1	1	18.089	18.045	0.044	4.90001	4.91183	1.85
9	1	2	3	19.365	19.354	0.01	4.58006	4.58248	1.76
10	-2	1	4	21.117	21.111	0.006	4.20384	4.20503	1.67
11	-1	0	5	23.119	23.099	0.02	3.84401	3.8473	1.96
12	2	3	3	25.565	25.588	-0.023	3.48158	3.4785	1.4
13	-3	3	3	26.818	26.813	0.005	3.32162	3.32223	1.46
14	5	1	1	28.248	28.228	0.019	3.15672	3.15886	1.14
15	-2	1	6	29.307	29.29	0.017	3.04494	3.04672	0.97
16	-3	0	6	30.638	30.584	0.053	2.9157	2.92065	1.09
17	5	3	1	32.986	32.985	0	2.71333	2.71336	0.76
18	-4	0	6	33.284	33.301	-0.016	2.68967	2.68838	0.77
19	5	2	3	33.715	33.72	-0.005	2.65629	2.6559	0.76
20	1	4	5	34.163	34.167	-0.004	2.62243	2.62215	0.78
21	3	3	5	34.618	34.675	-0.057	2.58902	2.58492	0.75

4.6.2. X-ray Crystallography

***Description of Crystal Packing Patterns*:**The favourable α angles (angle between the line connecting Cg, H atom and the normal to the phenyl ring plane) whereas the β angles (Annexure 17) are large enough to facilitate CH... π interactions found in normal range, reflects strength of particular interactions.

Table A2. Significant intermolecular interactions [Interatomic distances (Å), and bond angles (°)] found in compounds **5-7**.

Interactions	**D─H…A**	**D─H**	**H…A**	**D…A**	**<DHA**	**<α**	**<β**
		5					
CH…π	**H24...π** (Cg: C22 C60 C53 C46 C63 C44) **10 atoms**	0.932	2.590	3.521	176.87	5.3	176.87
	H61...π(Cg: C49 C59 C57 C52 C33 C55) **10 atoms**	0.930	2.751	3.583	149.11	11.99	149.11
	H49...π(Cg: C35 C11 C13 C20 C54 C42) **10 atoms**	0.931	2.908	3.682	141.48	2.12	141.48
	H62...π(Cg: C11 C35 C42 C54 H49 C20 C13) **10 atoms**	0.930	2.850	3.529	130.80	7.62	130.80
CH…O	**H8...O5/O15** H8...O5	0.931	2.471	3.278	145.20	…	…
	(Bifurcated) H8...O15	0.931	2.491	3.321	148.66	…	…
	H21...O15	0.931	2.519	3.205	130.71	…	…
	H59...O6	0.929	2.586	3.378	143.48	…	…
		6					
CH…π	**H6...π** (Cg: C70 C69 C32 C27 C28 C29)	0.932	2.850	3.485	126.40	1.01	126.40
	H15...π(Cg: C46 C37 C38 C43 C44 C45)	0.929	2.779	3.663	159.22	13.45	159.22
	H21...π(Cg: N4 C59 C60)	0.931	2.960	3.478	116.62	0.70	116.62
	H34...π(Cg: C17 C18 C13 C14 C15 C16)	0.929	3.419	4.140	136.23	40.68	136.23
	H42...π(Cg: C56 C57 C48 C49 C54 C55)	0928	3.758	4.443	132.99	44.91	132.99
	H55...π(Cg: C66 C65 C60 C59 C68 C67)	0.931	2.928	3.806	157.80	13.12	157.80
	H61...π(Cg: C56 C57 C48 C49 C54 C55)	0.931	3.190	3.826	126.42	5.44	126.42
π…π	**π...π** (Cg1: C7 C8 C9 C10 C11	…	…	3.586	…	…	…

	C12, Cg2: C46 C37 C38 C43 C44 C45)							
CH…O	**H70...O3**		0.930	…	3.084	124.51	…	…
			7.DMSO					
CH…π	**H35...π** (Cg: **10 atoms**)		0.930	2.561	3.488	173.99	3.32	173.99
	H39...π (Cg: **10 atoms**)		0.930	2.773	3.589	148.33	4.47	148.33
	H40...π (Cg: **10 atoms**)		0.931	2.800	3.444	127.26	2.78	127.26
CH…O	**H12/H64...O2**	H12...O2	0.930	2.580	3.452	156.33	…	…
	(Bifurcated)	H64...O2	0.930	2.595	3.427	149.16	…	…
	H32/H45...O3	H32...O3	0.930	2.491	3.337	151.39	…	…
	(Bifurcated)	H45...O3	0.930	2.520	3.197	129.81	…	…
	H32...O7		0.930	2.511	3.306	143.63	…	…
	H19/H68a...O4	H19...O4	0.971	2.655	3.558	154.86	…	…
	(Bifurcated)	H68a...O4	0.970	2.528	3.458	160.67	…	…
	H57...O4		0.929	2.588	3.398	145.90	…	…
O…S	**O9…S1**		…	…	3.277	…	…	…
			7.MDC					
CH…π	**H18...π** (Cg: C1-C6)		0.949	3.240	3.913	129.53	25.45	129.53
	H25...π (Cg: C14-C19)		0.950	2.991	3.811	145.26	7.56	145.26
	H26...π (Cg: C19C20N2)		0.951	2.745	3.517	139.04	11.9	139.04
CH…O	**H11B...O1/O3**	H11B...O1	0.990	2.632	3.434	138.23	…	…
	(Bifurcated)	H11B...O3	0.990	2.543	3.328	136.24	…	…
	H11A...O2		0.990	2.462	3.393	156.64	…	…
π…π	**π...π** (Cg1: C8 C13 C12 C11 C10 C9, Cg2: 9 atoms)		…	…	3.586	…	…	…
Cl…O	**Cl2…O3**		…	…	3.161	…	…	…

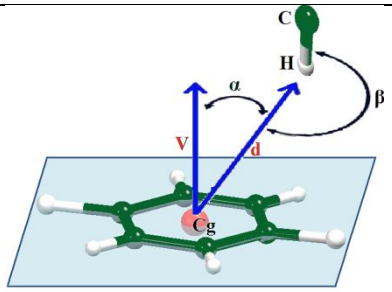

Annexure 17. Protocol for CH...πinteractions: d is the distance between the phenyl ring centroid (Cg) and the H atom; V is the vector normal to the plane of phenyl ring; α is the angle between the d and V vector, and β is the C–H...Cg angle.

5.*2H₂O:* Interestingly, the **H61...π** (Cg: C49 C59 C57 C52 C33 C55) interactions can be used to generate 1D infinite helicate along *b*-axis whereas **H49...π** (Cg: C35 C11 C13 C20 C54 C42) interactions forms another helicate along *c*-axis, with helical pitch 28.963Å (Annexure 18). The **H24...π** (Cg: C22 C60 C53 C46 C63 C44) interactions are associated with two CH...O interactions viz. **H8...O5/O15** and **H21...O15**,which are closing contact, hence forms macrocyclic assembly.

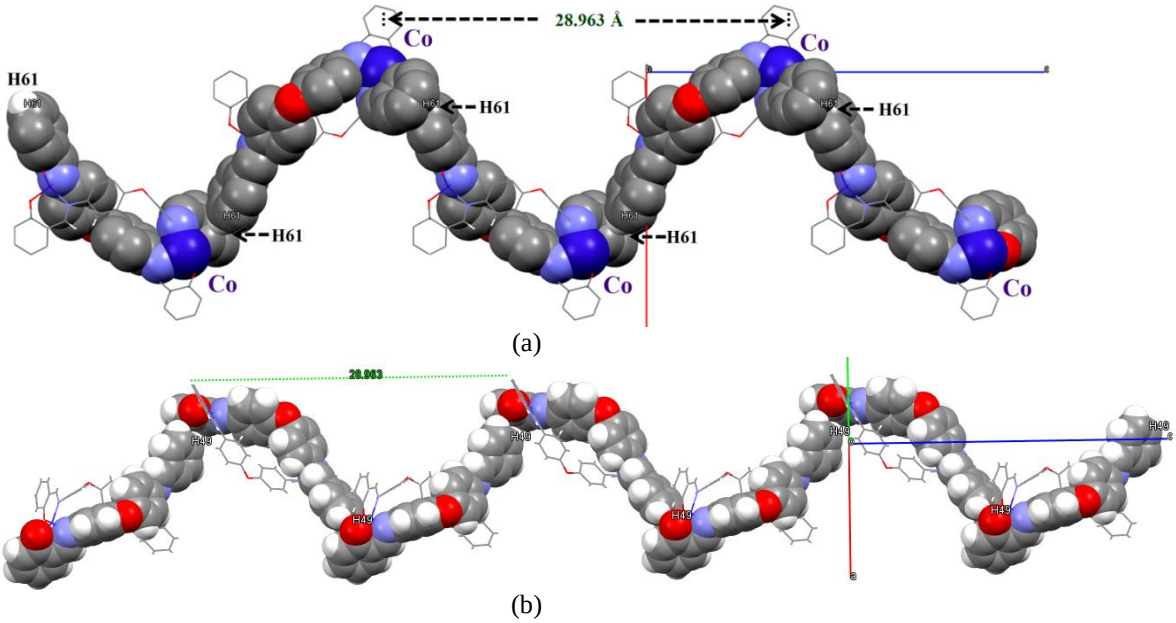

(a)

(b)

Annexure 18. (a) and (b) Formation of helicates along b- and c-axisthrough noncovalent interactions.

6.*2H₂O:* The H21...π(Cg: N4 C59 C60) donor-acceptor interactions are closing contact which holds two molecules exactly in *anti* manner and are associated with **H61...*π*** interaction, which leads to the formation of two molecular finite '*S-shaped*' self-assembly. Additionally, 1D wavy arrangement along *c*-axis and 1D stacking along *a*-axis have been formed through **H42...*π*** and **H42...*π*** interactions, respectively. (Annexure 19 a-b) Four double helical macrocyclic molecular units are situated at four diagonal corners of the unit cell of **6** whereas dimenstionality is extended predominantly through CH...π and CH...O interactions to the formation of infinite 3D architecture consisting of number of voids.

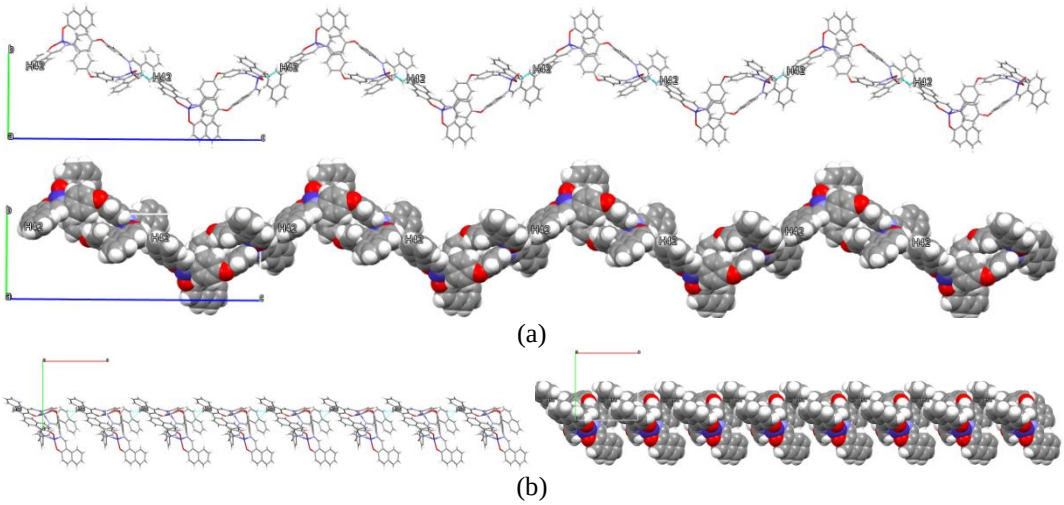

(a)

(b)

Annexure 19. (a-b)Formation of 1D wavy arrangement along *c*-axis and 1D stacking along *a*-axis have been formed through **H42...*π*** and **H42...*π*** interactions, respectively.

7.*CH_2Cl_2:* The **π...π** interactions align molecules in *anti* and lead to 1D packing (Annexure 20a) and Cl...O interactions in cooperation with CH...O interactions, pack the molecules in *ac* plane *via* dichloromethane (Annexure 20b). Notably, distinct crystal packing pattern is observed when DMSO is switched over to CH_2Cl_2, for instance smaller voids are generated due to crystal packing which are occupied by CH_2Cl_2 molecules. Hydrogen of CH_2Cl_2 molecules are also involved in CH...O interactions with both the chelated phenolic oxygens of either side.

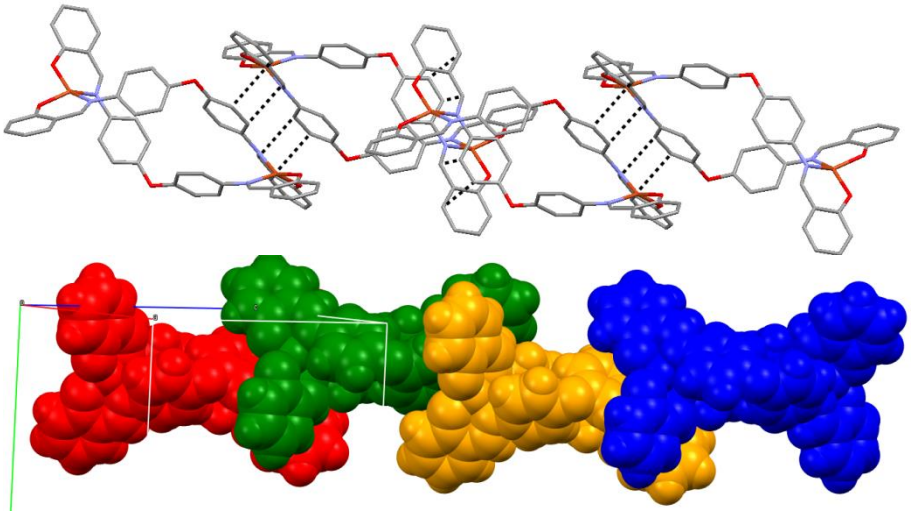

(a)

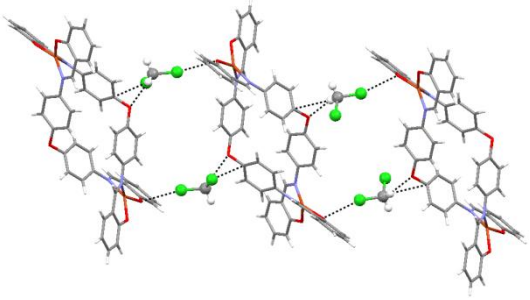

(b)

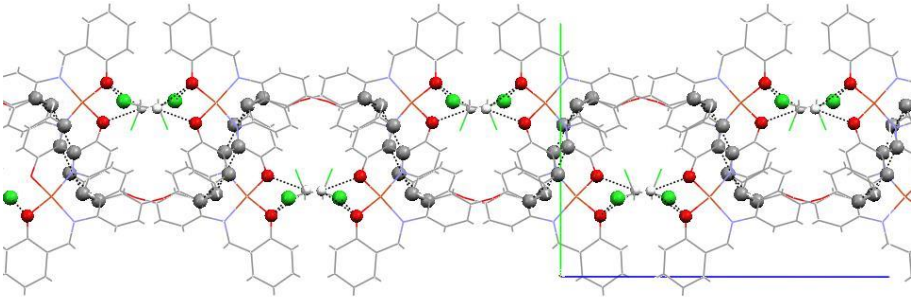

(c)

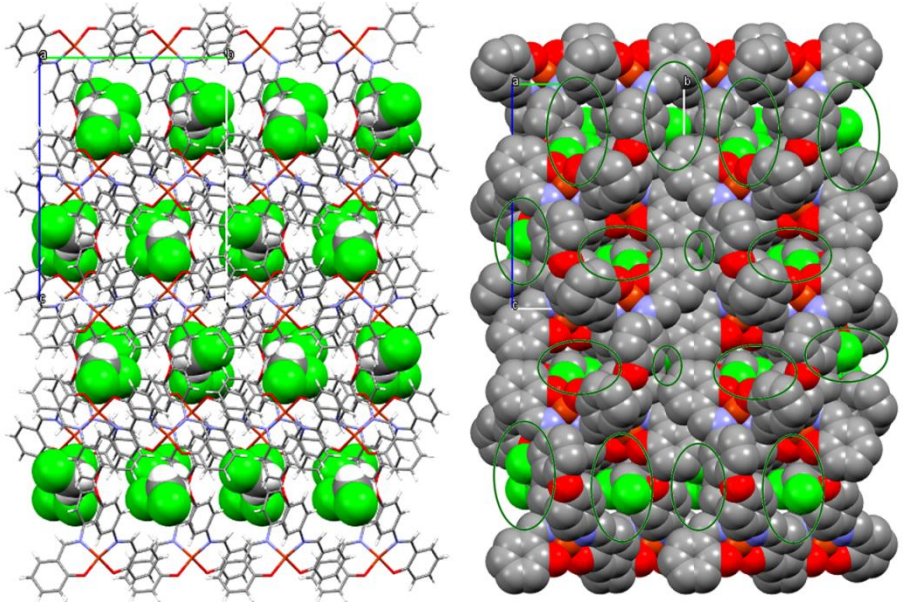

(d)

Annexure 20. (a) View of the layer formed by the $\pi\ldots\pi$-stacking interactions (b) Molecular packing in *ac* plane *via* dichloromethane molecules. (c) Helical chain-like packing along the c-axis. (d) Molecular packing view along *a*-axis (2.2.2) in complex **7**.CH_2Cl_2, H atoms and solvent molecules were omitted for clarity.

2.6.3. Cytotoxicity Study

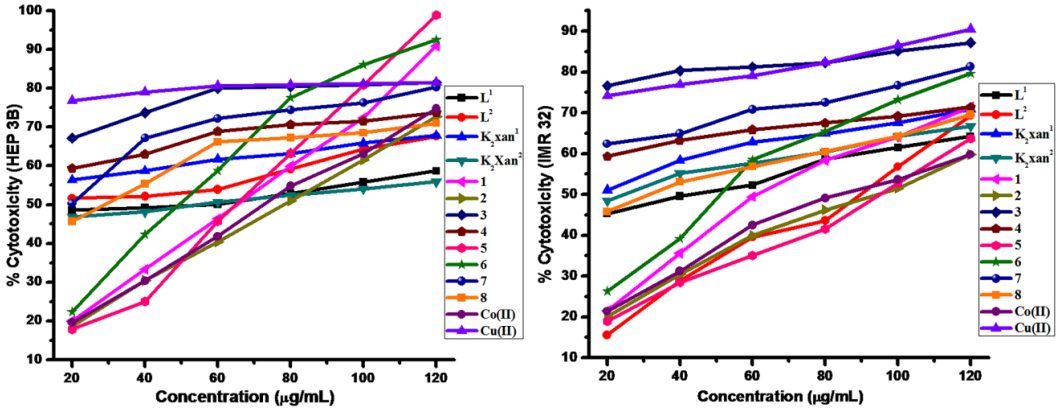

(a) **(b)**

Annexure 21. % Cytotoxicity observed for investigated compounds against HEP 3B (a) and IMR 32 (b) at different concentrations.

Table A5. Parameters obtained from the computational investigations and cytotoxic activity for model compounds.

Compound	E_{HOMO} (eV)	HOMO-LUMO gap (eV)	Dipole moment (Debye)	Charges on chelated atoms (S/N,O) and metal centre	IC_{50} values	
					HEP 3B µM (1mL) ±SE	IMR 32 µM (1mL) ±SE
L_1	-5.59	3.7829	3.4765	N,O – (0.568-0.600)	137.76±13.93	103.985±3.30
Kxan-1	-5.0127	3.2543	17.2480	S –(0.380-0.394), K (0.821-0.824)	17.8135±2.94	23.194±1.36
1	-5.5524	3.4646	2.6945	S – (0.020-0.036), Co (0.052)	52.943±1.30	51.802±2.86
3	-5.5772	3.3941	1.1886	S (0.015-0.028), Cu –(0.103-0.109)	8.1349±0.82	1.848±0.31
5	-5.4240	3.5688	0.4366	N – (0.566-0.571), O – (0.654- 0.661), Co (0.749-0.750)	69.725±3.57	99.658±6.55
7	-5.4801	3.6303	0.0139	N – (0.545), O – (0.606), Cu (0.607)	19.163±2.05	13.211±1.07

2.6.4. Thermogravimetric Analysis

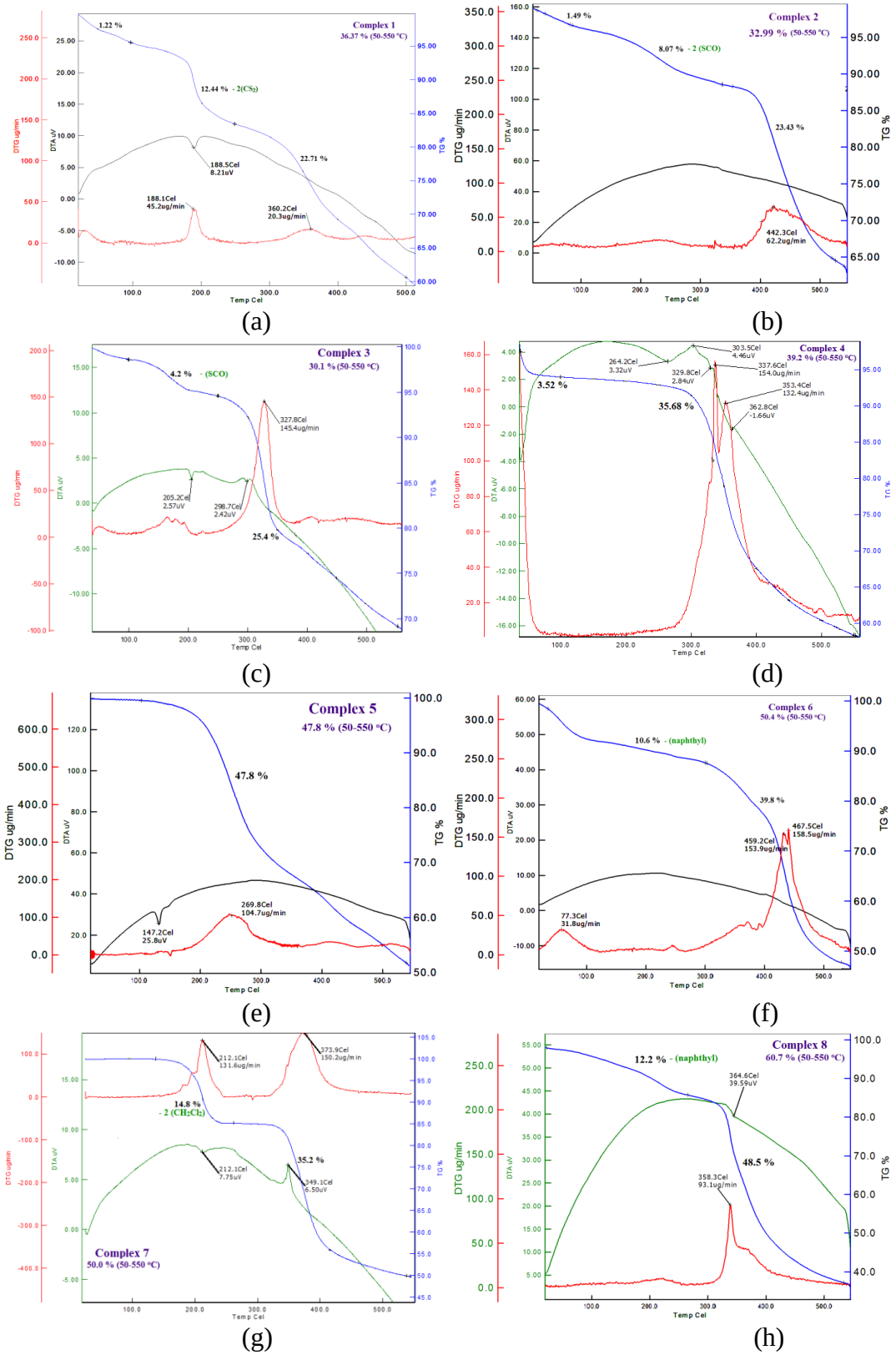

Annexure22. DTG/DTA/TG curves a-h for binuclear xanthate/ *N,O*-Schiff base macrocyclic complexes**1-8**, respectively.